Development of new channelrhodopsin versions with enhanced plasma membrane targeting and high calcium/sodium conductance

Dissertation zur Erlangung des
naturwissenschaftlichen Doktorgrades
der Julius-Maximilians-Universität Würzburg

vorgelegt von

Xiaodong Duan

Hunan, China

Würzburg, 2019

Eingereicht am:

Mitglieder der Promotionskommission:

Vorsitzender:

Gutachter: Prof. Dr. Georg Nagel

Gutachter: Prof. Dr. Robert J. Kittel

Tag des Promotionskolloquiums:

Doktorurkunde ausgehändigt am:

Eidesstattliche Erklärungen nach §7 Abs. 2 Satz 3, 4, 5 der Promotionsordnung der Fakultät für Biologie

Eidesstattliche Erklärung

Hiermit erkläre ich an Eides statt, die Dissertation: „**Development of new channelrhodopsin versions with enhanced plasma membrane targeting and high calcium/sodium conductance**“, eigenständig, d. h. insbesondere selbständig und ohne Hilfe eines kommerziellen Promotionsberaters, angefertigt und keine anderen, als die von mir angegebenen Quellen und Hilfsmittel verwendet zu haben.

Ich erkläre außerdem, dass die Dissertation weder in gleicher noch in ähnlicher Form bereits in einem anderen Prüfungsverfahren vorgelegen hat.

Weiterhin erkläre ich, dass bei allen Abbildungen und Texten bei denen die Verwertungsrechte (Copyright) nicht bei mir liegen, diese von den Rechtsinhabern eingeholt wurden und die Textstellen bzw. Abbildungen entsprechend den rechtlichen Vorgaben gekennzeichnet sind sowie bei Abbbildungen, die dem Internet entnommen wurden, der entsprechende Hypertextlink angegeben wurde.

Affidavit

I hereby declare that my thesis entitled: „ **Development of new channelrhodopsin versions with enhanced plasma membrane targeting and high calcium/sodium conductance**” is the result of my own work. I did not receive any help or support from commercial consultants. All sources and/or materials applied are listed and specified in the thesis.

Furthermore, I verify that the thesis has not been submitted as part of another examination process neither in identical nor in similar form.

Besides I declare that if I do not hold the copyright for figures and paragraphs, I obtained it from the rights holder and that paragraphs and figures have been marked according to law or for figures taken from the internet the hyperlink has been added accordingly.

Würzburg, den Univ. Wuerzburg
Inst. Physiology - Neurophysiology
Röntgenring 9, D-97070 Würzburg, Germany

Signature PhD-student

Abstract

The technique to manipulate cells or living animals by illumination after gene transfer of light-sensitive proteins is called optogenetics. Successful optogenetics started with the use of the light-gated cation channel channelrhodopsin-2 (ChR2). After early demonstrations of the power of ChR2, further light-sensitive ion channels and ion pumps were recruited to the optogenetic toolbox. Furthermore, mutations and chimera of ChR2 improved its versatility.

However, there is still a need for improved optogenetic tools, e.g. with higher permeability for calcium or better expression in the plasma membrane. In this thesis, my work focuses on the design of highly functional channelrhodopsins with enhanced Na^+ and Ca^{2+} conductance.

First, I tested different N-terminal signal peptides to improve the plasma membrane targeting of Channelrhodopsins. We found that a N-terminal peptide, named LR, could improve the plasma membrane targeting of many rhodopsins. Modification with LR contributed to three to ten-fold larger photocurrents (than that of the original version) of multiple channelrhodopsins, like ChR2 from *C. reinhardtii* (*Cr*ChR2), *Ps*ChR, Chrimson, CheRiff, *Ce*ChR, ACRs, and the light-activated pump rhodopsins KR2, Jaw, HR.

Second, by introducing point mutation, I could further improve the light sensitivity and photocurrent of different channelrhodopsins. For instance, ChR2-XXM 2.0, ChR2-XXL 2.0 and *Ps*ChR D139H 2.0 exhibited hundred times larger photocurrents than wild type ChR2 and they show high light sensitivity. Also, the Ca^{2+} permeable channelrhodopsins *Ps*CatCh 2.0f and *Ps*CatCh 2.0e show very large

photocurrents and fast kinetics. In addition, I also characterized a novel bi-stable *Ce*ChR (from the acidophilic green alga *Chlamydomonas eustigma*) with a much longer closing time.

Third, I analysed the ion selectivity of different ChRs, which provides a basis for rational selection of channelrhodopsins for different experimental purposes. I demonstrate that ChR2, Chronos, Chrimson, CheRiff and *Ce*ChR are highly proton conductive, compared with wild type *Ps*ChR. Interestingly, Chronos has the lowest potassium conductance among these channelrhodopsins. Furthermore, I found that mutation of an aspartate in TM4 of ChR2 (D156) and *Ps*ChR (D139) to histidine obviously increased both the sodium and calcium permeability while proton conductance was reduced. *Ps*ChR D139H 2.0 has the largest sodium conductance of any published channelrhodopsin variants. Additionally, I generated *Ps*CatCh 2.0e which exhibits a ten-fold larger calcium current than the previously reported Ca^{2+} transporting *Cr*ChR2 mutant CatCh.

In summary, my research work

1.) described strategies for improving plasma membrane trafficking efficiency of opsins;

2.) yielded channelrhodopsins with fast kinetics or high light sensitivity;

3.) provided optogenetic tools with improved calcium and sodium conductance.

We could also improve the performance of channelrhodopsins with distinct action spectra, which will facilitate two-color neural excitation, both *in-vitro* and *in-vivo.*

Zusammenfassung

Die Technik, Zellen oder lebende Tiere nach dem Gentransfer lichtempfindlicher Proteine durch Belichtung zu manipulieren, wird als Optogenetik bezeichnet. Erfolgreiche Optogenetik begann mit der Verwendung des lichtgesteuerten Kationenkanals Channelrhodopsin-2 (ChR2). Nach frühen erfolgreichen Versuchen mit ChR2 wurden weitere lichtempfindliche Ionenkanäle und Ionenpumpen als optogenetische Werkzeuge etabliert. Darüber hinaus verbesserten Mutationen und Chimären von ChR2 seine Vielseitigkeit.

Es besteht jedoch immer noch ein Bedarf an verbesserten optogenetischen Werkzeugen, z. mit höherer Permeabilität für Calcium oder besserer Expression in der Plasmamembran. In dieser Arbeit beschäftige ich mich mit dem Design hochfunktioneller Channelrhodopsine mit verbesserter Na^+- und Ca^{2+}-Leitfähigkeit.

Zuerst habe ich verschiedene N-terminale Signalpeptide getestet, um die Anreicherung von Channelrhodopsinen in der Plasmamembran ("Plasmamembran-Targeting") zu verbessern. Wir fanden heraus, dass ein N-terminales Peptid namens LR das Plasmamembran-Targeting vieler Rhodopsine verbessern kann. Die Modifikation mit LR trug zu drei- bis zehnfach größeren Photoströmen (als die der Originalversion) von mehreren Channelrhodopsinen bei, wie ChR2 von *C. reinhardtii* (*Cr*ChR2), *Ps*ChR, Chrimson, CheRiff, *Ce*ChR, ACRs und der lichtaktivierten Pump-Rhodopsine KR2, Jaw, HR.

Zweitens konnte ich durch Mutagenese die Lichtempfindlichkeit und/oder den Photostrom verschiedener Channelrhodopsine weiter verbessern. Beispielsweise zeigten ChR2-XXM 2.0, ChR2-XXL 2.0

und PsChR D139H 2.0 hundertmal größere Photoströme als Wildtyp-ChR2 und sie zeigen eine hohe Lichtempfindlichkeit. Auch die Ca^{2+}-permeablen Kanalrhodopsine *Ps*CatCh 2.0f und *Ps*CatCh 2.0e zeigen sehr große Photoströme und eine schnelle Kinetik. Außerdem habe ich ein neues bistabiles *Ce*ChR (aus der azidophilen Grünalge *Chlamydomonas eustigma*) mit einer viel längeren Schließzeit charakterisiert.

Drittens analysierte ich die Ionenselektivität verschiedener ChRs, die eine Grundlage für die rationale Selektion von Channelrhodopsinen für verschiedene experimentelle Zwecke bietet. Ich zeige, dass ChR2, Chronos, Chrimson, CheRiff und *Ce*ChR im Vergleich zu Wildtyp-*Ps*ChR eine hohe Protonenleitfähigkeit aufweisen. Interessanterweise weist Chronos die niedrigste Kaliumleitfähigkeit unter diesen Channelrhodopsinen auf. Außerdem fand ich, dass die Mutation eines Aspartats in TM4 von ChR2 (D156) und *Ps*ChR (D139) zu Histidin offensichtlich sowohl die Natrium- als auch die Calciumpermeabilität erhöht, während die Protonenleitfähigkeit verringert ist. *Ps*ChR D139H 2.0 weist die größte Natriumleitfähigkeit aller veröffentlichten Channelrhodopsin-Varianten auf. Zusätzlich erzeugte ich *Ps*CatCh 2.0e, das einen zehnmal größeren Calciumstrom als die zuvor berichtete Ca^{2+}-transportierende *Cr*ChR2-Mutante CatCh aufweist.

Zusammenfassend ergab meine Dissertationsarbeit:

1.) Strategien zur Verbesserung der Expression von Opsinen in der Plasmamembran;

2.) Gut exprimierende Channelrhodopsine mit schneller Kinetik oder hoher Lichtempfindlichkeit;

3.) Neue optogenetische Werkzeuge mit verbesserter Calcium- und Natriumleitfähigkeit.

Auch konnte ich die Leistung von Channelrhodopsinen mit unterschiedlichen Aktionsspektren verbessern, was die zweifarbige neuronale Anregung sowohl *in vitro* als auch *in vivo* erleichtern sollte.

Material and methods

1.1Molecular biology

1.1.1Reagents and genetic material

The principal reagents for biological engineering experiments

Reagents /Kit	***Source***
DNA polymerase	Thermo Fisher Scientific
Restriction enzyme	Thermo Fisher Scientific
Ligase enzyme	Thermo Fisher Scientific
Synthesized primer	Thermo Fisher Scientific
Chemicals and antibiotics	Sigma Aldrich

Table 1.1 Material for molecular biology and their source

Synthesized and optimized opsin genes for molecular cloning.

Opsin	**species**	**Accession Number**
*Ce*ChR	*Chlamydomonas eustigma*	This study
*Ps*ChR	*alga Platymonas subcordiformis*	JX983143
ChR2	*Chlamydomonas reinhardtii*	EF474017
Chronos	*Stigeoclonium helveticum*	KF992040
Chrimson	*Chlamydomonas noctigama*	KF992060
*Gt*ACR1	*cryptophyte Guillardia theta*	KP171708
*Gt*ACR2	*cryptophyte Guillardia theta*	KP171709
*zip*ACR	*Proteononas sulcata*	KX879679

Table 1.2 All template genes for constructs generation

Opsin genes are inserted into the different expression vector

Vector	*resistance*	*Purpose*
pGEM	ampicillin	Oocytes expression
opAAV	ampicillin	Mammalian cell expression
pCDNA	ampicillin	Mammalian cell expression
pBKCMV	ampicillin	Stem cell expression
PTL515	ampicillin	*Drosophila* neuron expression
pAD5	ampicillin	*C. elegans* in vivo expression

Table 1.3 List of commonly used vectors for expression of microbial rhodopsin

1.1.2 PCR and digestion

PCR reaction system	**Total 20 μL**
Template	1
5× HGD buffer	4.6
forward primer (10 μM)	0.8
Reverse primer (10 μM)	0.8
dNTP (10 mM)	0.8
Phusion DNA Polymerase	0.3
BSA	0.1
ddH_2O	12.6

steps	repeats	Temperature	Duration
Step 1		98℃	45s
Step 2	6	98℃	15s
		72℃	15s per kb
Step3	6	98℃	15s
		66℃	15s
		72℃	15s per kb
Step4	26	98℃	15s
		56℃	15s
		72℃	15s per kb

1.1.3 DNA purification, ligation and sequencing

QIAquick PCR Purification Kit (Qiagen, Hilden, Germany) was used for DNA fragment purification. The purified DNA was eluted with cleaning water and stored at -20 ℃ for further use. The DNA insert was ligated to the vector by T4 DNA ligase (Fermentas, Thermo, Waltham, USA) at room temperature for at least 30 minutes. The molar ratio of DNA fragment to vector range from 2∶1 to 10∶1. The ligated product was transformed to *E. Coli* for future work. After double-digested confirmation, the recombinant plasmid was checked by DNA sequencing. The samples were sent to GATC Biotech (GATC Biotech, Constance, Germany).

Enzyme digestion	Total 10μL
Template	1
5× buffer	2
restriction enzyme I	1
restriction enzyme II	1
ddH_2O	5

DNA ligation	Total 10μL
T4 ligase	1
T4 ligation buffer	1
DNA segment / vector	molar ratio = 5:1 to 10:1
ddH_2O	Adjust to 10μL

1.1.4 DNA transformation and amplification

The transformation was done by heat-shock method. Classical heat shock method was adopted for transformation of DNA plasmids in this study. The competent MRF cells were put on ice before transformation and gently mixed with plasmid. The cell-DNA suspension was incubated on ice for 15-20min. and then transferred to 42 ◦C for 90 s was followed by another 2 min incubation on ice. The mixture was plated on agar plates containing 30 μg/ml kanamycin or 100 μg/ml ampicillin. For plasmids with ampicillin resistance, the mixture can be spread directly to the agar plates with ampicillin and incubated at 37 ℃ overnight. For plasmids with kanamycin resistance, 400 μL SOC medium (Table 2.5) was added to the mixture and incubated at 37 ℃ for 30 min, then 200 μL mixture can be spread

directly to the agar plates with kanamycin and incubated at 37 ℃ overnight.

1.1.5 Cracking of E. coli

Mix the colony with 10 μL H_2O by pipetting up and down. Add the same volume of cracking buffer into EP tube or strips and centrifuge shortly, put it at room temperature for 10 minutes. Then add the loading dye, run the DNA gel and check the size of the band. 2-4 colonies with correct band size were picked for overnight incubation.

Cracking buffer
0.2N NaOH
0.5 SDS
20 sucrose

1.1.6 Site-directed mutagenesis

To get single or multiple amino acids of interesting opsin genes the QuikChange method was performed. primer pairs containing single or multiple amino acid substitution were rationally designed using Benching software (Benchling, San Francisco, CA). QuickChange PCR reaction system and condition were description in the following table. The DpnI enzyme was added to PCR products and incubated for at 1-3 hours at 37℃, and then directly transformed the digested DNA into *E. coli.* Plasmids were extracted as described before and send for sequencing to confirm the correct mutations.

QuikChange PCR cycling condition

steps	repeats	Temperature	Duration
Step 1		98℃	45s
Step 2	6	98℃	15s
		72℃	15s per kb
Step3	6	98℃	15s
		66℃	15s
		72℃	15s per kb
Step4	26	98℃	15s
		56℃	15s
		72℃	15s per kb

QuikChange PCR reaction system

PCR reaction system	Total 20μL
Template	1
5× HGD buffer	4.6
forward primer (10μM)	0.8
Reverse primer (10μM)	0.8
dNTP (10mM)	0.8
Phusion DNA Polymerase	0.3
BSA	0.1
ddH_2O	12.6

1.1.7 RNA preparation

cDNA-derived mRNA (cRNA) of interesting genes were injected into Oocytes to estimate their functionality. In vitro transcription assay was performed to generate cRNA, AmpliCap-MaxT7 High Yield

Message Maker Kit (Epicentre Biotechnologies) was used for cRNA production. Constructs containing the interesting genes were linearized by NheI, then the linearized DNA fragment was purified for RNA preparation. The reaction starts from the T7 promoter using T7 RNA polymerase. The reaction was prepared as the following table. The mixture was incubated at 42 degrees for three hours. After short centrifugation, each sample was mixed with 12 μL methanol. Putting the mix in-20 ℃ for half-hour, and then centrifuge at 4℃ for at least 15 minutes. Discarding the supernatant and 75% ethanol were used to wash the white precipitation. After at least 15 minutes centrifugation, discard the supernatant. Keeping the EP tube for dry and then add RNAase free water to dissolve the RNA.

1.1.8 RNA injection

The concentration of RNA product was adjusted to 600ng/ μL or 1000ng/ μL with RNAase free water. cRNA was injected to Oocytes by the nano injection machine (Nanoject, Drummond Scientific Company). The injection capillary (3.511 Drummond #3-000-203-G/X; Drummond Scientific Company) was made by a vertical Puller (PP-83; Narishige). After injection, the oocytes are incubated in ND96 medium of the following composition (mM): 96mM NaCl, 5mM KCI, 1 mM $MgC1_2$, 1mM $CaC1_2$, 5mM HEPES, pH 7.4. The antibiotic gentamycin (50 mg/ml) is also added. The cells are stored at 16°C and the solution is changed daily. During this latter process, the cells should be inspected daily under a microscope, and unhealthy ones discarded.

1.2 Electrophysiology

1.2.1 Preparing Experiments

	Proton to sodium permeability			Proton to potassium permeability		
	pH7.6 High NaCl	**pH7.6 Low NaCl**	**pH9.6 High NaCl**	**pH7.6 High KCl**	**pH7.6 Low KCl**	**pH9.6 High KCl**
NaCl	120	1.2	120	120	1.2	120
KCl	/	/	/	/	/	/
NMG	/	119	/	/	119	/
HEPS	5	5	/	5	5	/
CAPSO	/	/	10	/	/	10

Table 1.4 Measuring solution for evaluation of monovalent ion permeability

	$CaCl_2$	**$BaCl_2$**	**NMG**	**HEPES**	**CAPO**
pH 7.6 High Ba^{2+}	0	80	0	5	0
pH 7.6 High Ca^{2+}	80	0	0	5	0
pH 7.6 Low Ba^{2+}	0	0.8	238	5	0
pH 9.0 High Ba^{2+}	0	80	0	0	10
pH 9.0 High Ca^{2+}	80	0	0	0	10

Table 1.5 Measuring solution for evaluation of divalent ion permeability

Before patching, it is necessary to remove the vitelline membrane. This is done manually with fine forceps. The oocyte is placed in a hyperosmotic medium (mM) with 500 mosmol/kg: 50 mL ND96++ containing 2.7g D-sorbitol,7.4. After 3-10 min in this solution, the cell shrivels. The vitelline membrane can now be observed and be gently

teased away from the cell using forceps. Once it is removed, the cells are extremely fragile and will easily rupture if exposed to air. The cells are also very sticky and will adhere to plastic or glass within a few minutes, and so they should immediately be transferred to the recording chamber.

1.2.2 Inside-out patch clamp in *Xenopus* oocytes

Entering the Bath:

Before putting pipette into the bath solution, a small amount of positive pressure to the pipette is very necessary. When moving the pipette tip into the bath, the current trace may disappear, in that case, we need to reduce the amplifier gain until the current trace reappears. Then cancelling any offset potentials between pipette and reference electrode by setting the holding potential of the patch-clamp amplifier to 0mV.

Forming a Gigaseal:

After the pipette has entered the bath, one should proceed as fast as possible to obtain a gigaseal, as the probability of floating particles, such as peptides, proteins, tend to cover the pipette tip and interfere with seal formation. When the pipette is pushed against a cell, the current pulses will become slightly smaller, indicating an increase in resistance. When the positive pressure is released from the pipette, the resistance usually increases further. Application of gentle suction should increase the resistance further and result in the formation of a gigaseal, which is characterized by the current trace becoming essentially flat again. To verify gigaseal formation, one may increase

the amplifier gain; the trace should still appear essentially flat except for capacitive spikes at the start and end of the voltage pulse.

Breaking the Patch:

After a gigaseal is formed, the patch membrane can be broken by additional suction or, in some cells, by high-voltage pulses. Electrical access to the cell's interior is indicated by a sudden increase in the capacitive transients from the test pulse and, depending on the cell's input resistance, a shift in the current level or background noise. Additional suction pulses sometimes lower the access resistance, causing the capacitive transients to become larger in amplitude but shorter in duration. Low values of the access (series) resistance *(R.)* are desirable, and when *R.* compensation is in use, it is important that the resistance be stable as well.

1.2.3 Two electrophysiology voltage-clamp recording of Xenopus laevis oocytes

cRNA-injected oocytes were incubated in ND96 solution containing 1 μM all-trans-retinal at 16 ℃. Two-electrode voltage-clamp (TEVC) recordings were performed with solutions as indicated in figures. Osmolality was adjusted to 220 mosmol/kg with D-sorbitol.

For calcium selectivity measurements, to avoid calcium triggered larger chloride current in *Xenopus* oocyte, calcium ions were replaced by barium. To block the Ca^{2+} activated chloride current in oocytes, we injected 50 nL 200 mM of the fast Ca^{2+} chelator BAPTA (1,2-bis (o-aminophenoxy) ethane-N,N,N',N'-tetraacetic acid, potassium-salt) into each oocyte (~10 mM final concentration in the oocyte), incubated for 90 mins at 16 ℃ and then performed the TEVC measurement. For

monovalent ions permeability measurements, the relative permeability was calculated as described previously. Standard voltage protocol was as follows: Starting from a holding potential of -60 mV, single voltage pulses were applied in -20 mV steps from +30 to -90 mV.

1.3 Light stimulation

Illuminations were performed with 473 nm, 445 nm, 532 nm and 635 nm lasers from Changchun New Industries Optoelectronics Tech as indicated in every figure. Action spectrum measurements were performed by combining narrow bandwidth interference filters of different wavelengths (Edmund Optics) and a white light generator PhotoFluor II (89 North). Wavelengths were further confirmed with a spectrometer (Ocean Optics). The light intensities were measured with a PLUS 2 Power & Energy Meter (LaserPoint s.r.l). For light sensitivity measurements, light intensities applied were ranging from 1.67, 5.56, 16.7, 55.6, 167, 556 and 1667 to 5000 $\mu W/mm^2$. All oocyte experiments were done with LED laser illumination, with nominal wavelength 473nm,445nm,532nm and 635nm. Action spectrum data were taken with narrow bandwidth interference filters of different wavelengths (Edmund Optics), which give us light with different wavelengths. Light power was controlled by a white light generator PhotoFluor II light source(89North). Equal photon fluxes of about 2×10^{18} photons/s/cm^2 were used across wavelength for each channelrhodopsin measurement. But LED has broader spectra. The wavelength was further confirmed with a spectrometer (Ocean Optics). The light intensities at different

wavelengths were measured with a Laser point meter (Coherent Technologies).

1.4 Protein quantification by fluorescence

All Channelrhodopsins' expression levels in oocytes were quantified by the fluorescence emission values of the tagged YFP protein. Fluorescence emission was measured at 538 nm by a Fluoroskan Ascent microplate fluorometer (Thermo Scientific) with 485 nm excitation.

1.5 Fluorescence imaging

Fluorescence pictures of *Xenopus* oocytes were taken with a Leica DM6000 confocal microscope after 2 days' expression. To determine the action spectra of channelrhodopsins, we used narrow bandwidth interference filters together with a PhotoFluor II light source to generate light of the desired wavelength. The light wavelength was further examined with a photo-spectrometry. Same amount photon flux of each wavelength was set for irradiation.

1.6 Data processing

Data analysis were performed with pClamp7.0, OriginPro, Microsoft Excel and GraphPad Prism. All values were plotted or presented with mean values and error bars represent the standard deviations (SD) or standard error mean (SEM) as indicated in each figure. Differences were considered significant at $p < 0.05$. *** $p < 0.001$, ** $p < 0.01$, * $p < 0.05$.

Introduction

2.1 Microbial rhodopsin

Rhodopsin is an organic complex that consists of retinal and opsin protein. The retinal molecule is a vitamin A-related organic photon-absorbing cofactor that enables light sensitivity for rhodopsin[1]. Most rhodopsins comprise seven-transmembrane helixes forming an interior protonated retinylidene Schiff base chromophore covalently binding to a conserved lysine residue located on seven-TM helix [2, 3]. The retinal chromophore isomerization initialized by photon absorption resulting in photocycle with several distinct intermediates, therefore give rises to light-gated channel or pump activities as well as recently discovered enzyme activity [1, 4-6]. Rhodopsin is typically divided into two different families: type I microbial rhodopsin and type II animal rhodopsin. Even though microbial rhodopsin and animal rhodopsin show low sequence homology, both exhibit similar structure and functionality[7].

Type I microbial rhodopsin are identified from prokaryotes or simple eukaryotes, like algae and fungi. These opsins utilize the all-trans-retinal, which isomerizes from all-trans-retinal to 13-cis configuration. Microbial rhodopsin function as light-gated cation[8] or anion channel[9], light-driven proton[10], chloride and sodium pump[11], and enzyme rhodopsin[5, 6, 12] (**figure2.1**). As its fast and reversible photochemical reaction directly trigger ions pass the plasma membrane by light illumination and enough levels of retinal in the

mammalian system, channelrhodopsin became an ideal tool to modulate neural activity in all kinds of animals[13, 14].

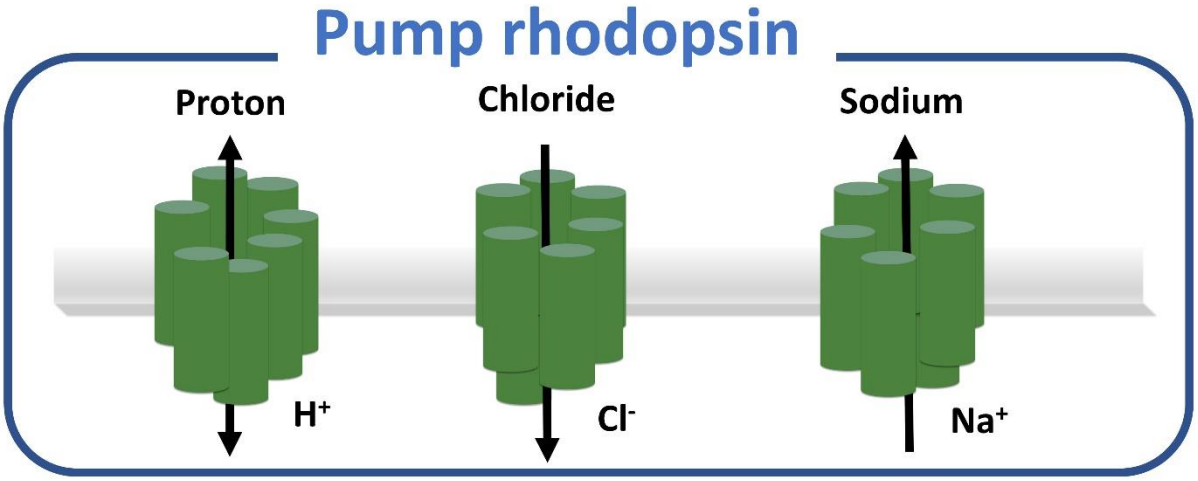

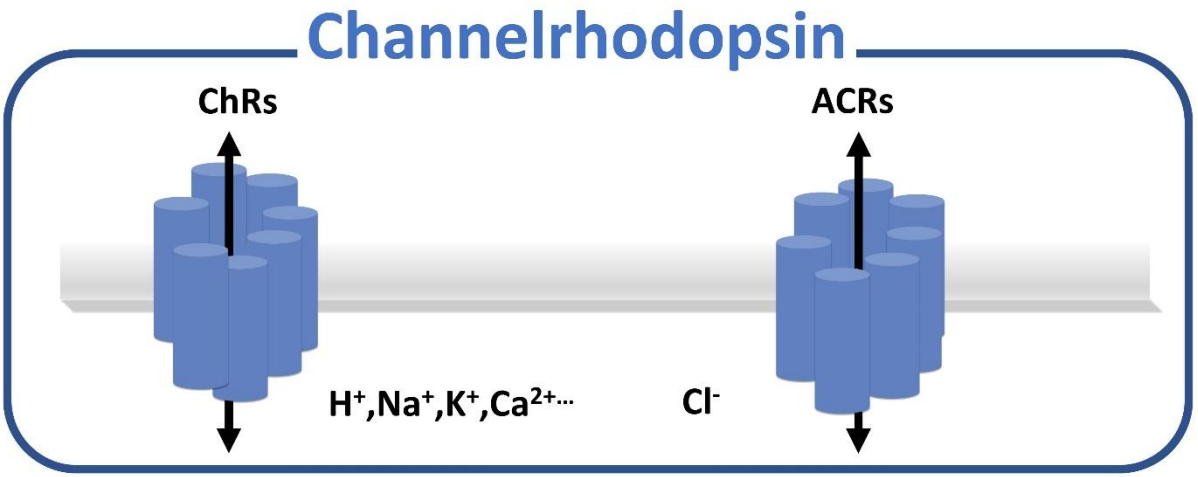

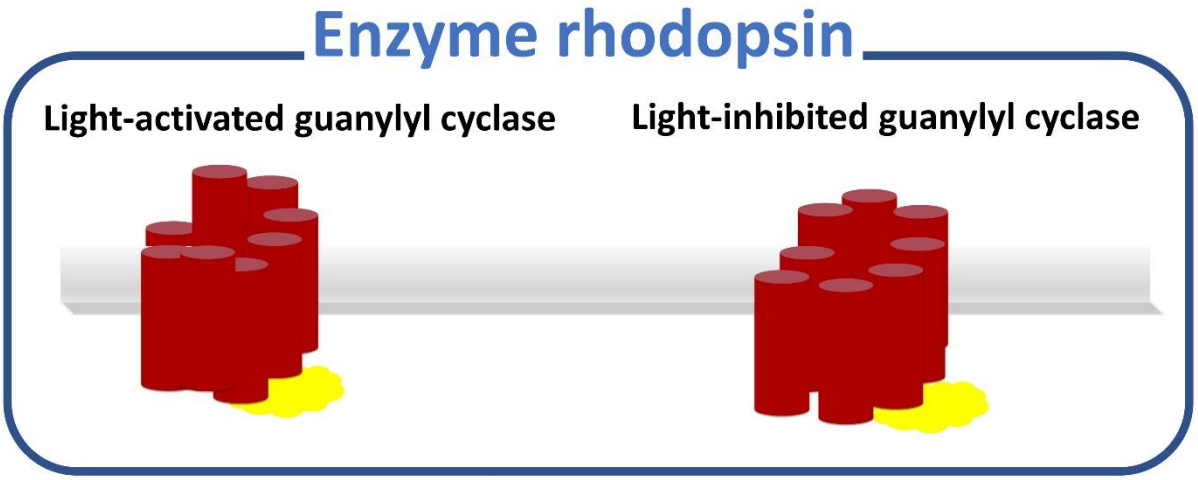

Figure 2.1 Type I Microbial Rhodopsin.
BR is a light-driven outward proton pump, and HR pump chloride into the cytoplasm; KR2 pump sodium ion from intracellular to extracellular side. ChR2, *Ps*ChR and Chrimson is a light-gated cation channel; ACRs is a light-gated chloride channel. *Be*CyClOp and *2C*-CyClOp exhibits light-activated and inhibited guanylyl cyclases.

In contrast, animal rhodopsin which are eukaryotic-derived opsin proteins mainly responsible for vision. Type II opsins primarily function as G protein-coupled receptors (GPCRs). Upon photon absorption, it triggers complex visual phototransduction initialized by isomerization of 11-cis retinal into the all-trans configuration[7, 15].

2.1.1 Proton-pumping rhodopsin

The first discovered type I microbial rhodopsin is bacteriorhodopsin BR, a light-driven outward proton pump[15]. Light-driven outward proton pump is abundant and widespread in nature, converting sunlight energy into proton force. Later, another two bacteriorhodopsin-type Archaerhodopsin-3 from *H. sodomense* [16] and Mac from fungus *Leptosphaeria maculans* were identified and proposed to be an outward proton pump[17, 18]. Recently, a new class of microbial rhodopsin was reported to exhibit inward proton pump activity. For example, *Po*XeR and *Ns*XeR are confirmed to be an inward proton[10, 19].

2.2.2 Chloride-pumping rhodopsin

In 1977, distinct class rhodopsins capable of outward photocurrent was identified as the first light-driven inward chloride pump termed Halorhodopsin. Another chloride pump from *Natronomonas pharaonis* was discovered by Lanyi in 1990[20, 21]. Experimental screen studies revealed that light-driven chloride pump from *Natronomonas pharaonis* named *Np*HR was able to use as an optically inhibitory tool for neural suppression[22]. In contrast, chloride pump from *Halobacterium salinarum Hs*HR unable to generate stable photocurrent when express in Oocytes or mammalian neurons. While both chloride pumps generate small photocurrents, which prevented them from further application in controlling living animals' behavior. Fortunately, improved version for enhancing plasma membrane targeting termed eNpHR2.0 and eNpHR3.0 have widely used for neural inhibition. Later, Edward S Boyden group screened a red-shifted crushalrhodopsin from *H. salinarum* (strain Shark), with less than 60% homology to the *Natronomonas pharaonis* halorhodopsin, termed Jaw with two points mutations K200R and W214F[23].

2.2.3 Sodium-pumping rhodopsin

In 2013, *Hideki Kandori* research group identified the first light-driven sodium pump from *marine flavobacterium Krokinobacter eikastus* termed KR2[24-27]. Structural and spectroscopic studies revealed that KR2 is an outward sodium pump. The ratio permeability of sodium to proton was around 8000 [25-27]. In the resting state, sodium transport was blocked by the protonated Schiff base. Upon photon absorption, photoisomerization of all-trans-retinal and N-H

flipping, the positive charge of Schiff base provides proton to Asp116 which breaks the electrical barrier. In M intermediate, the flipping of protonating Asp116 reduces the energy barrier to sodium transport and thereby allows sodium to pass the chromophore region. In O intermediate, the re-protonated of the Schiff base would rebuild the electrical barrier within chromophore which inhibits sodium conduction[28]. In addition, diverse light-driven sodium pump has been discovered from many flavobacteria, such as *Ny*NaR, *Nd*NaR, GLR, NdR2, *Sr*NaR and *Tr*NaR1 and *Tr*NaR2[29-32]. These studies provide many possibilities of engineering powerful light-driven sodium or potassium pumps to expand the optogenetic toolbox. However, the small photocurrent amplitude and heavily intracellular aggregation prevent it from wide application in neuroscience[33].

2.2.4 Enzyme rhodopsin

The first microbial rhodopsin capable of the enzyme function was identified in fungus *Blastocladiella emersonii*, referred to BeGC1, consisting of a type I microbial rhodopsin domain and guanylyl cyclase catalytic domain[34]. By functional characterization of BeGC1 in heterologous cells (*Xenopus* oocytes, HEK293T cells, neurons) and Caenorhabditis elegans, it was then called cyclase opsin CyclOp and RhGC rhodopsin-guanylyl cyclase[5, 35]. BeCyClOp is the first opsin with cytosolic N and C terminal and eight transmembrane helices with strongest light-regulated guanylyl cyclase activity so far, providing us powerful optogenetic tools to manipulate cellular cGMP signaling in a spatiotemporal precised manner[36].

The second member of enzyme rhodopsin is a unique gene-encoded microbial rhodopsin with C-terminal phosphodiesterase domain termed *Sr*RhoPDE which was identified in the genome of the choanoflagellate *Salpingoeca rosetta*. It was expressed in mammalian cells and turned out to be a slightly light-activated phosphodiesterase which is 10-fold more active with cGMP as substrate than with cAMP. Later, our group present strong evidence showed that RhoPDE capable of hydrolysis of cGMP which is around 100-fold higher turnover than that of cAMP[6]. Interestingly, they also confirmed that *Sr*RhoPDE shows cytosolic N and C-termini with an additional N terminal transmembrane helix, most likely an eight transmembrane helix opsin protein[4].

Recently, our group report a novel opsin family: *Cr2c*-Cyclop1 from *C. reinhardtii* and *Vc2c*-Cyclop1 from *V. carteri*. The function of *Cr2c*-Cyclop1 and *Vc2c*-Cyclop1 turned out to be a light inhibited guanylyl cyclase activity in an ATP dependent manner[12]. It is possible that combine 2c-Cylop with Cyclop could achieve bidirectional manipulated cGMP signaling by light. However, more studies need to be focus on its molecular characteristics, subcellular location, and application in mammalian systems.

2.2.5 ACRs

Two natural anion channelrhodopsin ACRs were identified and characterized from chlrophyte algae *Guillardia theta* [9]. ACRs could exhibit robust inhibition of behavior responses in multiple animal systems, including fish, *Drosophila*, *Caenorhabditis elegans* and mice[37-39]. There are several obvious advantages of ACRs when

compared to other optogenetic silencing tools. First, it generates the largest photocurrent among all the reported natural microbial rhodopsins due to its high expression level and large single-channel conductance. Second, ACRs exhibit 10^2~10^4-fold higher light sensitivity than other rhodopsin pumps, meaning it requires less light for neural silencing either in vitro or in vivo applications. Third, slow-off kinetic is suitable for long-term inhibition experiments in certain type neurons.

Furthermore, many other new ACRs homologs were reported from diverse cryophyte species. A red-shifted absorption anion conductance ChRs, named *Ps*ACR1, was identified from *Proteomonas sulcate[40]*. In 2017, Elena G. Govorunova found another light-gated anion channel *Zip*ACR[41], which shows much faster off-kinetics than previous reported ACRs. Later, they reported *Rap*ACR[42], an ACR from *Rhodomonas salina*, that exhibits channel half-closing times below 10 ms but shows 100-fold higher light sensitivity than *Zip*ACR and generate comparable photocurrent than other ACRs as well.

2.2.6 Channelrhodopsin

In 2003, it was first demonstrated that light-induced currents by heterologous expressed ChR2 can be used to control neural activity with high spatiotemporal resolution, the technology of optogenetics was born[8]. The wide application of optogenetics in neuroscience starting by expression ChR2 in neurons[43-47]. Channelrhodopsin belongs to the large family of type I microbial rhodopsin, the seven-helical transmembrane protein containing retinal as a chromophore.

This section describes key properties associated with channelrhodopsin, including crystal structures and photocycle, membrane targeting strategies, photocurrent and ion selectivity.

2.2.6.1 Crystal structure and photocycle

Recently, the high-resolution structure of native ChR2 was revealed, the crystal structure data demonstrated that wild type ChR2 contains four cavities, three gates and in the center is the retinal Schiff base[2]. They are connected by extended water-mediated and hydrogen-bonding networks. Four cavities are separated by three gates, close to the retinal Schiff base is the central gate. Within the central gate exists a DC gated comprised of a water-mediated bond between C128

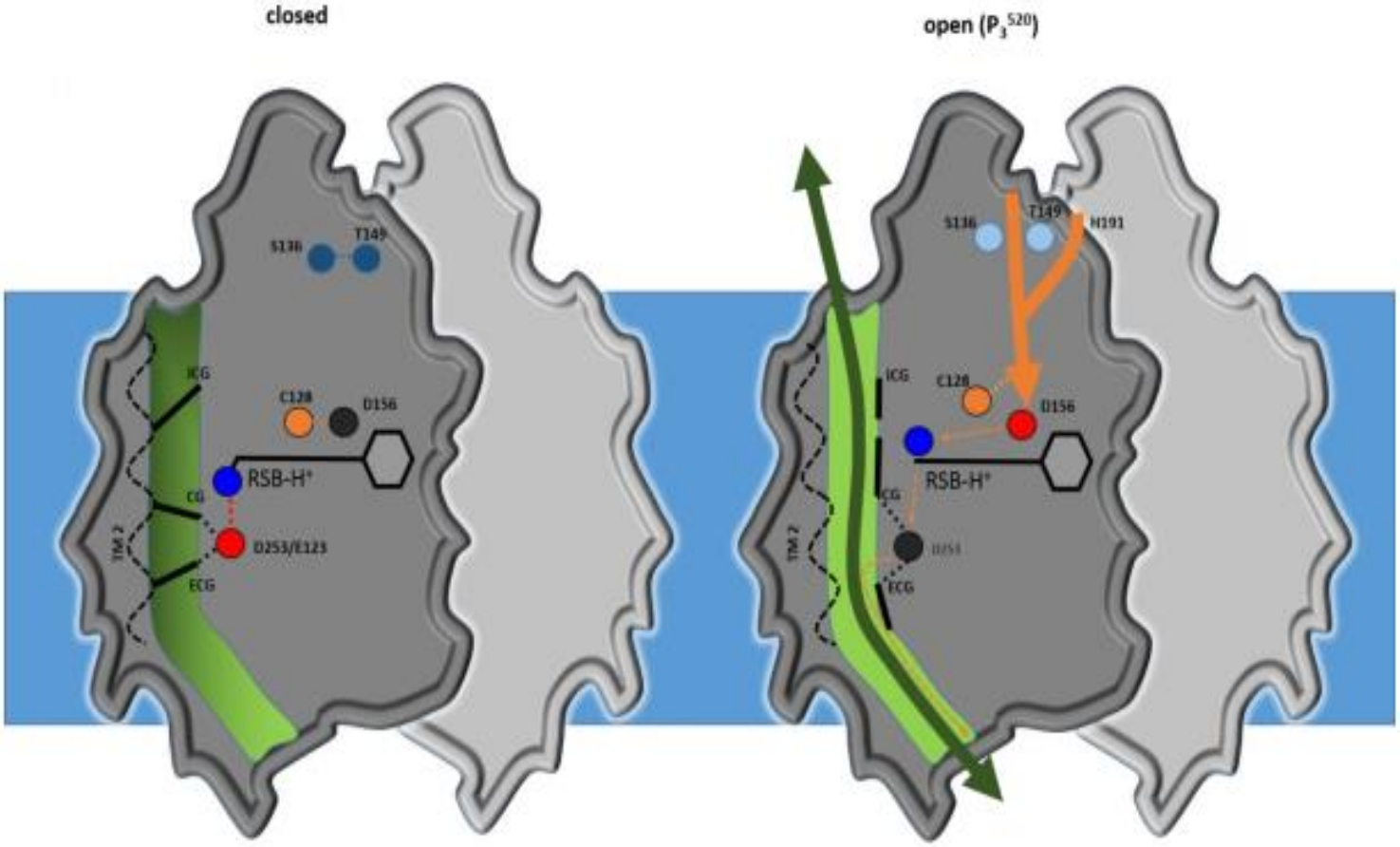

Figure 2.2 Structure and gating mechanism of ChR2.

In the dark state, the complexed hydrogen-bonding network connected gates and cavities that form channel closing state. After photon absorption, the retinal isomerization destroys the existing hydrogen-bonding network and causes rearrangement of interaction network formed by key residues and water molecules which, in turn, triggers a synchronized opening of two gates. These steps create $P3^{520}$ intermediate state which represents the conducting state, Picture were taken from Oleksandr Volkov,2017.

and D156 and interacts directly with the retinal Schiff base[48, 49]. Towards the cytoplasmic side, intracellular gate ICG separates two intracellular cavity IC1 and IC2. Moving to the extracellular side, the CG connects first to extracellular cavity EC1, followed by the extracellular gate ECG and extracellular cavity EC1.

Like many other microbial rhodopsins, ChR2 initiates retinal isomerization by photon absorption [50]. The photocycle of ChR2 is defined by five spectrally distinct intermediates state. In the dark-adapted state, the closing state of ChR2 is stabilized by chromophore which adopts all-trans transformation. After light-absorbing, retinal isomerization from the all-trans to 13-cis (P^{500}) state converts quickly to a hot (K-like) intermediate that relaxes to the P^{500} state. Then, deprotonation of the Schiff base by D253 which leads to disrupt the H-bonds and causes the M-like pre-open channel state P^{390}. A water influx partially hydrates the helices. Water penetration leads to the complete opening of the channel. This transition is followed by the re-protonation of the Schiff base by D156 and the formation of the P^{520} conducting state. The channel closes within several milli-second, but P^{520} can decay

to either the closed D^{470} state or to a P^{480} inactive state that desensitizes the protein[2, 48, 50].

The structural feature of its retinal binding, photocycle and cation conductance pathway provides insight into the molecular basis for designing powerful ChRs variants.

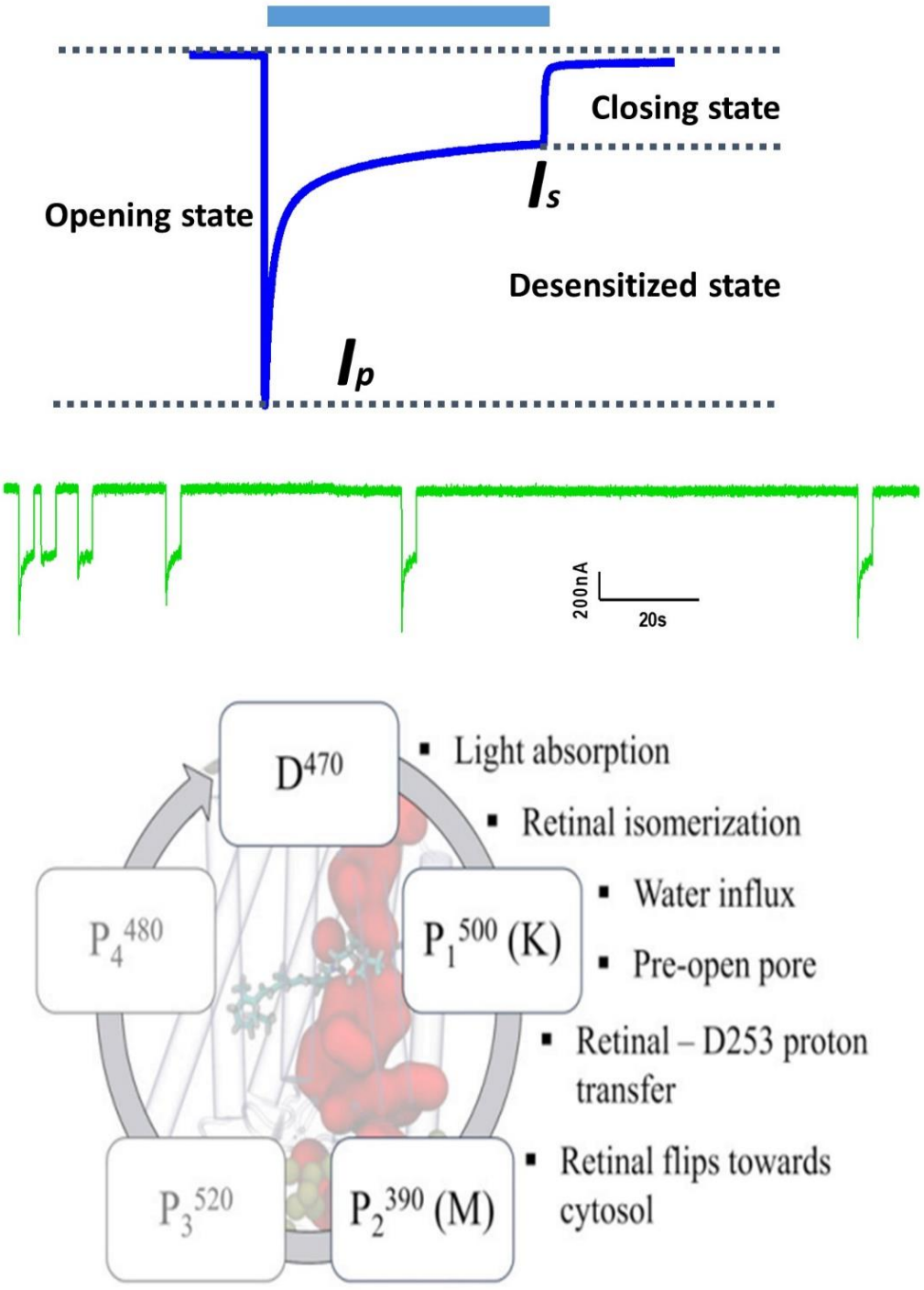

Figure 2.3 ChR2 photocurrent and photocycle.

Illustration of ChR2 photocurrent (up), The representative photocurrent trace of wild type ChR2 under short light pulse with a different dark period (middle), schematic depiction of ChR2 photocycle(down), the picture was taken from Albert Ardevol[48].

2.2.6.2 ChRs membrane trafficking

Plasma membrane: It has been known that plasma membrane expression level for many opsin genes was heavily impaired at early endoplasmic reticulum trafficking step, leading to intracellular accumulation[51]. Several molecular strategies, such as fusion of the ER export and Golgi trafficking signal to the C terminal of opsin genes have been applied to generate channelrhodopsin with high plasma membrane targeting[51-53], we still lacking a universal trafficking module for improving cellular surface targeting for multiple opsin proteins.

Mitochondria: Currently, several approaches have been applied to localized sensors in mitochondria matrix or inner membrane by addition of N terminal targeting sequence of cytochrome c oxidase subunit IV or VIII (Cox-8), allowing monitors mitochondrial metabolic and signaling activity [54]. Similar approaches have also been used to achieve mitochondrial-targeting bacteriorhodopsin in yeast by the N-terminal addition of the signal sequence from COX IV. Recently, a study described an optometabolic strategy that allows highly specific, light-dependent regulation of membrane potential across the IMM by targeting engineered mitoChR variants which provided additional

strategies to manipulate proton-driving force or potential over the inner membrane in mitochondrial[55].

Endoplasmic reticulum: Endoplasmic reticulum is the largest calcium store in the cell, playing a vital role in regulating intracellular calcium homeostasis. Recently, Toshifumi Asano and Hiroyuki Igarashi engineered an ER/SR localized chimeric channelrhodopsin ChRGR, with a sequence of the 3rd-4th transmembrane helices of mouse ryanodine receptor 2 at its C-terminal[56]. This first demonstration that successfully achieved the expression of optogenetic tools in the ER/SR membrane. Further improvement in calcium permeability and ER membrane targeting efficiency of optogenetic tools will provide neuroscientists a better way to control neural calcium dynamics in vivo.

Lysosome and vesicle: The acidification of synaptic vesicles is the power source of the electrochemical driving force for neurotransmitter accumulation. However, subcellular optogenetic approaches to manipulate proton accumulation of these acidic subcellular compartments are still poorly established. Benjamin R Rost generated novel optogenetic tools that can be used to acidify synaptic vesicle and lysosome by light[57]. They incorporated a light-gated proton pump between the third and fourth helix of a vesicular synaptophsin, together with a pH sensor and fluorescence protein at the luminal and cytosolic side, respectively. They demonstrated that the construct termed pHoenix was able to target to the presynaptic terminal and rapidly acidified synaptic vesicles. Furthermore, based on the design of pHoenix, they also try to target this pump to the lysosome by insertion

of this protein between helix one and two of tetraspanin CD63. However, the same strategies cannot be successfully applied to channelrhodopsin.

Endosome: Neurotransmitter and AMPA receptor endocytosis mediated synaptic transmission has been confirmed as a cellular substrate for learning and memory. Wataru Kakegawa developed a new optogenetic tool, PhotonSABER (photon-sensitive ASR-based endocytosis regulator) by fusing the C-terminal cytoplasmic region of the chloride channel protein 5 and the FLAG tag to the proton pump *Anabaena* sensory rhodopsin variant ASR^{D217E}, which can regulate early endosomal pH by light temporally and reversibly [58]. They demonstrated that PhotonSABER inhibited AMPA receptor endocytosis during long term depression and motor learning in vivo.

2.2.6.3 Novel ChRs variants

Channelrhodopsin was first discovered and characterized from *C. reinhardtii*[59]. After showing the light-switched large passive cation conductance in HEK293 and BHK cells by Nagel et al., the ChR2 was immediately applied in neuroscience by several independent groups for studies in the hippocampal neuron, *Caenorhabditis elegans*, inner retinal neurons and PC12 cells[8, 43, 44, 47]. ChRs has six key properties including expression and photocurrent, light-sensitivity and kinetics, ion selectivity and action spectrum.

ChRs variants can be divided into three groups: wild type ChRs, chimeric ChRs and mutated ChRs[60]. H134R was the first and most

common used ChR2 gain-of-function mutant which showed enhanced plasma membrane expression and larger stationary photocurrents in comparison to ChR2 wild type. Here, we summarize the latest and the most useful ChRs variants in **table2.1**.

Opsins	Distinguishing characters	Ref
*Ps*CatCh	high conductance, high Na^+ and Ca^{2+}selectivity	This study
CheRiff	high light sensitivity, large photocurrent	[61]
ChRger1/2/3	high light sensitivity, large photocurrent	[62]
ChromeT/Q	low proton and calcium permeability	[63]
ChR2-XXM	high light sensitivity, large photocurrent	[64]
ChR2-XXL	large photocurrent, very slow kinetics	[65]
ChronosME	fast kinetic, large photocurrent	[66]
bReaChES	fast closing time with relatively large photocurrent	[67]
ChrimsonSA	20nm red-shift, very fast off kinetics	[68]

Table2.1 Overview of the latest ChR variants with distinct properties for optogenetic applications.

All summarized ChR variants are published during the last five years, different color represents their different peak action spectrum.

Channelrhodopsin with large photocurrent and high light sensitivity enable either minimally invasive neural manipulation or non-invasive control neural activities when combining with upconverting nanoparticles[69]. However, current ChRs cannot match this experiment setting very well. Based on structural-based or machine-learning guided method, engineered ChRs, such as Chgers and ChR2-XXM generated larger photocurrents in comparison with ChR2(H134R) even at hundred-fold less light power density[62, 64]. Nowadays, many ChRs variants quickly came out to meet the requirements of different research areas, but simultaneously engineering multiple properties of ChRs to obtain a useful and powerful channelrhodopsin seems not easy[47].

Even though all ChRs are high selective for protons, ionic photocurrent composition differs between ChRs, ion selectivity of ChRs should be taken into consideration when choosing appropriate ChRs variants[70]. In order to study the calcium signaling, high calcium-permeable ChRs, like *Ps*ChR and CatCh^{+} Could be an ideal option[71, 72]. Intracellular acidification would occur when high proton conductance ChRs, like Chronos, CheRiff and Chrimson, were selected for neural excitation. The effects on designing a specific ion-permeable channelrhodopsin are still on the way.

Functional color tuned ChRs are highly demanded and most interesting optogenetic tools, as it can be used to combine with diverse genetical encoded sensors[73, 74]. Furthermore, integration of red-shifted ChRs (ChrimsonSA) with blue-shifted ChRs (*Ps*ChR) enable

two-color independent optogenetic manipulation. However, engineering functional ChRs with large spectrum shift is very difficult.

2.2.6.4 Unitary conductance and Ion selectivity

The single-channel conductance of ChR2 was lower than any known ion channel in a conducting state, except for the 15fs of voltage-gated proton channel[75]. Single-channel current generated by ChR2 was below the limit of electrophysiological recording. The stationary noise analysis method was adopted to evaluate this parameter. Their single-channel conductance estimated to range from 50~300fs, this parameter would be in the range of conductance of membrane transporters. Among discovered Channelrhodopsins, *Ps*ChR and *Gt*ACR1 has 3-fold and 25 times larger single-channel conductance than ChR2, respectively[76, 77]. However, this parameter is hard to measure in a precise way and can be easily influenced by electrical noise or mechanical and variability during the measurement process.

Channelrhodopsin was initially identified as a light-gated proton channel (ChR1). Subsequently, ChR2 proved to be a light-gated cation channel. The relative cation permeability for ChR2: $p(Li^+) > p(Na^+) > p(K^+) > p(Cs^+) > p(Ca^{2+}) > p(Mg^{2+})$[8]. Besides, some other uncommon organic cations like guanidinium+, methyl-ammonium, di-methyl-ammonium, and even for tetra-methyl-ammonium are also permeable but much lower compared to other ions. All published Channelrhodopsin were primarily conducting protons, comparable to that of highly selective mammalian proton channels (e.g., H+Hv1; $P_{H^+}/P_{Na^+} \geq 10^6$). The relative permeability of proton to sodium for

Channelrhodopsin like *Cr*ChR1/2, *Vc*ChR1/2, Chrimson, Chronos and CheRiff was determined to $P_{H^+}/P_{Na^+}10^6$~10^7.Channelrhodopsin like *Ps*ChR, *Mv*ChR1and *Gt*CCR2/3 has relative higher sodium conductance, as larger reversal potential shifts (60~70mV) occured when reducing 100-fold Na^+ concentration [40, 78].

Under physiological conditions, the dominant monovalent charge carriers of ChRs photocurrent are protons and sodiums. In ChR2-expressing cells, light evoke photocurrent are carried appropriately 60% by H^+ and 30% by Na^+ and the rest 10% is generated by other ions like calcium ion[79]. Under continuous light irritation, this could cause some artificial effects, mainly like intracellular acidification. Therefore, secondary side-effects like neurotransmitter release, activation of pH-sensitive channel and change in the reversal potential of the endogenous channel. Extensively modified ChR2 variants that exhibit an increase in P_{Na^+}/P_{H^+} ratio. For example, mutated H134 to arginine, serine or asparagine increased the P_{Na^+}/P_{H^+} ratio, replaced E90 by A and Q decreased proton selectivity compared to wild type ChR2[49]. In our previous study, we found that mutated the aspartate in TM4 to histidine significantly elevated the P_{Na^+}/P_{H^+} ratio 3-fold for ChR2 and 5 times larger for *Ps*ChR. In contrast, ChrimsonR showed more than 20 times larger P_{Na^+}/P_{H^+} ratio than the wild type, however, reduction of proton selectivity came along with decreases photocurrent amplitude and altered their kinetics[80].

Divalent ion permeability was relatively lower than monovalent ion, but ChR2 was still permeable for some divalent ions like calcium or barium. The most famous ChR2 variants with increased calcium

conductance termed CatCh (ChR2 ^{L132C}) which exhibits higher calcium selectivity by a factor of 1.6 compared to wild type ChR2[81]. Furthermore, by the combination of CatCh with another mutation ChR2 $^{T159C/S}$ give rise to CatCh^{+}, a slightly improve calcium permeability in comparison with CatCh[72]. In contrast, the novel ChR2-XXM and *Ps*ChR-D193H generated more than two times larger calcium current than CatCh, indicating larger calcium conductance than previous ChR variants. However, the mechanism of elevated calcium selectivity is still elusive and attempts to get ChRs with a high calcium conductance and large photocurrent is always welcome.

2.2 Research objective

Combining opsin-based optogenetics with optical strategies has been widely used in exploring the mechanism underlying neural circuits[82, 83]. Despite extensive characterization and modification of channelrhodopsin, current tools still cannot satisfy multiple needs for neuroscience research. So far, refining performances of channelrhodopsin was still a high value work. Engineering optogenetic tools with improved properties should consider six key parameters, including plasma membrane targeting efficacy, photocurrent amplitude, light sensitivity, kinetics, ion selectivity and actional spectra.

Poor plasma membrane localization was often a problem for heterologous expression of opsin proteins. Here, we found a universal plasma membrane targeting signal peptide that could enhance plasma membrane expression levels of multiple channelrhodopsins and light-driven ion pumps.

Light-induced unphysiological effects from in *vivo* application was another problem[84]. Channelrhodopsin with high calcium-selectivity would be useful for studying calcium signaling in a temporal precision way. Channelrhodopsins with less proton conductance can overcome side-effects, like intracellular acidification and extracellular alkalization. However, efforts on modifying ChRs ion selectivity while simultaneously maintaining the fast kinetics and the large photocurrent are difficult. In our research work, we engineered diverse ultra-fast or

slow channelrhodopsin variants with less proton, high calcium and sodium permeability as well as large photocurrent amplitude.

Result

3.1 Part I

3.1.1 LR signal peptide boost channelrhodopsin performance

Previous studies have demonstrated that the Leucine-rich repeat 17-amino acid signal peptide could enhance surface expression for some GPCRs in cell culture[86]. To test whether LR could be used as an effective plasma membrane-trafficking peptide to improve the photocurrent of microbial rhodopsin[51]. First, I integrated LR with excitatory optogenetic tools such as CeChR wild type, ChR2 (H134Q/D156H) double mutation, *Ps*ChR (H117Q/D139H) double mutation and Chrimson wild type **(figure3.1a)**. Interestingly, all the LR fused Channelrhodopsins generated three to four-fold larger photocurrents as well as significant increased its expression level compared to channelrhodopsins without LR fusion **(figure3.1b)**. Thus, I termed these improved tools as *Ce*ChR 2.0, ChR2(HQ/DH)2.0, *Ps*ChR (HQ/DH) 2.0 and Chrimson2.0.

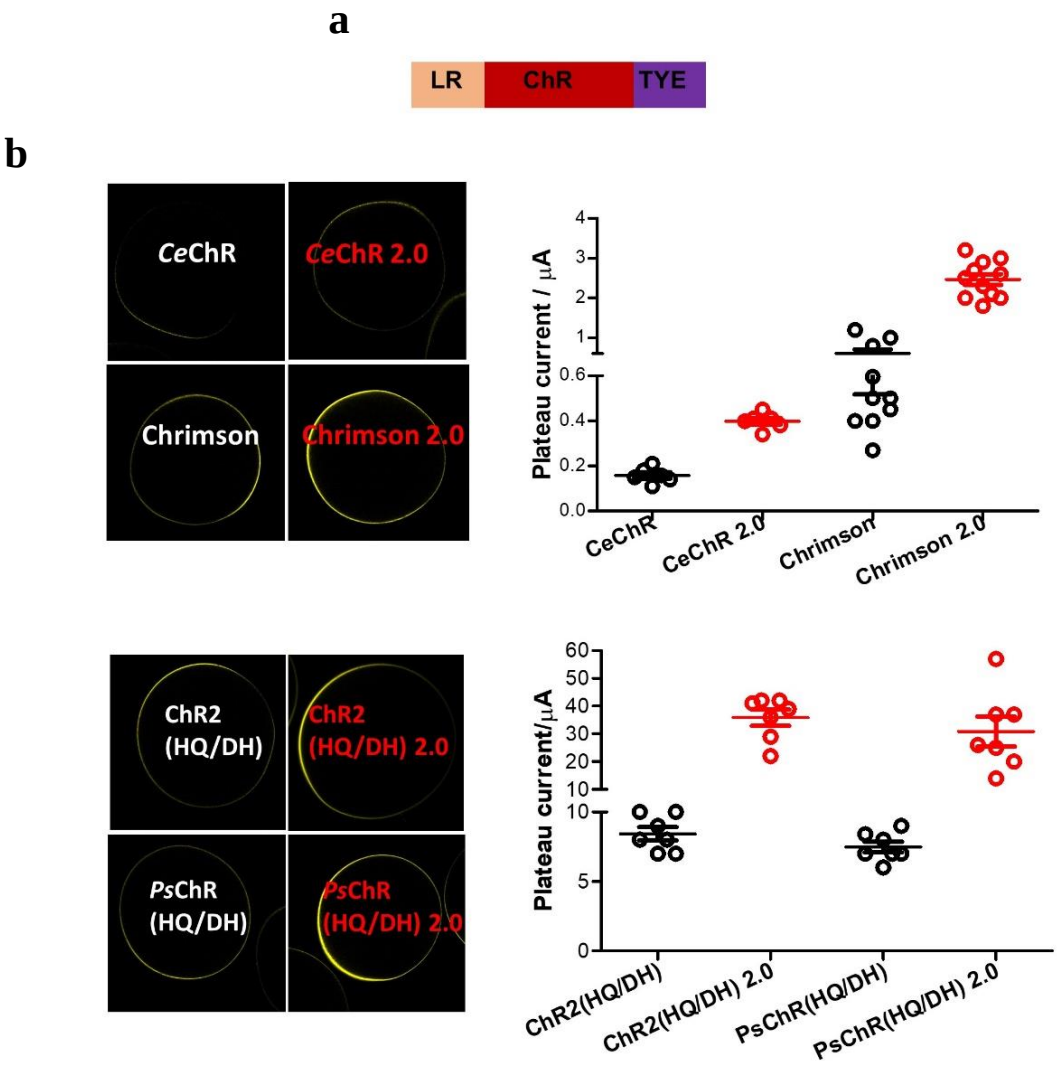

Figure 3.1 LR signal peptide improves ChR plasma membrane trafficking and photocurrent amplitude.

(a) Schematic of microbial opsins chimera. pink box, LR signaling peptide; red box, microbial opsin gens; purple box, TYE motif**:** trafficking signal(T), enhanced yellow fluorescence protein(Y) and endoplasmic reticulum exports signal(E). **(b)** Left side, the fluorescence images of corresponding channelrhodopsin: *Ce*ChR wild type, ChR2 (HQ/DH), *Ps*ChR (HQ/DH) and Chrimson wild type, as well as improved version: *Ce*ChR 2.0, ChR2 (HQ/DH) 2.0, *Ps*ChR (HQ/DH) 2.0 and Chrimson 2.0. All of them were fused with LR at its N terminal and TYE motif at its C terminal. right side, comparison of stationary photocurrent among these

ChRs. 20 ng cRNA of these constructs were injected into Oocytes for two days expression, Bath solution: 110mM NaCl,5mM KCl,2mM $BaCl_2$, 1mM $MgCl_2$, 5mM HEPES, pH7.6. Illumination with blue light 450nm for *Ps*ChR, 473nm for *Ce*ChR and ChR2, red light 635 nm for Chrimson at saturation light intensity under -100mV. Stationary photocurrent value was collected from at least seven Oocytes.

Second, new inhibitory tools like ACRs for neural inactivation were identified recently [37, 39]. Here I fused LR signal peptide at the N terminal of ACR1, ACR2 and *Zip*ACR generating ACR1 2.0, ACR2 2.0 and *Zip*ACR 2.0. Because ACRs showed strong expression levels and large photocurrents in Oocytes after one day cRNA injection. To avoid saturated photocurrent that may cover up the differences among these ACRs, I injected 2ng cRNA of each construct for one-day expression. Consistent with the above results, LR fused ACRs exhibited larger photocurrent amplitude by a factor of three to five **(figure3.2a and b)**. Later, I compared kinetic of photocurrent decay of ACR1 2.0, ACR2 2.0 and *Zip*ACR 2.0. as well as their light sensitivity **(figure3.3a and b)**. From this data, we can know that LR fusion does not change its kinetic and light sensitivity[42].

In conclusion, all the above data demonstrated that N terminal fusion of LR signal peptide could be an ideal and universal strategy for improving plasma membrane trafficking efficiency for multiple opsin proteins.

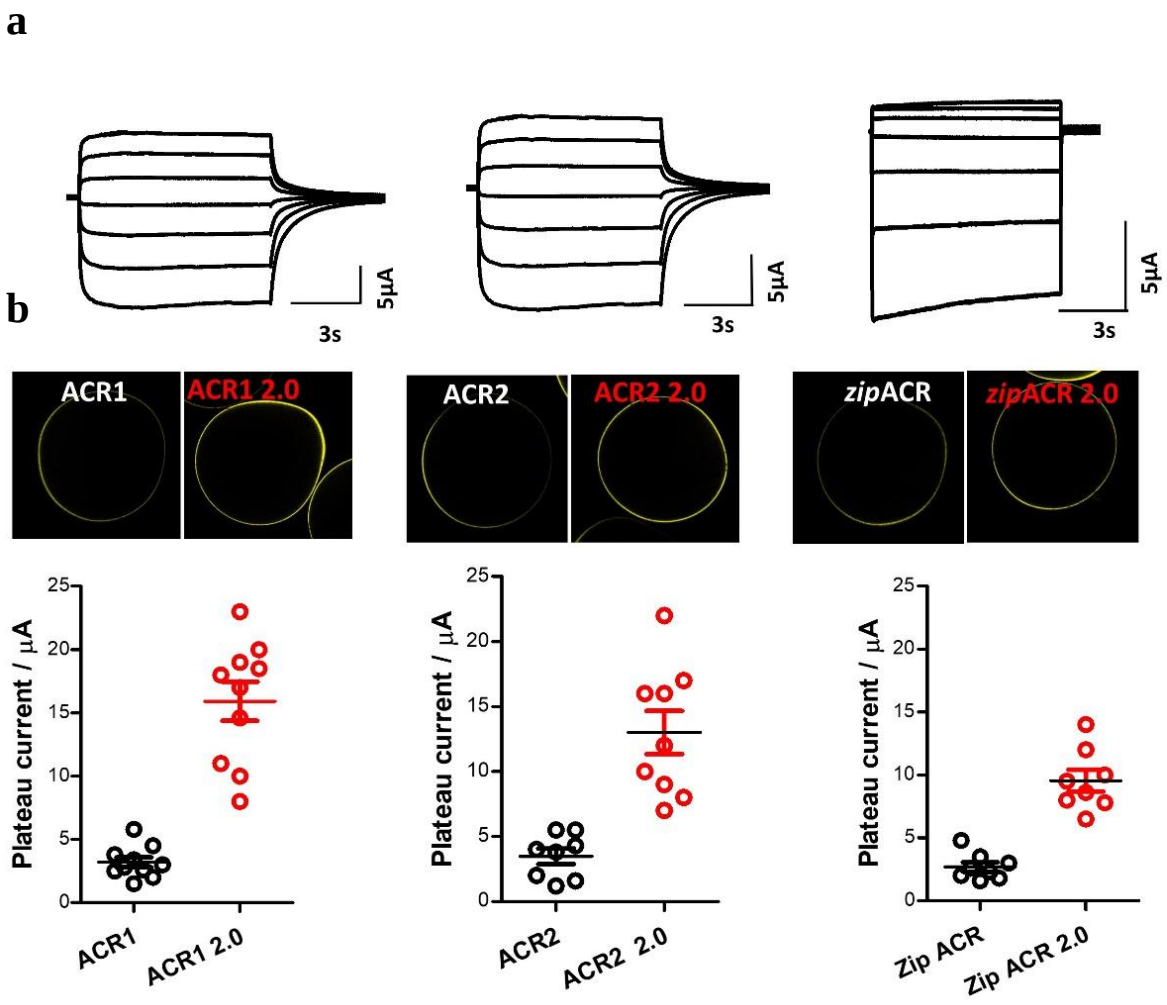

Figure 3.2 LR signal peptide enhances ACRs plasma membrane targeting and photocurrent magnitude.

(a) the upside, representative photocurrent traces of ACR1 2.0, ACR2 2.0 and *zip*ACR 2.0; the downside, the fluorescence images of corresponding channelrhodopsins. **(b)** Comparison of plateau photocurrent amplitude. two electrophysiological voltage-clamp recording from Oocytes, expressing ACR1, ACR2 and *zip* ACR, ACR1 2.0, ACR2 2.0 and *zip* ACR 2.0, in solution (110mM NaCl,5mM KCl,2mM $BaCl_2$, 1mM $MgCl_2$, 5mM HEPES, pH7.6). Illumination with blue light 473nm for ACR2, green light 532nm for ACR1 and *Zip* ACR at saturation light intensity under -100mV. Stationary photocurrent value was collected from at least seven Oocytes.

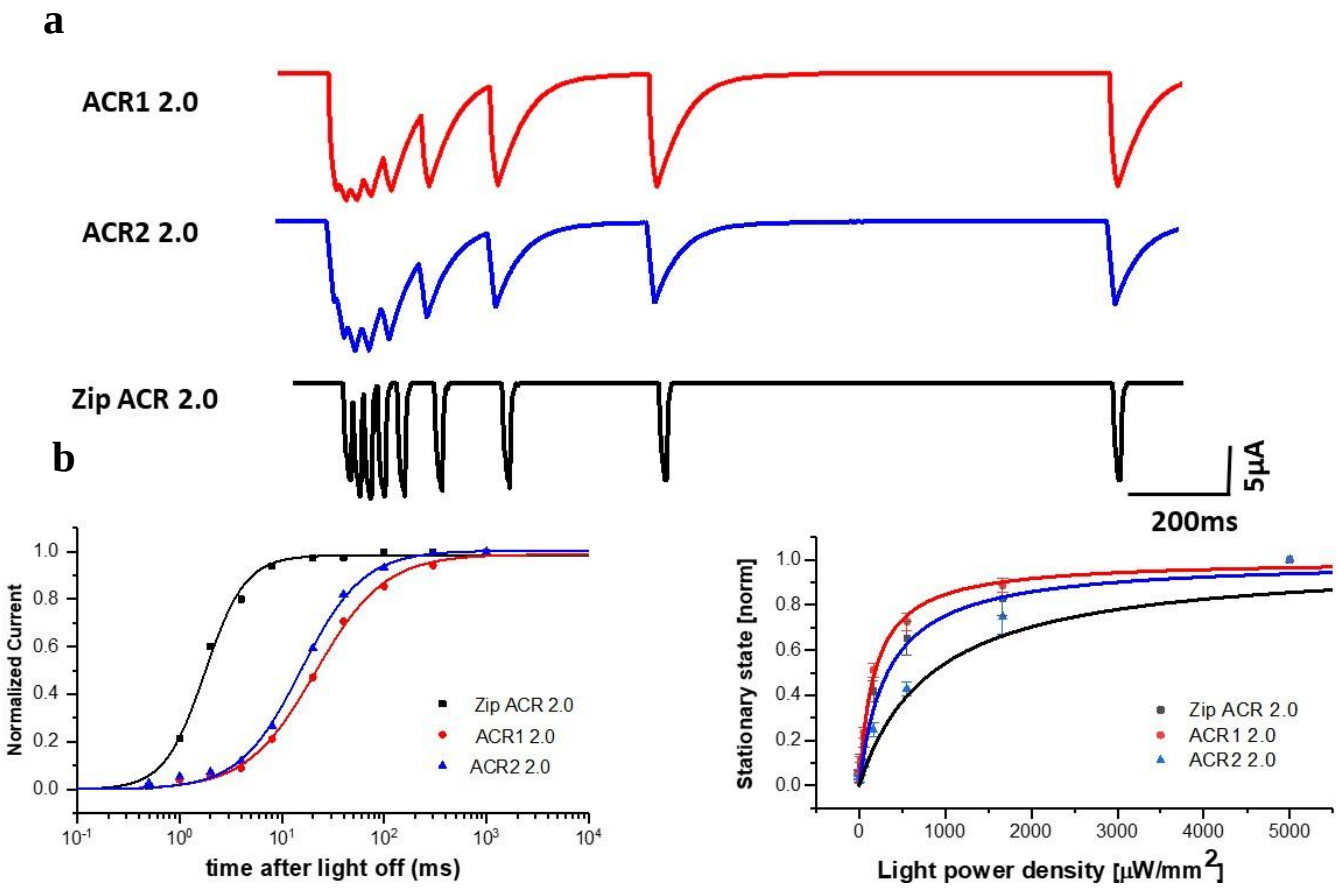

Figure 3.3 Comparison of kinetics and light sensitivity of ACR1 2.0, ACR2 2.0 and *Zip*-ACR 2.0.

(a) Representative photocurrent trace of ACR1 2.0， ACR2 2.0 and *Zip*-ACR 2.0 after 5ms 473nm light pulse during 0.5,1,2,4,8, 20, 40,100,300,1000ms darkness period. **(b)** The kinetics of the photocurrent decay after switching off the continuous light and the light sensitivity of ACR1 2.0， ACR2 2.0 and *Zip*-ACR 2.0.

3.1.2 Improving ChR2 function by N terminal modification

Giving endogenous signal peptide may suffer from poor compatibility or less tolerability with mammal's expression system [73], it is possible that replaces self-derived signal peptide of ChR2 with

mammal derived LR signal peptide may further improve the efficiency of plasma membrane targeting. Here, I truncated 11,13,15,17,19,24 N terminal amino acid from LR-fused ChR2(H134Q/D156H) variant **(figure3.4 a and c)**. As we expected that truncated 24 amino acid at N terminal (#10) dramatic decreased photocurrent, but all other ChR2 variants displayed an increase in photocurrent than that of not truncated ChR2. Among them, both 13(#3) and 17(#6) N terminal amino acid truncated ChR2 variants generated the largest photocurrent amplitude **(figure3.4 b)**. As our study indicated that a proton pump CvRh exhibited high plasma membrane targeting (data not shown), I inserted 10 or 12 amino acid from N terminal of CvRh following LR sequence for number (#3) and (#6) ChR2 variant, which give rise to number (#4), (#7) and (#8) ChR2 variants. Despite all of them do not show obvious differences in terms of the photocurrent, finally, I selected number (#7) ChR2 variant for further application as it has less effect on damaging cell conditions **(figure3.4 b)**.

In order to get high-functional channelrhodopsins with large photocurrent and high light sensitivity, I used ChR2-XXM and ChR2-XXL as a template. Based on point mutation and N terminal modification strategies, I obtained ChR2-XXM 2.0 and ChR2-XXL 2.0 **(figure3.4 d and e)**. The improved version has three differences in comparison with the original version. First, LR fusion and 11 amino acid truncations at N terminal; Second, additional H134Q mutation; Third, TYE motif fusion at C terminal. As it was shown in (**table 3.1)**.

	I_s	Inactivation (%)	Closing rate		EC50, μW/mm²
			τ fast **ms** (%‡)	τ slow **ms** (%‡)	Plateau
ChR2	**1×†**	**72±2.7**	**7.5±0.6**(>98)	**NA**	**~714**
ChR2-XXM	**34×†**	**23±0.6**	**81±13.2**(8±1.6)	1086±65(92±1.5)	~102
ChR2-XXM2.0	**150×†**	**21±1.1**	**673±49**(10±1.2)	1896±76(90±2.5)	~**90**
ChR2-XXL	**53×†**	**13±0.9**	NA	**70000±3919**(>96)	~5.4
ChR2-XXL2.0	***232×†***	***18±1.6***	**NA**	***82000±1500***(*>96*)	***~2.8***

Table 3.1 Basic properties of ChR2 variants.

†, expression or photocurrent of the corresponding wild type was normalized as 1×. Is, stationary (plateau) current. ‡, as most ChRs exhibit biphasic off-kinetics which comprised a fast and a slow component, here the % indicated the percentage of the amplitude of the fast (τ1) or slow (τ2) component to the whole photocurrent. Data are shown as mean ± SEM, n = 4-5. Values were presented as approximates.

ChR2-XXM 2.0 and ChR2-XXL 2.0 has ~150 and ~232 times larger photocurrent than wild type ChR2, respectively. The EC50 of ChR2-XXM 2.0 was ~90μW/mm^2 and ChR2-XXL 2.0 was ~2.8μW/mm^2, which was nearly 10 times and 255 times higher than wild type ChR2, respectively **(figure3.5 a and b)**. To our knowledge, ChR2-XXM 2.0 and ChR2-XXL 2.0 belong to the most powerful channelrhodopsin for low light application.

a

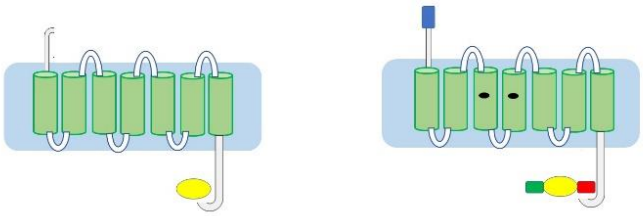

b

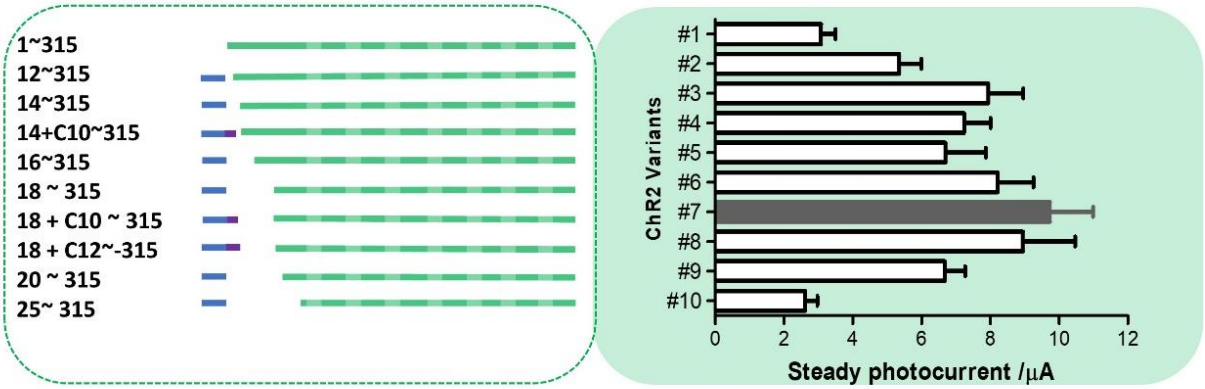

c

	MDYGGALSAVGRELLFVTNPVVVNGSVLVPEDQCYCAGWIESRGTN
#1	MRPQILLLLALLTLGLANGTEGPNFYVPFSNKTGVVRSGSMDYGGALSAVGRELLFVTNPVVVNGSVLVPEDQCYCAGWIESRGTN
# 2	MRPQILLLLALLTLGLANGTEGPNFYVPFSNKTGVVRSGS RELLFVTNPVVVNGSVLVPEDQCYCAGWIESRGTN
# 3	MRPQILLLLALLTLGLANGTEGPNFYVPFSNKTGVVRSGS LLFVTNPVVVNGSVLVPEDQCYCAGWIESRGTN
# 4	MRPQILLLLALLTLGLANGTEGPNFYVPFSNKTGVVRSGSMAVHQIGEGG LLFVTNPVVVNGSVLVPEDQCYCAGWIESRGTN
# 5	MRPQILLLLALLTLGLANGTEGPNFYVPFSNKTGVVRSGS FVTNPVVVNGSVLVPEDQCYCAGWIESRGTN
# 6	MRPQILLLLALLTLGLANGTEGPNFYVPFSNKTGVVRSGS TNPVVVNGSVLVPEDQCYCAGWIESRGTN
# 7	MRPQILLLLALLTLGLANGTEGPNFYVPFSNKTGVVRSGSMAVHQIGEGG TNPVVVNGSVLVPEDQCYCAGWIESRGTN
# 8	MRPQILLLLALLTLGLANGTEGPNFYVPFSNKTGVVRSGSMAVHQIGEGGLV TNPVVVNGSVLVPEDQCYCAGWIESRGTN
# 9	MRPQILLLLALLTLGLANGTEGPNFYVPFSNKTGVVRSGS PVVVNGSVLVPEDQCYCAGWIESRGTN
# 10	MRPQILLLLALLTLGLANGTEGPNFYVPFSNKTGVVRSGS GSVLVPEDQCYCAGWIESRGTN

d

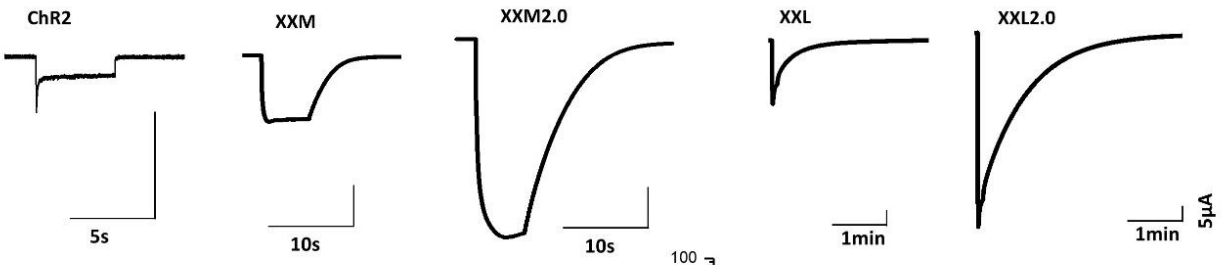

e

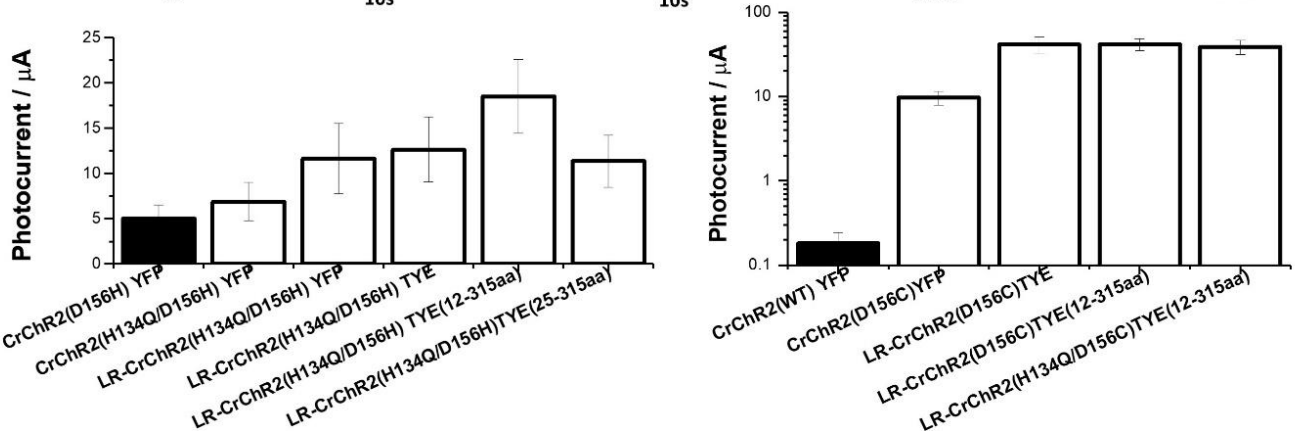

Figure3.4 Improving ChR2 variants by N terminal modification.

(a) schematic comparison of wild type ChR2 with modified ChR2. **(b)** left side: Schematic of plasma membrane targeting, and trafficking sequence used to generate enhanced ChR2s; right side: stationary photocurrent of truncated ChR2 variants. **(c)** The sequence of N terminal modification of ChR2 variants. orange, LR signal peptide; blue, linker; back, N terminal from ChR2; red, the first amino acid of the first transmembrane helix from ChR2. **(d)** typical photocurrent traces of ChR2-XXM, ChR2-XXL, ChR2-XXM 2.0 and ChR2-XXL 2.0. **(e)** comparison of photocurrent among several modified ChR2-XXM and ChR2-XXL variants. I injected 10ng cRNA of each construct in Oocytes and kept in 16 ℃ incubator for two days expression. Bath solution (110mM NaCl,5mM KCl,2mM $BaCl_2$, 1mM $MgCl_2$, 5mM HEPES, pH7.6). Illumination with blue light 473nm for ChR2 variants at saturation light intensity under -60mV. The stationary photocurrent value was collected from at least seven Oocytes.

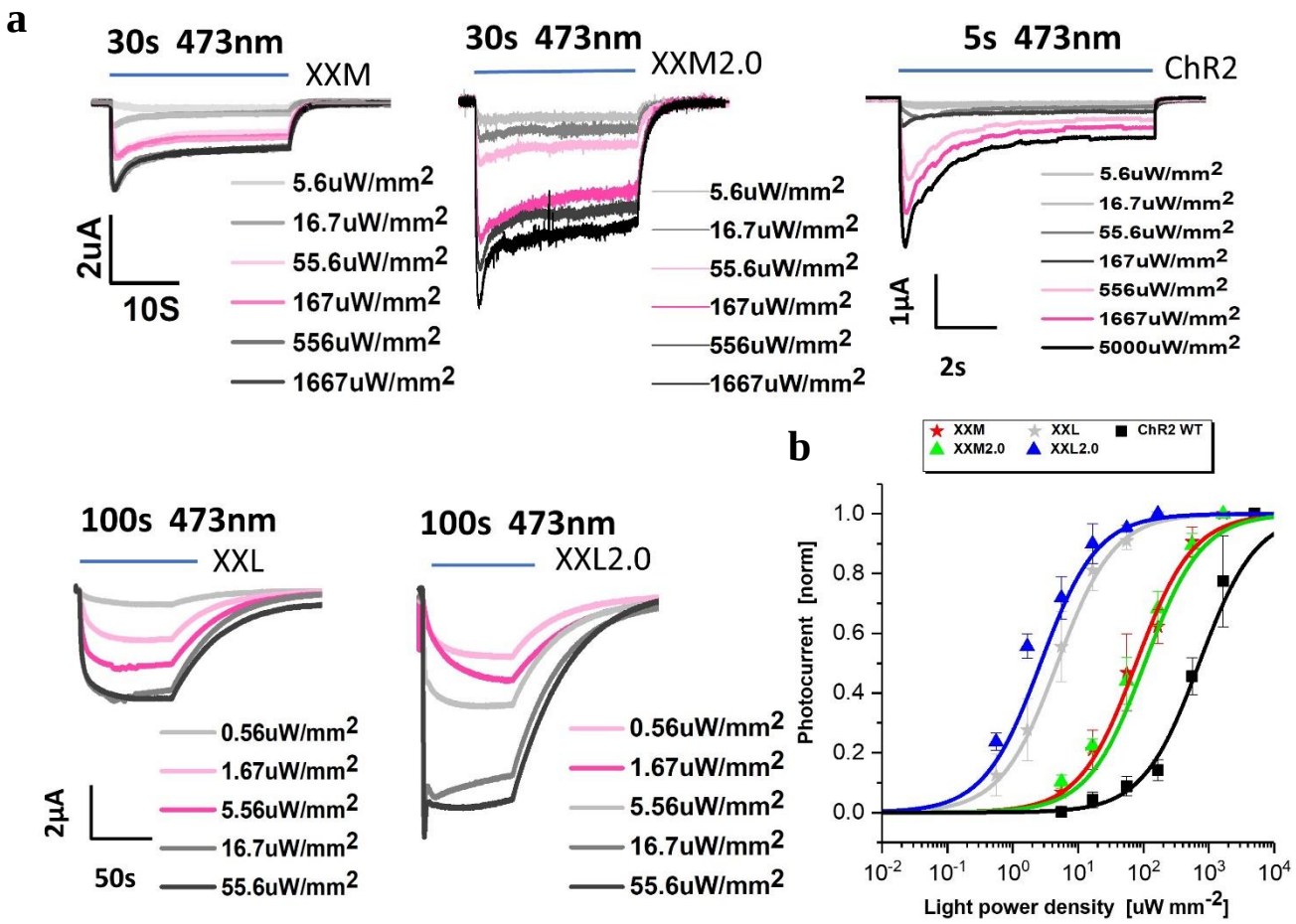

Figure3.5 Comparing the light sensitivities of ChR2 variants.

(a) represent photocurrent traces of ChR2 variants under different light illumination conditions. **(b)** 5 s, 30 s and 100 s continuous 473 nm blue light illumination Were applied to ChR2, XXM/XXM 2.0 and XXL/XXL 2.0, respectively. Photocurrent at a maximum light power density of each oocyte was normalized as 1.20 ng cRNA of above constructs were injected into *Xenopus* oocyte. Measurements were performed 2 days after injection. All measurements were done in standard solution with $BaCl_2$ (110 mM NaCl, 5 mM KCl, 2 mM $BaCl_2$, 1 mM $MgCl_2$, 5 mM HEPES and pH 7.6). Photocurrents of XXM/XXM 2.0 and XXL/XXL 2.0 were measured at -60 mV because of the larger current and slow kinetics; other constructs were measured at -100 mV. Data points were presented as mean ± SD, n = 3 - 4. Curves were fitted with the Hill equation.

3.1.3 Characterization of ion permeability of ChR2 variants

Influencing kinetics by mutating ChR2 position C128 and D156 were reported quite intensively[65, 87, 88]. But no attention was paid to the potential influence of ion selectivity. To investigate this, I measured the photocurrent at different potentials and calculated the reversal potentials shift of these mutants when systematically changing bath solutions with different pH and Na^+ or K^+ concentrations. I estimated channelrhodopsin ion permeabilities using the Goldman-Hodgkin-Katz (GHK) equation.

ChR2 is a non-selective cation channel which is mostly permeable to H^+. Both changing of outside pH from 7.6 to 9.6 and changing outside Na^+ concentration from 120 mM to 1 mM altered ChR2 reverse potential. As it is shown in **(table 3.2)**, the ChR2 permeability ratio of Na^+ to H^+ (P_{Na+}/P_{H+}) or K^+ to H^+ (P_{K+}/P_{H+}) was determined as P_{Na+}/P_{H+} = ~ 3.1×10^{-7} and P_{Na+}/P_{H+} = ~ 2.7×10^{-7},which was consistent with previous study. Interestingly, ChR2(D156H) (XXM) showed increase in sodium selectivity compared to wild type ChR2, as obvious reversal potential shift was detected when changing sodium concentrations (wild type ChR2=*23.5±1.29*mV, ChR2(D156H) =*48.7±2* mV) **(figure 3.6b)**. Reversal potential shift of ChR2 (H134Q/D156H) (ChR2(134Q/D156H) =*58.3±1.5* mV) was larger than ChR2(D156H), indicating further increase sodium permeability. Additional N terminal modification of ChR2(134Q/D156H) seems no change in sodium and proton conductance (ChR2(134Q/D156H) P_{Na+}/P_{H+} = ~ 20×10^{-7}, ChR2-XXM2.0 P_{Na+}/P_{H+} = ~ 20×10^{-7}). In contrast, the ChR2(D156C) (XXL)

changes P_{Na+}/P_{H+} only slightly. And both ChR2 (H134Q/D156C) as well as ChR2-XXL2.0 has identical ion selectivity with wild type ChR2 in terms of proton and sodium ions.

Principally, ideal optogenetic tool for depolarization should be more Na^+ conductive and less K^+ conductive, because K^+ efflux across the plasma membrane would lead to disturbing extracellular potassium ion concentration. To test the potential influence on K^+ permeabilities of different ChRs mutations, I measured and calculated the reversal potentials shift of these mutants when systematically changing bath solutions from 120 mM K^+ to 1 mM K^+ in comparison to changing pH from 7.6 to 9.6. ChR2 has slightly low K^+ conductance in comparison to Na^+, with a P_{Na+}/P_{K+} = ~ 1.2. Interestingly, I found that Chronos shows very low potassium permeability, with a P_{Na+}/P_{K+} = ~7.1 (data not shown here), indicating a relatively low potassium conductance ChR. XXM showed higher Na^+ permeability than K^+, as the P_{Na+}/P_{K+} of XXM and XXM2.0 reached ~ 2.2 and ~ 2.2, respectively **(figure 3.6a)**. XXL and XXL2.0 increased the Na^+ and K^+ permeability slightly and equally **(table 3.2)**.

	Reversal potential shift(mV)				**Ratio of Permeability**		
	V_r shift Na^+	**V_r shift H^+†**	**V_r shift K^+**	**V_r shift H^+‡**	**Na^+/H^+**	**K^+/H^+**	**Na^+/K^+**
ChR2	***23.5±1.29***	***20±1.83***	***20.5±1.29***	***21.8±2.75***	***~3.1×10^{-7}***	***~2.5×10^{-7}***	***~1.2***
ChR2-XXM	***48.7±2***	***8±1***	***31.7±1.53***	***10.3±1.52***	***~12×10^{-7}***	***~5.1×10^{-7}***	***~2.2***
ChR2-XXM2.0	***59±2.58***	***3±1.4***	***40.4±7.63***	***8.2±2.77***	***~20×10^{-7}***	***~8.1×10^{-7}***	***~2.5***
ChR2-XXL	***29.6±4.56***	***10.4±1.82***	***26.8±1.94***	***10.3±1.03***	***~4.5×10^{-7}***	***~3.8×10^{-7}***	***~1.2***
ChR2-XXL2.0	***38.2±5.07***	***7.4±1.34***	***29.6±3.78***	***7.8±0.84***	***~7.2×10^{-7}***	***~4.5×10^{-7}***	***~1.7***

Table3.2 Ion selectivity of ChR2 variants.

Reversal potentials and permeability ratio were determined from stationary currents in the indicated solution. Values represent mean ± SD, *n* = 4–6. Values without SD are presented as approximates. †, with the existence of 120 mM Na+. ‡, with the existence of 120 mM K+.

a

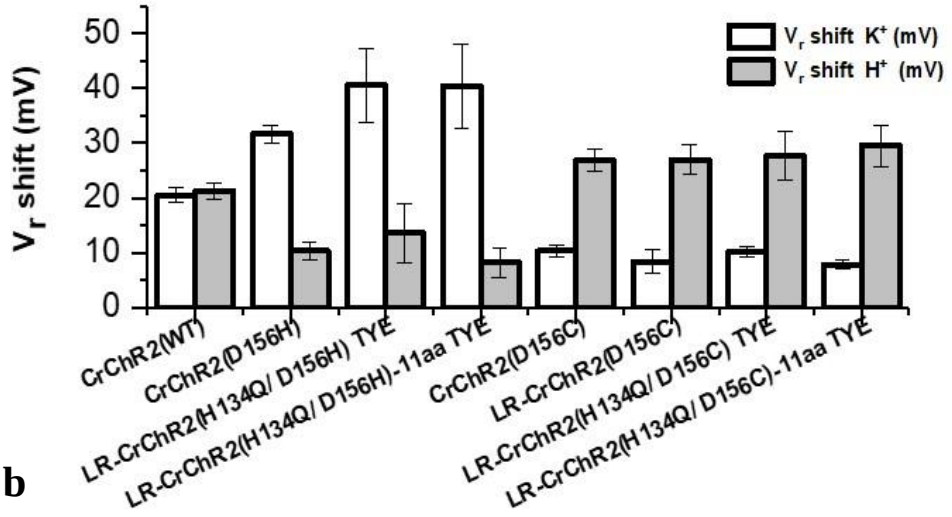

b

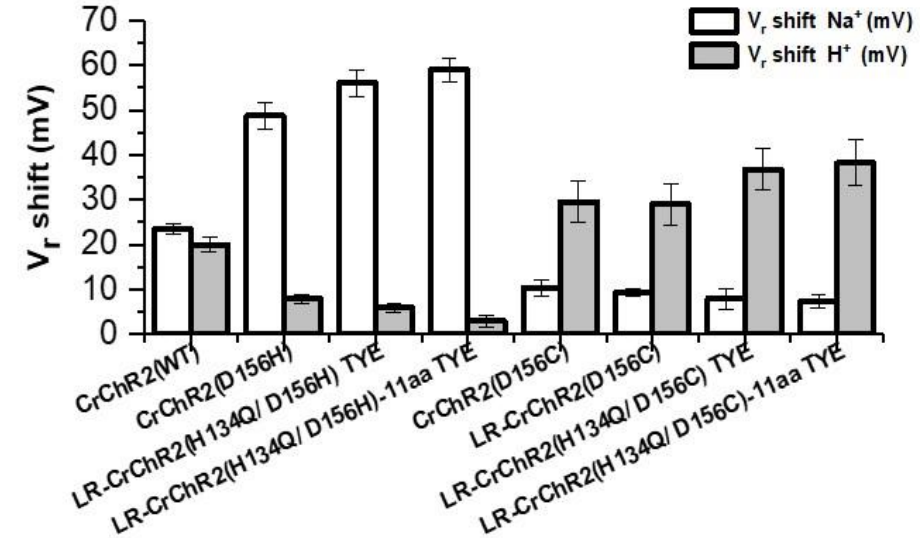

Figure3.6 Comparison of sodium and potassium permeabilities of ChR2 and its variants.

Reversal potentials were determined after photocurrent measurements from -90 mV to +10 mV. Reversal potential shift for Na^+**(b)**, K^+ **(a)** was calculated by the reversal potential differences in two different solutions containing 120 mM NaCl/KCl pH 7.6 and 1 mM NaCl/KCl pH 7.6. Reversal potential shift for H^+ was determined by the reversal potential differences in two different solutions of pH 7.6 and 9.6 containing 120m NaCl/ KCl. Data points were presented as mean ± SD, n = 4-6.

In order to further compare the Ca^{2+} permeability of selected mutants like ChR2, CatCh, ChR2-XXM and ChR2-XXM 2.0, a final concentration of 10 mM BAPTA was injected to the oocyte to block the Ca^{2+} induced chloride current. Then photocurrent was measured in a bath solution containing 80 mM $CaCl_2$ with pH 9.0 at -100 mV, which was the condition that the inward current was only from the Ca^{2+} influx. ChR2 showed robust photocurrent with 80 mM $CaCl_2$ at pH 9.0, then dramatically reduced after injection of 10 mM BAPTA. Consistent with previous study, wild type ChR2 showed small Ca^{2+} current (0.46 $\pm$ 0.1μA). CatCh has much increased Ca^{2+} current (2.2 $\pm$ 0.3μA) than ChR2 which was identical to the previous report. Interestingly, ChR2-XXM (4.9 $\pm$ 0.6μA) and ChR2-XXM 2.0 (10.2 $\pm$ 1.1μA) showed further increase Ca^{2+} current than CatCh, indicating a high calcium conductance.

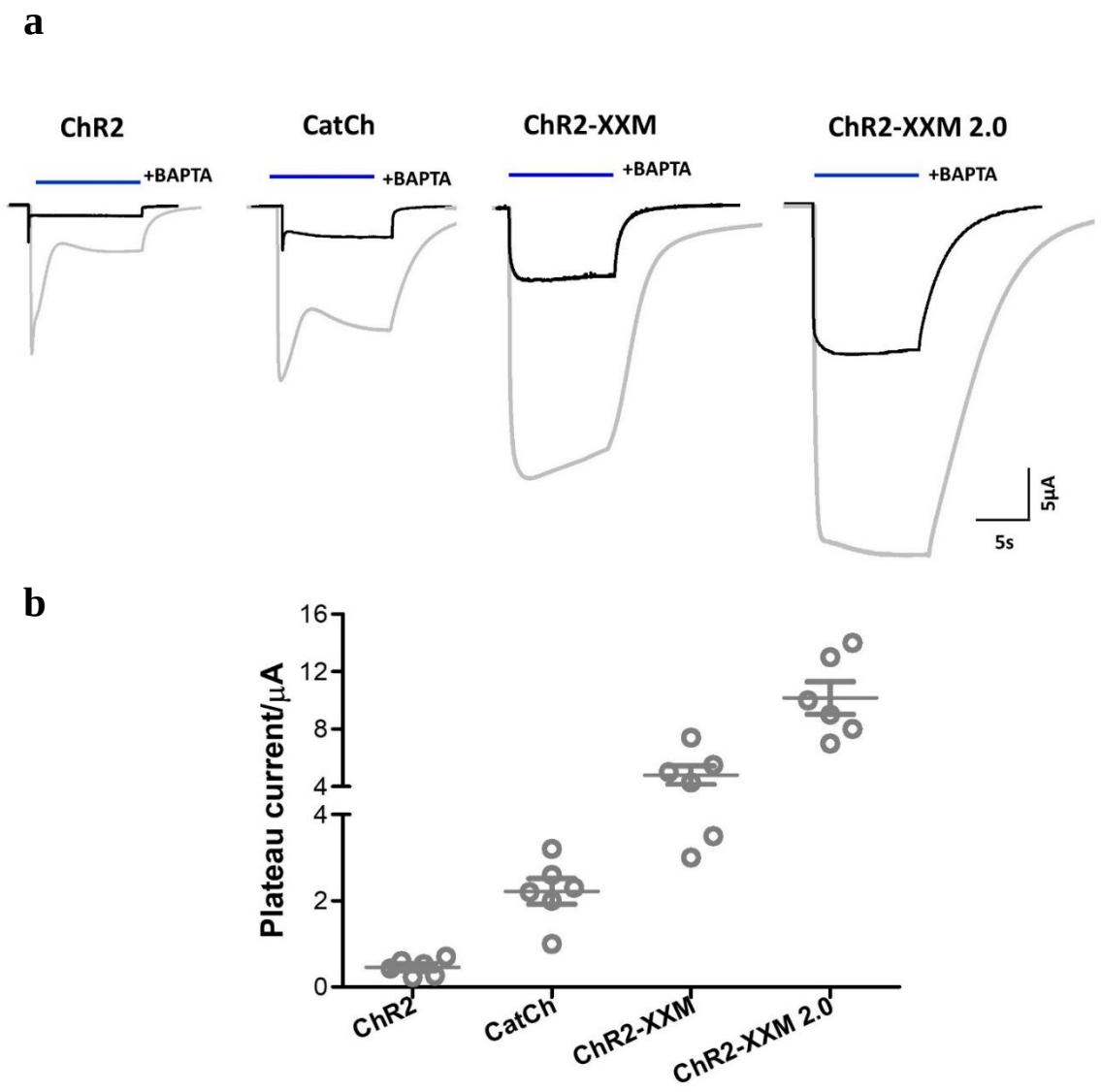

Figure 3.7 Calcium permeabilities of selected channelrhodopsin variants.

(a) Photocurrent traces of different channelrhodopsin before (black) and after (grey) BAPTA injection. Measurements were done in 80 mM $CaCl_2$, pH 9.0 at -100mV, 2 days after 20 ng cRNA injection. Blue bars indicate light illumination, 473 nm, 5 mW/mm^2 **(b)** Comparison of calcium permeability of ChR2, CatCh, ChR2-XXM and ChR2-XXM 2.0. All data points were plotted in the figure and mean ± SEM was indicated.

3.2 Part II

3.2.1 *Ps*ChR variants

As *Ps*ChR from *Marine Alga Platymonas subcordiformis* exhibited high sodium selectivity and large single-channel conductance compared with other ChRs [71], I used *Ps*ChR as a template to design high-functional channelrhodopsin. I generated a number of *Ps*ChR variants. To compare the functionality of these *Ps*ChR mutations, TEVC technique was used to test its photocurrent amplitude. As it shown in (***figure 3.8*a and b)**.

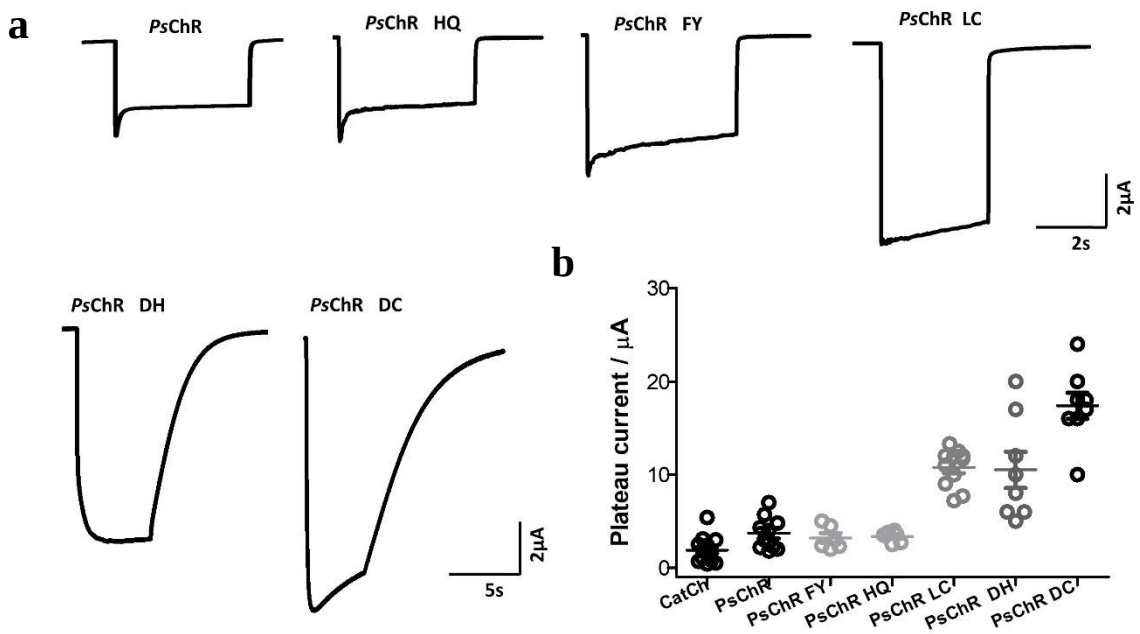

Figure 3.8 Generation of *Ps*ChR variants.

(a) representative photocurrent traces of different *Ps*ChR variants. Measured condition: 450nm light irradiation 5mW/mm^2 , -60mV, bath solution: ORI solution containing 2mm $BaCl_2$. **(b)** photocurrent comparison of different *Ps*ChR variations.

I found that *Ps*ChR L117C, *Ps*ChR D139H and *Ps*ChR D139C showed a significant increase in photocurrent amplitude compared to wild type *Ps*ChR **(figure 3.8a and b)**, while *Ps*ChR H134Q and *Ps*ChR F202Y have small and similar photocurrent. Because *Ps*ChR L117C was homolog to CatCh (CrChR2 L132C), I named this novel *Ps*ChR mutation: *Ps*CatCh. Imaging data showed strong retinal-dependent expression for both CatCh and *Ps*CatCh **(figure 3.9a)**. Interestingly, despite *Ps*CatCh showed relative weak fluorescence level, it generated three times larger photocurrent than CatCh. Furthermore, *Ps*CatCh exhibited 2-fold faster off closing time than CatCh **(figure 3.9b)**. Thus, *Ps*CatCh with large photocurrent and fast kinetics could be a useful depolarizing tool for neural excitation.

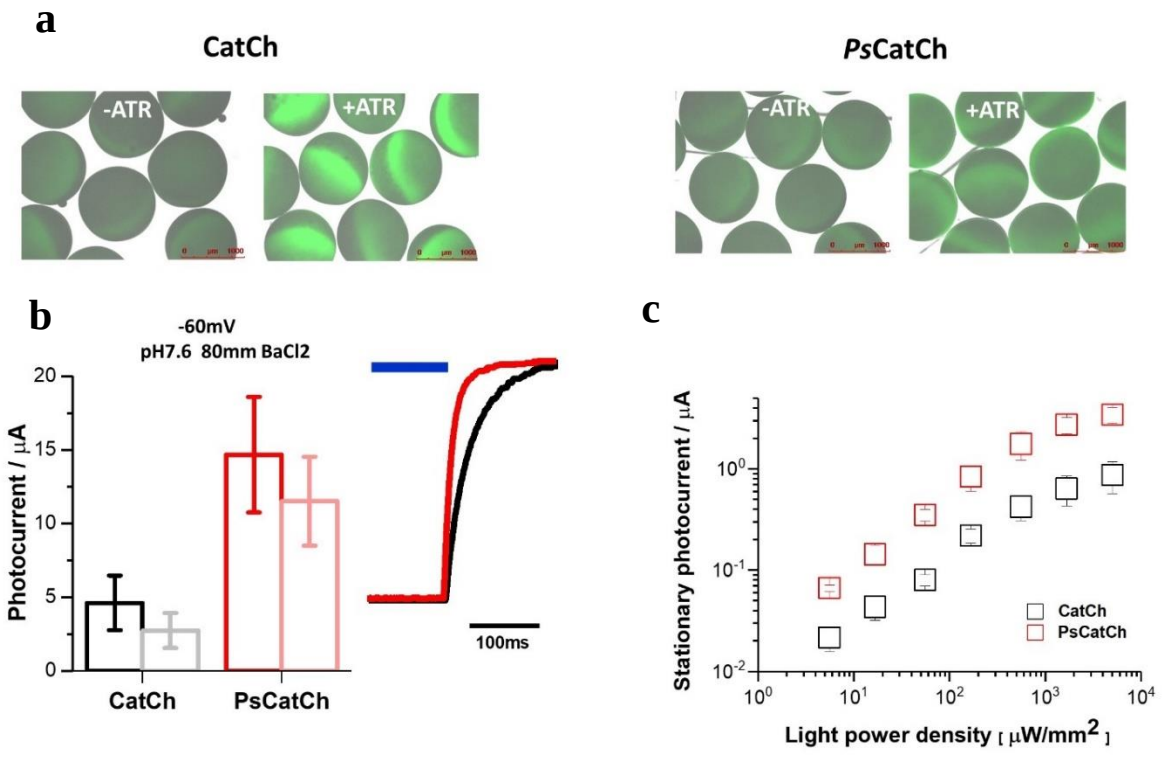

Figure 3.9 Characterization of CatCh and *Ps*CatCh.

(a) representative imaging pictures show retinal dependent expression of CatCh and *Ps*CatCh, C-terminal tagged YFP or TYE motif, respectively. **(b)** right: measurement of steady photocurrent of CatCh and *Ps*CatCh; left: comparison of off kinetics from CatCh (black) and *Ps*CatCh (red), average values for time constants of channel closing (τ_{off}) and data points in figures are given as mean ± SEM. hold potential: -100mV. **(c)** stationary photocurrent evoked by CatCh (black box) and *Ps*CatCh (red box) after different blue light (450nm, 5.6, 16.7, 55.6, 167, 556, 1667, 5000μW/mm^2) irradiation, hold potential: -60mV. TEVC recording condition: bath solution, ORI 2mM $BaCl_2$. Imaging picture and data value were taken and measured two days after 20ng cRNA injection.

I wanted to test whether *Ps*CatCh also shows high calcium permeability. Direct evaluation of calcium selectivity in Oocytes was difficult as it caused large calcium-induced chloride current during the voltage recording. Thus, first I prepared bath solutions containing low and high barium solution for voltage-clamp recording, as barium ion is usually used to mimic calcium ions. The current-voltage analysis data strongly demonstrated that PsCatCh has four times larger reversal potential shift than that of CatCh and generated more than 4-fold larger barium photocurrent **(figure 3.10a)**. This may suggest *Ps*CatCh has larger calcium conductance than that of CatCh. In order to further confirm *Ps*CatCh has high calcium conductance, I compared photocurrent amplitude of both CatCh and *Ps*CatCh at -100 mV in a bath solution containing 80 mM $CaCl_2$ at pH9.0 before or after BAPTA injection. Before BAPTA injection, both CatCh and *Ps*CatCh showed strong calcium evokes chloride current. Interestingly, when calcium-

induced chloride current was blocked by BAPTA, the remaining inward current was the absolute calcium current, *Ps*CatCh still generated three times larger calcium current than CatCh **(figure 3.10 b)**. Finally, all these data demonstrated that *Ps*CatCh was a high calcium conductance channelrhodopsin.

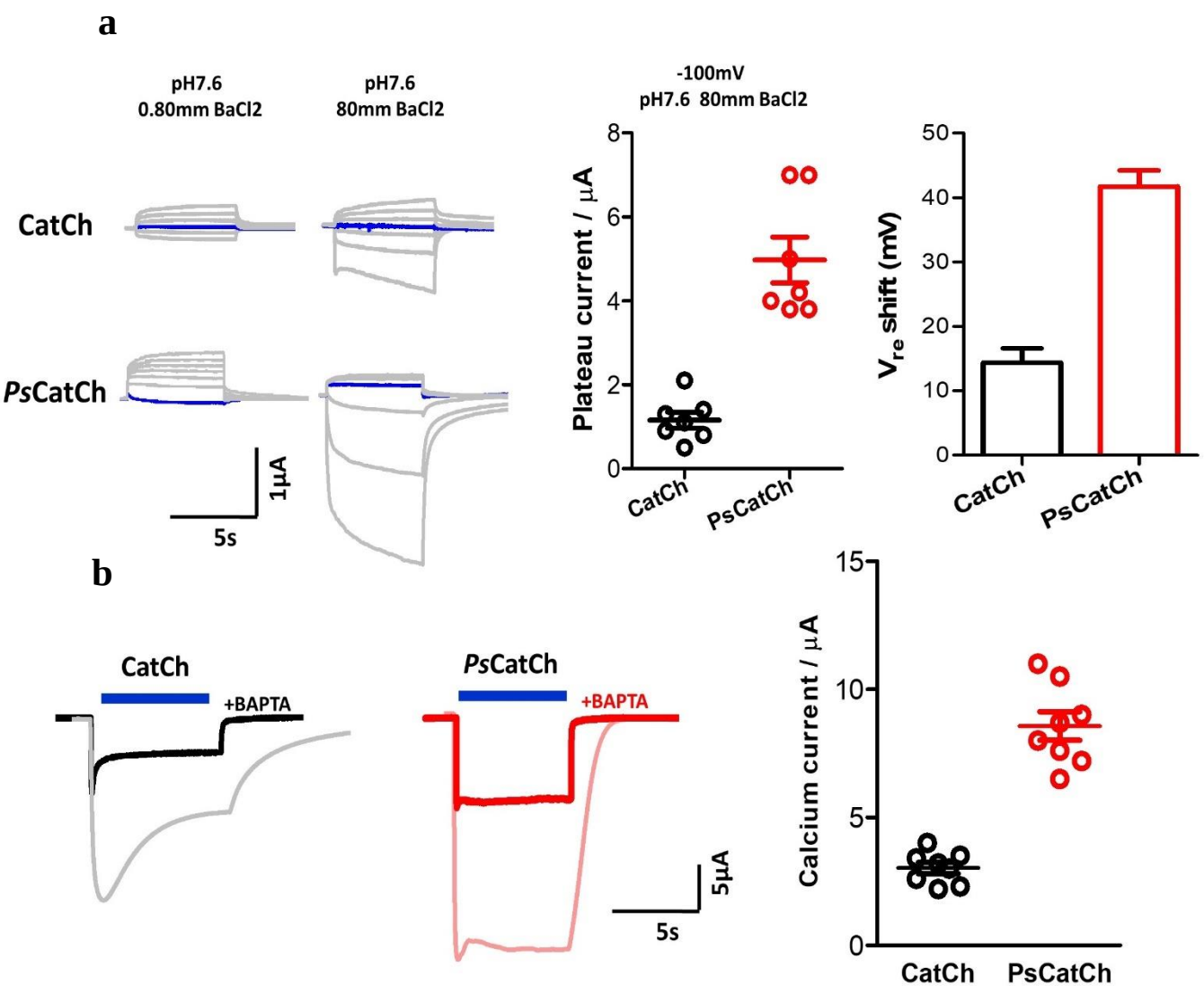

Figure 3.10 Divalent ion selectivity of CatCh and *Ps*CatCh.

(a) left: Representative traces of CatCh and *Ps*CatCh under low and high $BaCl_2$ bath solution at pH 7.6, holding potential is from -90mV in 20mV steps. middle: plateau photocurrent of CatCh and *Ps*CatCh at high $BaCl_2$ solution at -100mV. right: quantification of reversal potential shift between CatCh and *Ps*CatCh. **(b)** Photocurrent traces of CatCh and *Ps*CatCh before (grey) and after (black)

(BAPTA) injection. Measurement Were done in 80 mM $CaCl_2$ pH 9.0 at -100mV. BAPTA was injected into the oocyte to a final concentration of ~10 mM, to block the $Ca2^+$-induced chloride current. Blue bars indicate light illumination. calcium photocurrent of CatCh and *Ps*CatCh was shown on the right. All data points Were plotted in the figure and mean ± SEM was indicated.

3.2.2 Refinement and characterization of *Ps*CatCh variations

To enhance plasma targeting efficiency of *Ps*CatCh, I fused LR signal peptide at its N terminal and generated several *Ps*CatCh variants with different lengths truncation at N or C terminal **(figure3.11a)**. From my results, we can see that only LR fusion *Ps*CatCh (#2) gives rise to 4-fold large photocurrent and nearly three times total fluorescence emission value compared to no modified *Ps*CatCh (#1). To optimize this plasma membrane trafficking determines, I designed *Ps*CatCh variants with 12,19,33 and 35 N terminal deletion combined with LR fusion. From our electrophysical recording data, I excluded 33(#11) and 35 (#12) N terminal truncated *Ps*ChR variants as it almost destroys its channel activity. I further truncated 18 and 29 amino acid from its C terminal. Unfortunately, C terminal 29 (#5) deletion dramatic decreased its expression and photocurrent. Interestingly, I found that *Ps*CatCh 2.0 with both N 19 and C 16 amino acid truncation (#8) was the best performer which gives rise to 5.5-fold larger photocurrent than *Ps*CatCh **(figure 3.11a)**. Base on this result, as it is shown in (**figure 3.11b)**, I generated improved *Ps*ChR D139H by both LR fusion and N 19 and C 16 amino acid truncation termed *Ps*ChR D139H 2.0. Even though truncation of *Ps*CatCh generated large photocurrent, N or C

terminal deletion indeed slowed channel closing. Thus, I choose no truncated *Ps*CatCh (#2) as a fast version tool called *Ps*CatCh 2.0f.

In order to further enhance its function. I generated several double mutations based on *Ps*CatCh 2.0. Among these new *Ps*CatCh2.0 mutations, *Ps*CatCh 2.0e (enhanced version) containing addition amino acid mutation (C165L) around the retinal binding site which gives rise to nearly two times larger photocurrent than *Ps*CatCh 2.0. Other *Ps*CatCh 2.0 doubled mutation does not show better performance (**figure 3.11b)**. While introducing D139H mutation to *Ps*CatCh 2.0 and *Ps*CatCh 2.0 (C165L) displayed even worse performance compared to *Ps*ChR D139H 2.0 (**figure 3.11b)**. Off kinetics analysis of these *Ps*ChR variants were shown in **table3.3**. Even though *Ps*ChR F202Y does not improve photocurrent but has two times faster off closing time than wild type *Ps*ChR. The light sensitivity of CatCh, *Ps*CatCh 2.0f, *Ps*CatCh 2.0e and *Ps*ChR D139H 2.0 were also measured, the light power density for channel half activation was shown in (**figure 3.12)**.

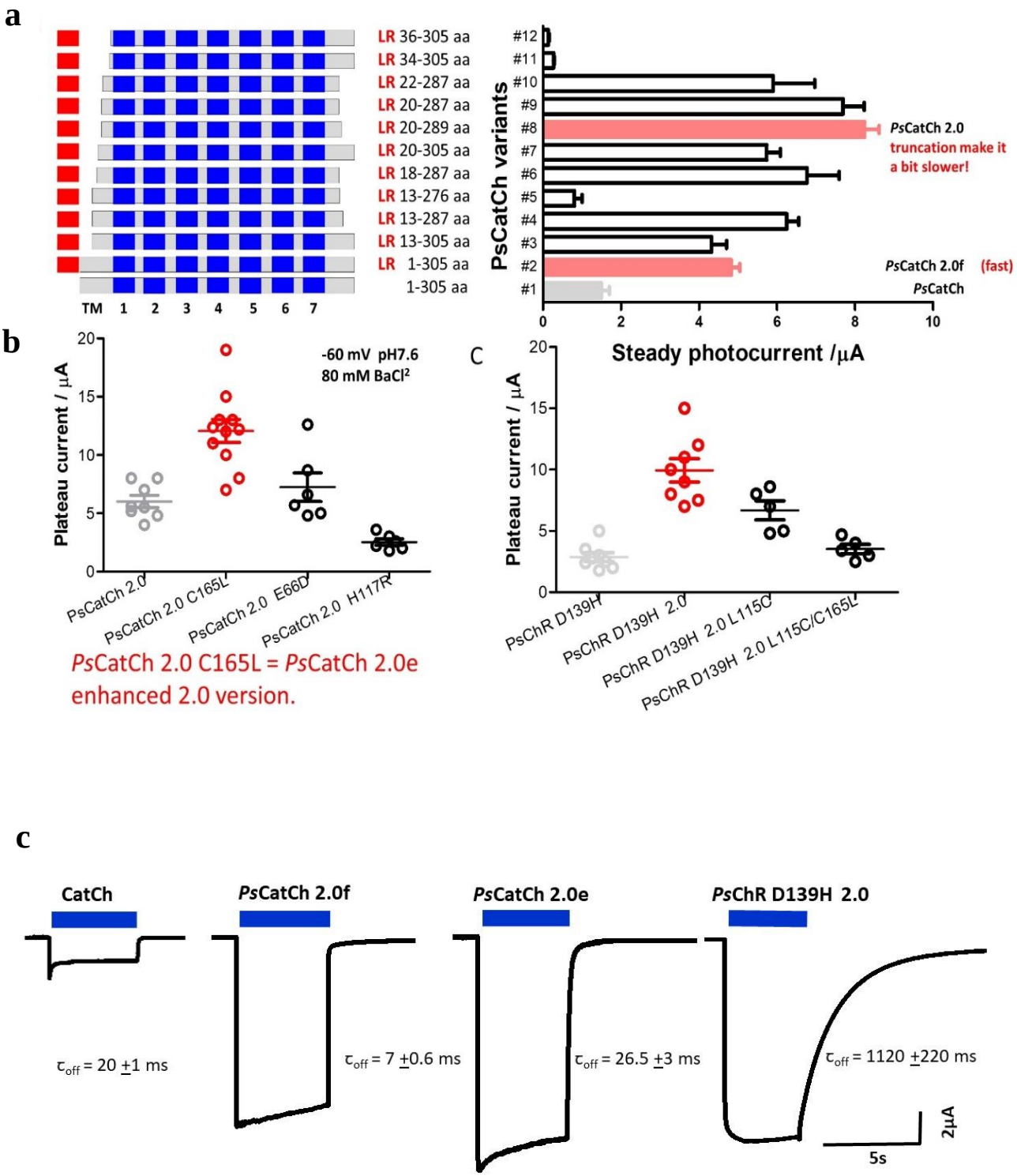

Figure3.11 Optimization of *Ps*CatCh.

(a) schematic description of wild type(left) and modified *Ps*CatChs. right side, blue box: transmembrane helix, red box: LR signal peptide, grey box:

extracellular loops. left side, Steady photocurrent of a number of *Ps*CatCh variants with 450nm light irradiation 5mW/mm^2 at -60mV. **(b)** photocurrent comparison of different *Ps*ChRs variants and photocurrent traces of indicated *Ps*ChRs variants. **(c)** representative photocurrent traces of CatCh, *Ps*CatCh 2.0f, *Ps*CatCh 2.0e and *Ps*CatCh D139H 2.0.

***Ps*ChR variants**	**Closing rate**	
	τ fast **ms** (%)	τ slow **ms** (%)
PsChR	***8.5±0.6***(>98)	*NA*
PsChR-F202Y	***3.5±0.6***(>90)	***NA***
PsChR-H117Q	***8.0±0.8***(>90)	***NA***
PsChR-L115C	***6.5±0.6***(>90)	***NA***
PsChR-L115C/F202Y	***6.9±0.7***(>90)	***NA***
PsChR-L115C/E66D	***21.0±0.7***(>90)	***NA***
PsChR-L115C/C165L	***26.5±29.9***(>90)	***NA***
PsChR-L115C/H117Q	***30.0±3.6***(>90)	***NA***
PsChR-L115C/H117R	***41.5±3.1***(>90)	***NA***
PsChR-L115C/E97D	***187.5±0.7***(~90)	***NA***
PsChR-D139H	***NA***	*807±175.8*(~80)
PsChR-L115C/D139H	***NA***	*1120±218*(~80)
PsChR-H117Q/D139H	***NA***	*980±200*(~80)
PsChR-D139C	***NA***	***74000±4278***(>95)
PsChR-H117Q/D139C	***NA***	***92000±4278***(>95)

Table3.3 Off kinetics of *Ps*ChR variants

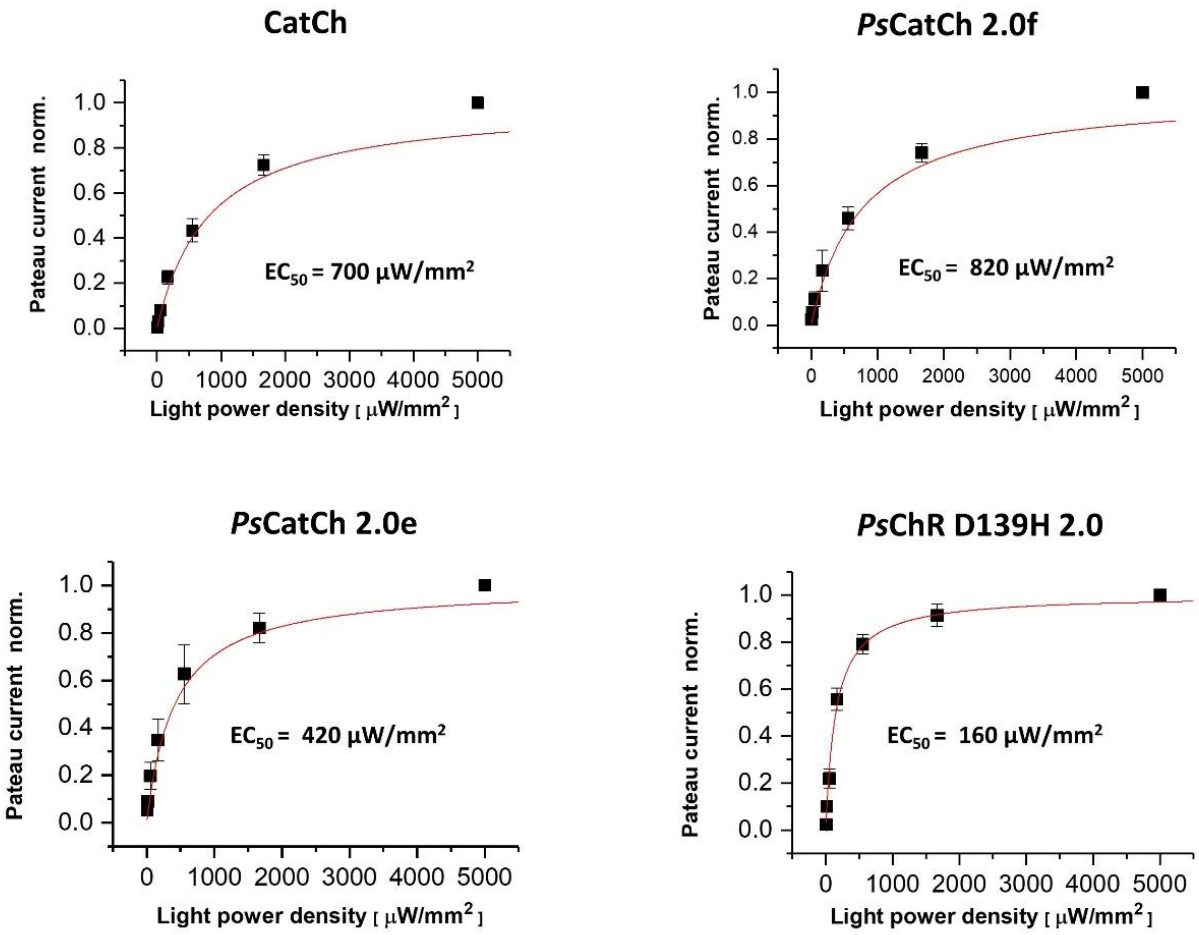

Figure3.12 Light sensitivity of *Ps*ChR variants.

5s, 30 s continuous 450 nm blue light illumination was applied to CatCh and PsChR variants, respectively. Photocurrent at maximum light poIr density of each oocyte was normalized as 1.20 ng cRNA of above constructs were injected into *Xenopus* oocyte. Measurements Were performed 2 days after injection. All measurements were done in standard solution with BaCl2 (110 mM NaCl, 5 mM KCl, 2 mM BaCl2, 1 mM MgCl2, 5 mM HEPES and pH 7.6) at -60 mV. Data points Were presented as mean ± SD, *n* = 3 - 4. Curves Were fitted with hill equation.

3.2.3 Ion selectivity of *Ps*ChR variants

To get an estimate of specific effects on proton versus sodium conductance among these ChR variants, I measured the current-voltage relationship and reversal potential of CatCh, *Ps*CatCh 2.0f, *Ps*CatCh 2.0e and *Ps*ChR D139H 2.0 by systematically changing the composition of bath solution.

First, I measured photocurrent changes for all constructs at different voltages using three different extracellular solutions with proton and sodium ion-concentration gradient. As the photocurrent traces shown in (**figure 3.13a)**, when I reduced extracellular sodium ion (from 120mM NaCl to 1mM NaCl pH7.6), the inward photocurrent of all constructs was much decreased, indicating high sodium conductance. While changing proton concentration does not show any change for CatCh, *Ps*CatCh 2.0f, *Ps*CatCh 2.0e. I calculated reversal potential shift when changing sodium concentration at pH7.6. I found *Ps*ChR D139H 2.0 has the largest reversal potential shift (mean ± SEM 90$\pm$1.3 mV, n=4) Which was almost three times larger than CatCh (mean ± SEM 34$\pm$0.8 mV, n=4). *Ps*CatCh 2.0f and *Ps*CatCh 2.0e has similar reversal potential. I quantified the permeability ratio of sodium to proton of these ChRs by the Goldmann-Hodgkin-Katz voltage equation. *Ps*ChR D139H 2.0 (P_{Na+}/P_{H+}= ~90×10^{-7}) exhibited thirteen times larger sodium conductance than CatCh (P_{Na+}/P_{H+}= ~7×10^{-7}). *Ps*CatCh 2.0f and *Ps*CatCh 2.0e has identical value (P_{Na+}/P_{H+}= ~20×10^{-7}) which was three times larger than that of CatCh (**figure 3.13b)**.

Finally, to compare the calcium selectivity among these ChRs, first I measured calcium-triggered chloride current in a solution containing 80mM $CaCl_2$ pH9.0 at -100mV. During light illumination, CatCh triggered robust inward photocurrent. This due to calcium influx activated endogenous calcium-sensitive chloride channel from Oocytes, after injection of 10mM BAPTA in the same Oocyte, inward photocurrent, reflecting the real size of calcium conductance, was dramatic reduced (grey trace), as it was reported previously. Consistent with previous research results, here I also observed high calcium conductance of *Ps*CatCh than that of Catch. In addition, *Ps*CatCh 2.0f, *Ps*CatCh 2.0e even generated much larger calcium current than *Ps*CatCh, indicating a significant increase of calcium selectivity (**figure 3.14a and b)**.

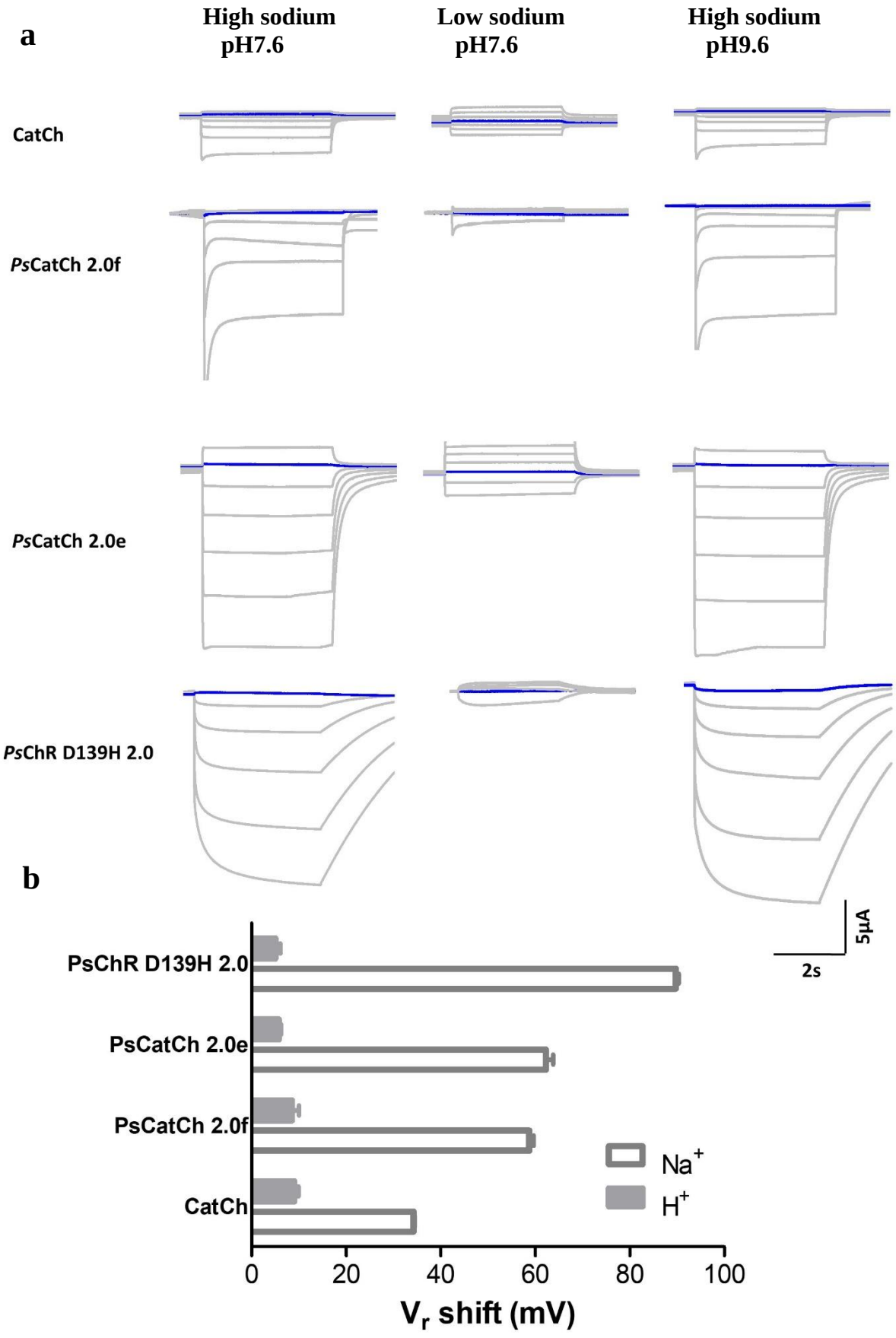
a
High sodium pH7.6
Low sodium pH7.6
High sodium pH9.6
CatCh
PsCatCh 2.0f
PsCatCh 2.0e
PsChR D139H 2.0
5µA
2s
b
PsChR D139H 2.0
PsCatCh 2.0e
PsCatCh 2.0f
CatCh
Na+
H+
0
20
40
60
80
100
Vr shift (mV)

Figure 3.13 Characterization sodium conductance of selected PsChR variants.

(a) representative photocurrents of CatCh, *Ps*CatCh 2.0f, *Ps*CatCh 2.0e and *Ps*ChR D139H 2.0 at different voltages and different extracellular solution of 120 mM NaCl and pHe7.6(left),1 mM NaCl and pH 7.6 (middle) and 120 mM NaCl and pH9.6 (right). **(b)** comparison of Na^+ permeabilities of CatCh, *Ps*CatCh 2.0f, *Ps*CatCh 2.0e and *Ps*ChR D139H 2.0. Reversal potentials (Vr) were determined after photocurrent measurements from -90 mV to + 10 mV. Reversal potential shift for Na^+ was calculated by the reversal potential differences in two outside buffers containing 120 mM NaCl pH 7.6 and 1 mM NaCl pH 7.6. Reversal potential shift for H+ was determined by the reversal potential differences in two outside buffers of pH 7.6 and 9.6 containing.120 mM NaCl. Data points Were presented as mean ± SD, n = 4–6.

However, this may due to higher plasma membrane expression level. Thus, patch-clamp analysis of calcium selectivity among these *Ps*CatCh variants is needed. *Ps*ChR D139H 2.0 was confirmed highest sodium selectivity channelrhodopsin, Interestingly, here I further observed a high calcium permeability of *Ps*ChR D139H 2.0 **(figure 3.14b)**.

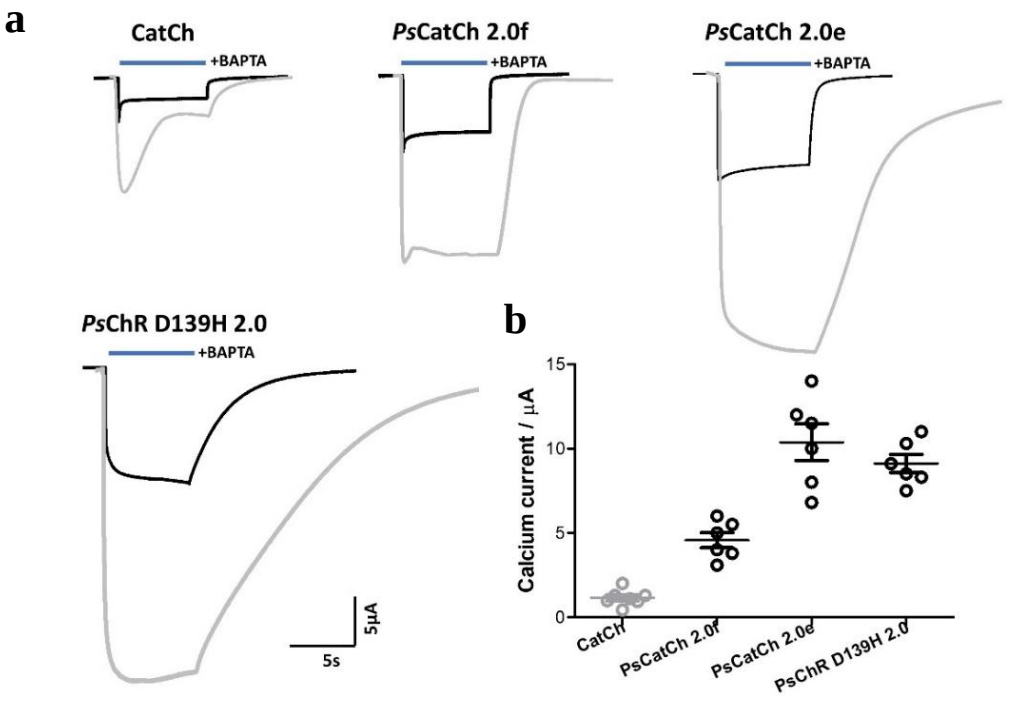

Figure 3.14 Investigation of calcium permeability of selected *Ps*ChR variants. **(a)** photocurrent in 80mM $CaCl_2$ pH9.0 at -100mV from the same *Ps*ChRs-expressing Oocyte (grey line and black line represent photocurrent traces before and after BAPTA injection, respectively), quantitative steady current show in the left. **(b)** comparison of calcium permeability among Catch, *Ps*CatCh and *Ps*CatCh 2.0f, *Ps*CatCh 2.0e and *Ps*ChR D139H 2.0. 20ng cRNA is injected in fresh Oocytes and incubate for 2 days expression. Photocurrent traces from the same Oocyte show in the left (grey line: with 10mM BAPTA injection), calcium induce current are shown in the right.

3.2.4 Independent two-color optogenetic excitation

The ability to achieve independent two-color optogenetic manipulates different neural populations would enable neuroscientist to study how multiple neural populations work together. So far, two-color excitation of neural activity was based on the principle of spectral separation between blue-shifted channelrhodopsin (ChR2, Chronos)

and red-shifted channelrhodopsin (C1V1, Chrimson)[73, 74]. Even though there was an implementation of using Chronos and Chrimson to achieve two-color independent neural excitation in brain slice, still no report about two-colour independent excitation in vivo to control animal behavior. All published channelrhodopsins have at least 10-20% activation of peak photocurrent towards the blue end of the spectrum, a fundamental property of retinal chromophore[7]. Due to this spectral overlap, previous studies could not reliably drive spikes with blue channelrhodopsin without eliciting spikes with red-shifted channelrhodopsin in the blue light irradiation, which will cause neural crosstalk. To overcome this challenge, we should combine high light sensitivity blue channelrhodopsin with low light sensitivity red channelrhodopsin. Based on our extensive modification and characterization of a series of optimized channelrhodopsin. I selected *Ps*CatCh 2.0f and Chrimson 2.0 as the candidate for achieving two-color independent optogenetic excitation. My study showed that *Ps*CatCh 2.0f generated identical photocurrent amplitude at 10μW/mm^2 as the CatCh triggered photocurrent size at saturated light power density **(figure 3.15a)**. This means the proper blue light power density of *Ps*CatCh 2.0 for evoking neural spiking can be reduced to several micro-watt scales, which was nearly hundred times less light power density than current depolarizing tools. Next, I tested blue light sensitivity of Chrimson2.0. The lowest blue light illumination that obviously activated Chrimson2.0 around 100 μW/mm^2 (data not shown).Therefore, the ideal blue light irradiation condition should be the range from 10 to 100 μW/mm^2, which can successful eliciting

neural spiking in *Ps*CatCh 2.0f-expressing neural population without perturbating Chrimson2.0-expressing cells. So, I chose 1-2mW/mm^2 red light power for activation of Chrimson2.0, no photocurrent was observed in *Ps*CatCh 2.0f-expressing cells.

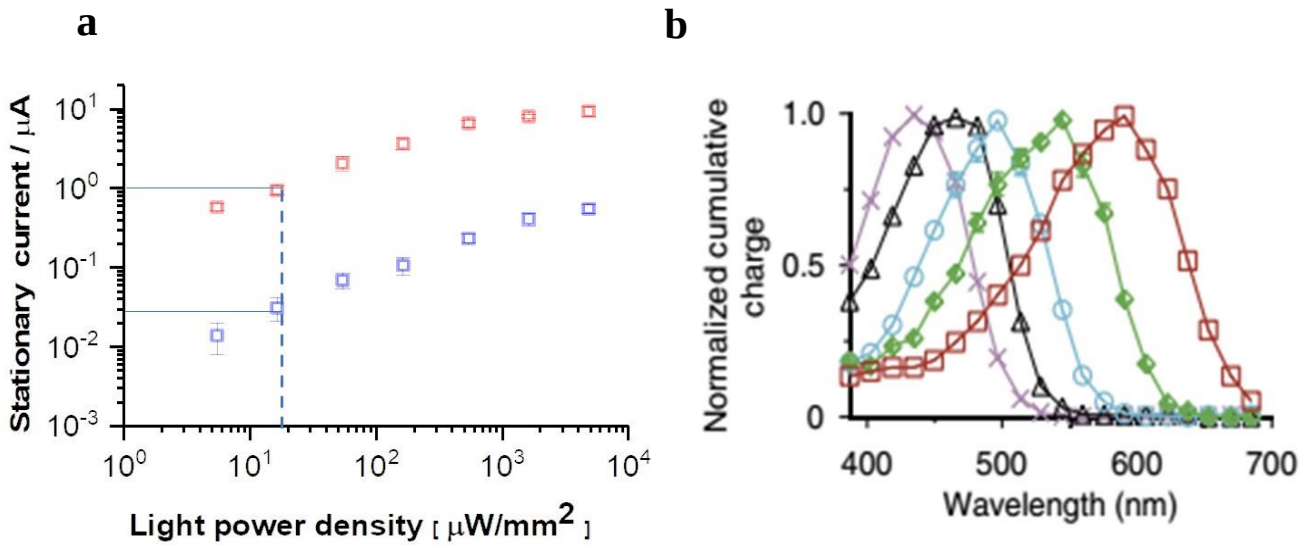

Figure 3.15 Light sensitivity of blue and red channelrhodopsin.

(a) 5s continuous 450 nm blue light illumination Were applied to CatCh (blue box) and PsCatCh 2.0f (red box), respectively. Photocurrent at maximum light poIr density of each oocyte was normalized as 1.20 ng cRNA of above constructs was injected into *Xenopus* oocyte. Measurements were performed 2 days after injection. All measurements were done in standard solution with $BaCl_2$ at -60 mV. Data points Were presented as mean ± SD, n = 3 - 4. Curves Were fitted with hill equation. **(b)** data of action spectra of different channelrhodopsin was taken from Nathan C Klapoetke,2014.

Based on the data from above, I selected 50 μW/mm^2 450nm for activating *Ps*CatCh 2.0f and 1mW/mm^2 635nm for driving Chrimson2.0. Then I evaluated the independent blue and red light response in only *Ps*CatCh 2.0f, Chrimson 2.0 injected Oocytes as well as two channelrhodopsins co-expression Oocytes under different frequency light pulse stimulation. As I expected, in *Ps*CatCh 2.0f-expressing cell, blue light triggered stable large inward photocurrent at 10,25,50Hz light pulse and no photocurrent was observed when the red light was applied. In contrast, in Chrimson2.0-expressing cell, almost no blue light response but robust red-light driving photocurrent was detected. Consequently, reliably inward photocurrent under either blue or red-light irradiation in two-channelrhodopsin expression cells at 10, 25, 50Hz were also observed, as is shown in (**figure 3.16a and b)**. Finally, our demonstrations provided pieces of evidence indicated that specific neural population can be activated independently by two-color light with no crosstalk.

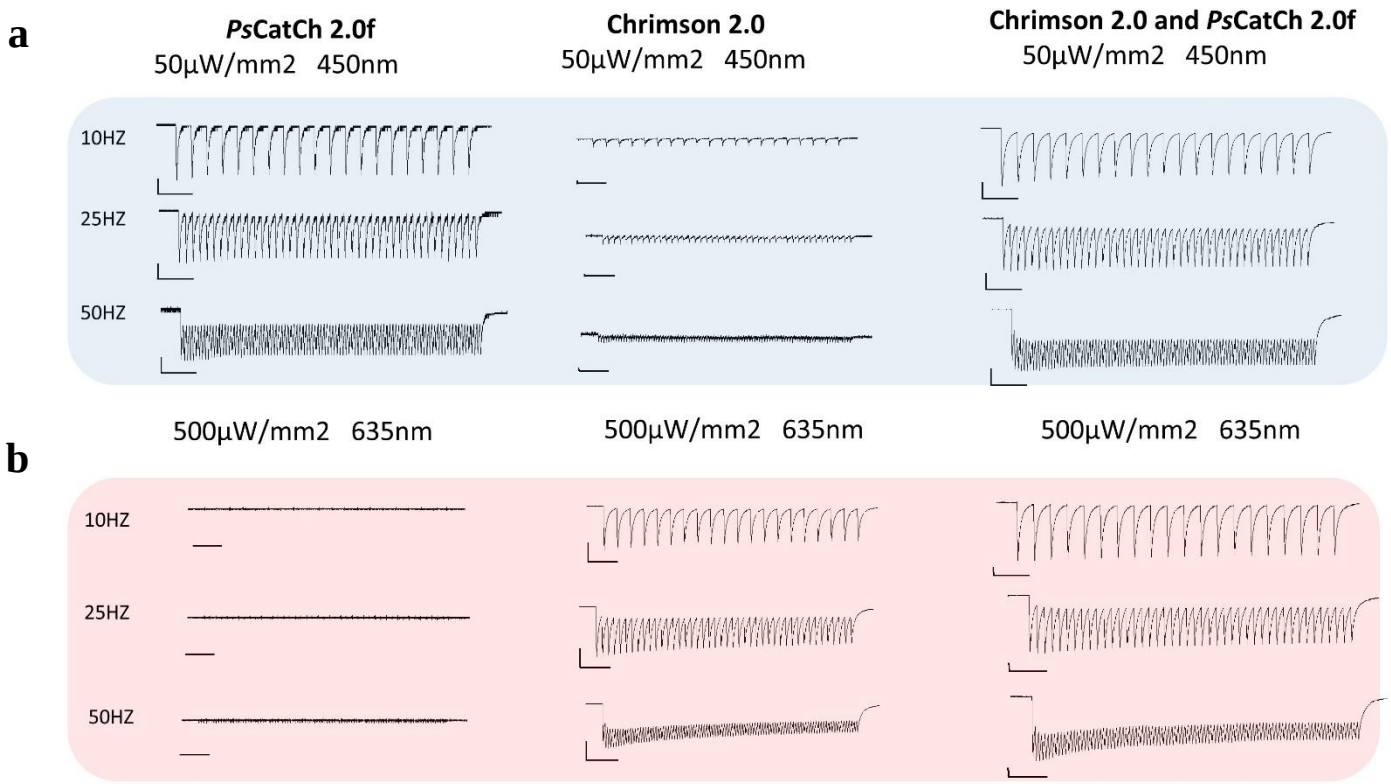

Figure 3.16 Implementation of two-colour optogenetic excitation in Oocytes. **(a)** light-induced photocurrent traces under 10,25,50Hz 450nm light stimulation in *Ps*CatCh 2.0f, Chrimson 2.0 and co-expression Oocytes. **(b)** light-induced photocurrent traces under 10,25,50Hz 635nm light stimulation in *Ps*CatCh 2.0f, Chrimson 2.0 and co-expression Oocyte. All measurements were done in standard solution with $BaCl_2$ at -60 mV.

3.3 Part III

3.3.1 Identification and characterization of *Ce*ChR

Channelrhodopsins derived from *Chlamydomonas reinhardtii* and *Volvox carteri* were identified and engineered for neuroscientific applications, and many other novel ChRs were found from opsin-like genome sequence[73]. Here, through searching the sequence database from acidophilic green alga *Chlamydomonas eustigma* **(figure3.17a)**, a novel channelrhodopsin *Ce*ChR was found [89]. From the sequence alignment result, *Ce*ChR showed high sequence homology with other characterized channelrhodopsin, in particular with ChR2 **(figure3.17b)**. I proposed that *Ce*ChR could be another functional channelrhodopsin. Initially, under two electrophysiology voltage-clamp conditions, I observed no photocurrent in standard ori pH 7.6 solution and very weak photocurrent in bath solution at pH 5.6 was detected (data does not show here). This may indicated that *Ce*ChR was a high proton-permeable channelrhodopsin with poor plasma membrane targeting **(figure3.18a)**. Putative N terminal of *Ce*ChR containing several methionines, the start codon of encoded *Ce*ChR sequence was not sure, thus I cloned four *Ce*ChR sequences with different lengths at N terminal. To reduce its intracellular aggregation, I fused beta-linker or LR at its N terminal. Remarkably, both signal peptides fused *Ce*ChR showed larger photocurrent, but LR signal peptide works better than beta-liker. LR fused *Ce*ChR generated at least three-fold larger photocurrent than

*Ce*ChR **(figure3.18b)**. Furthermore, it also significantly enhanced plasma membrane targeting efficiency.

To get an estimate of ion selectivity of *Ce*ChR, inward photocurrent was quantified in several bath solutions containing specific cation ions. my results indicated that *Ce*ChR was a novel light-gated cation channel with high proton conductance **(figure3.18c)**. Taken together, *Ce*ChR is a functional and new depolarizing tool for neural excitation. In order to get more information about *Ce*ChR, I compared *Ce*ChR with wild type ChR2 side by side. From electrophysiological data and photocurrent traces, I observed comparable photocurrent between LR-*Ce*ChR with wild type ChR2 Then, I explored the kinetics of recovery from desensitization during the different dark period. I delivered 2s blue light separated by varying intervals of darkness(Δt). I quantified the Δ*I*, the difference between peak and stationary photocurrent magnitude for each light pulse. and divided Δ*I* from the second pulse (Δ*I*2) by Δ*I* from the first pulse (Δ*I*1) and plotted the ratio against Δ*t*. I calculated the 50% recovery time from peak photocurrent. *Ce*ChR indeed has relative slow recovery(20s) than wild type ChR2(10s) **(figure3.18d)**. However. *Ce*ChR has two-fold higher light sensitivity compared to wild type ChR2 **(figure3.18e)**. In addition, the action spectrum of *Ce*ChR showed 20nm blue-shifted compared to ChR2 wild type **(figure3.18f)**.

a

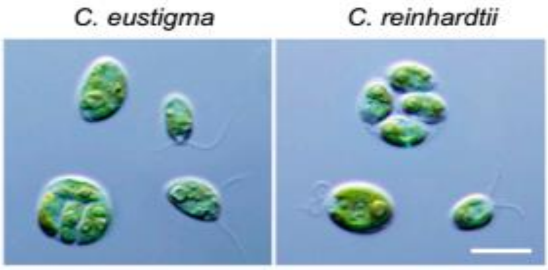

b

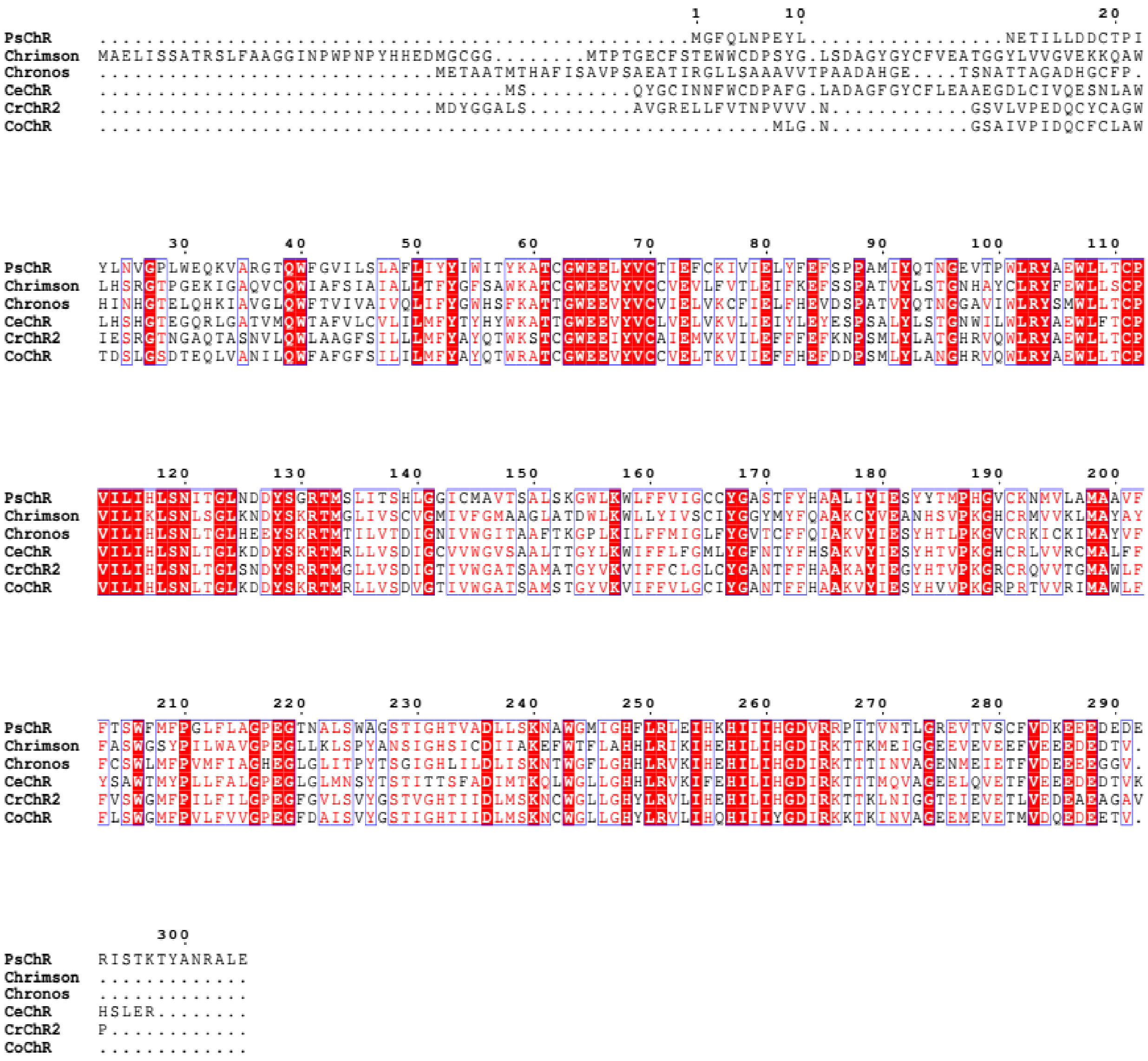

Figure 3.17 Identification of novel ChR from Chlamydomonas *eustigma*.

(a)cells of C. eustigma (Left) and C. reinhardtii (Right). (Scale bar: 10 µm.) **(b)** Sequence comparison of *Ce*ChR with other opsin genes.ChR2 (UniProt ID:Q8RUT8), Crimson (NCBI ID: KF992060), *Ps*ChR (NCBI ID: JX983143) *Co*ChR (NCBI ID: KF992041), *Ce*ChR sequence are from GenBank under the

accession code PRJDB5468.The C-termini of all presented ChRs is truncated.

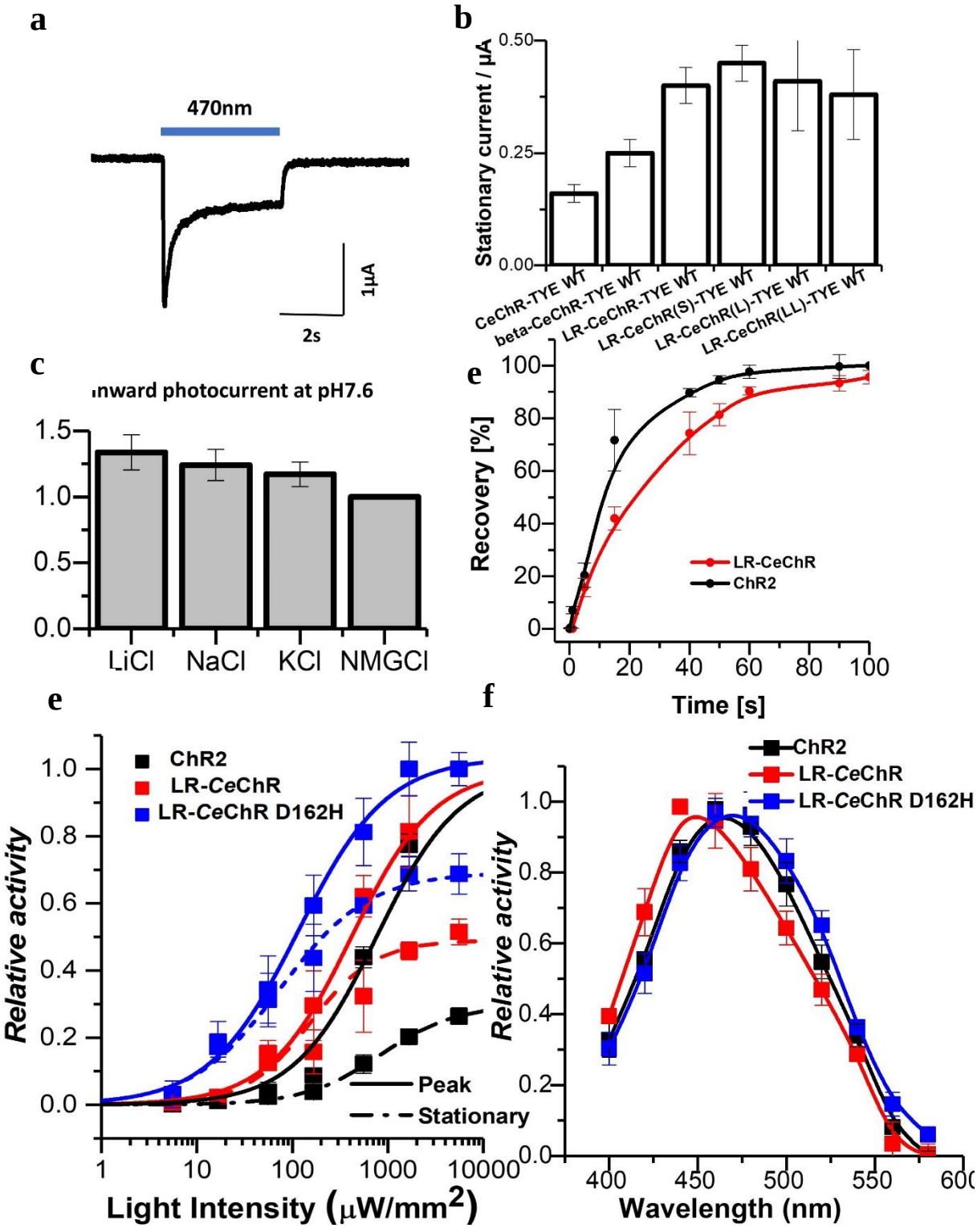

Figure 3.18 Biophysical characterization of *Ce*ChR.

(a) photocurrent trace of *Ce*ChR shows obvious light induce inward photocurrent

(b) photocurrent comparison of optimized *Ce*ChR-expressing Oocytes under -

100mV at pH7.6, 473nm laser. **(c)** Ion flux characteristics of *Ce*ChR. **(d)** comparison of channel recovery property between ChR2 and *Ce*ChR. **(e)** light sensitivity of CeChR and ChR2. **(f)** action spectral of ChR2, LR-*Ce*ChR and LR-*Ce*ChR D162H.

3.3.2 Mutation analysis of *Ce*ChR

*Ce*ChR belongs to the most blue-shifted channelrhodopsin with high light sensitivity. To obtain *Ce*ChR variants capable of interesting performance for optogenetic application, I generated a series of *Ce*ChR variants either with single or double mutation. I measured photocurrent of each *Ce*ChR variant-expressing Oocytes cultured with 10μM ATR (all-trans-retinal) or without any ATR. Photocurrent and fluorescence emission value were quantified **(figure3.19a)**. All these functional *Ce*ChR variants exhibited obvious retinal-dependent expression level. And all double mutations generated very weak photocurrent. I excluded *Ce*ChR variants with very small photocurrent. Interestingly, substitution of *Ce*ChR D162 to F, Y, H and C lead to long inactivation time. In particular, *Ce*ChR(D162C) has the slowest off-kinetics compared with other mutations, showing the longest opening time among all published ChRs **(figure3.19b)**. Finally, I selected step-function opsin like *Ce*ChR DC variants for further study.

a

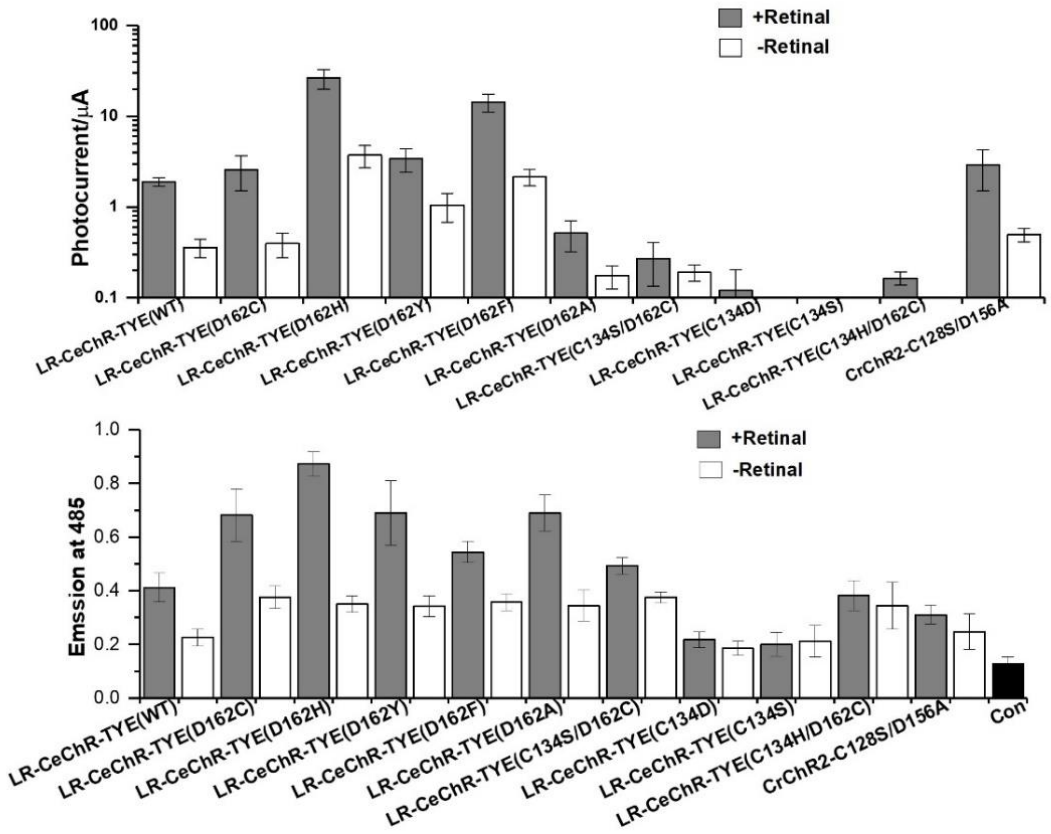
+Retinal
-Retinal
Photocurrent/μA
100
10
1
0.1
LR-CeChR-TYE(WT)
LR-CeChR-TYE(D162C)
LR-CeChR-TYE(D162H)
LR-CeChR-TYE(D162Y)
LR-CeChR-TYE(D162F)
LR-CeChR-TYE(D162A)
LR-CeChR-TYE(C134S/D162C)
LR-CeChR-TYE(C134D)
LR-CeChR-TYE(C134S)
LR-CeChR-TYE(C134H/D162C)
CrChR2-C128S/D156A
+Retinal
-Retinal
Emssion at 485
1.0
0.8
0.6
0.4
0.2
0.0
LR-CeChR-TYE(WT)
LR-CeChR-TYE(D162C)
LR-CeChR-TYE(D162H)
LR-CeChR-TYE(D162Y)
LR-CeChR-TYE(D162F)
LR-CeChR-TYE(D162A)
LR-CeChR-TYE(C134S/D162C)
LR-CeChR-TYE(C134D)
LR-CeChR-TYE(C134S)
LR-CeChR-TYE(C134H/D162C)
CrChR2-C128S/D156A
Con

b

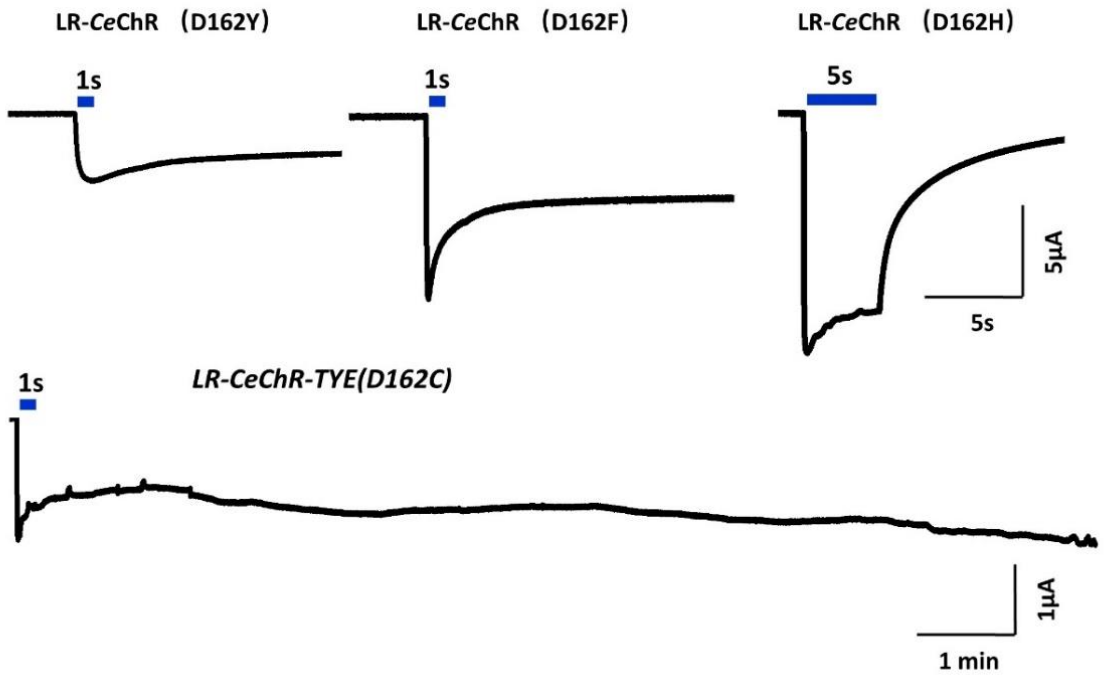
LR-CeChR （D162Y）
LR-CeChR （D162F）
LR-CeChR （D162H）
1s
1s
5s
5μA
5s
1s
LR-CeChR-TYE(D162C)
1μA
1 min

Figure 3.19 Photocurrent and expression level of *Ce*ChR variants.

(a) stationary photocurrent amplitude of *Ce*ChR mutations and qualification of emission fluorescence value at 583nm of YFP tagged *Ce*ChR mutations. The black box represents the group with additional 1uM all-trans-retinal ATR in $ND96^{++}$ solution. White box means the culture media has not additional ATR.20ng cRNA of each construct Were injected into fresh Oocytes for two days expression. **(b)** representative photocurrent traces of *Ce*ChR(D162H), *Ce*ChR(D162F), *Ce*ChR(D162Y) and *Ce*ChR(D162C). All measurements were done in standard solution with $BaCl_2$ at -100 mV.

3.3.3 Novel bi-stable function channelrhodopsin

Upon photon absorption, the photocycle of ChR2 is defined by five different intermediate conformational changes from its dark-adapted closed state (D470) to two nonconducting intermediate states (P500 and P390), and then enters the open-channel state (P520), until it finally reaches its dark-adapted closed state again and the cycle can be repeated. ChR2 mutation at DC gate has delayed inactivation and shows a prolonged open state after blue light illumination, which can be converted directly to the closed state by green light, this kind of ChR2 mutation called bi-stable function opsin[87]. As the above data demonstrated that *Ce*ChR(D162C) showed extremely slow off-kinetics, I proposed that this *Ce*ChR(D162C) mutation was a new step function opsin. As I expected, 1s blue-light activated *Ce*ChR(D162C) and 5s second yellow light could switch back channel to the closed state**(figure3.20a)**. This indicated *Ce*ChR(D162C) was a novel step-functional opsin. There are some advantages of SSFO (stable step function opsin), including less light delivery and continuous mild

depolarizing targeted cells[90]. Thus, here I engineered two novel SSFOs based on *Ce*ChR: LR-*Ce*ChR(D162C), LR-*Ce*ChR (C134S/D162A). Then I roughly compared their photocurrent and kinetics with SSFO (ChR2-C128S/D156A) under a long-time voltage-clamp recording. To avoid long time recording in damaging or causing leakage of Oocytes, I used relatively low sodium and high potassium bath solution, and holding at -60 mV. My measures indicated that LR-*Ce*ChR (C134S/D162A) and *Ce*ChR(D162C) was even slower than SSFO. *Ce*ChR (C134S/D162A) and SSFO have similar stable inward photocurrent. While *Ce*ChR (D162C) has slightly less photocurrent compared to SSFO (figure 3.20b). All these novel bi-stable channelrhodopsin could be used for nanoscale optogenetic application[91].

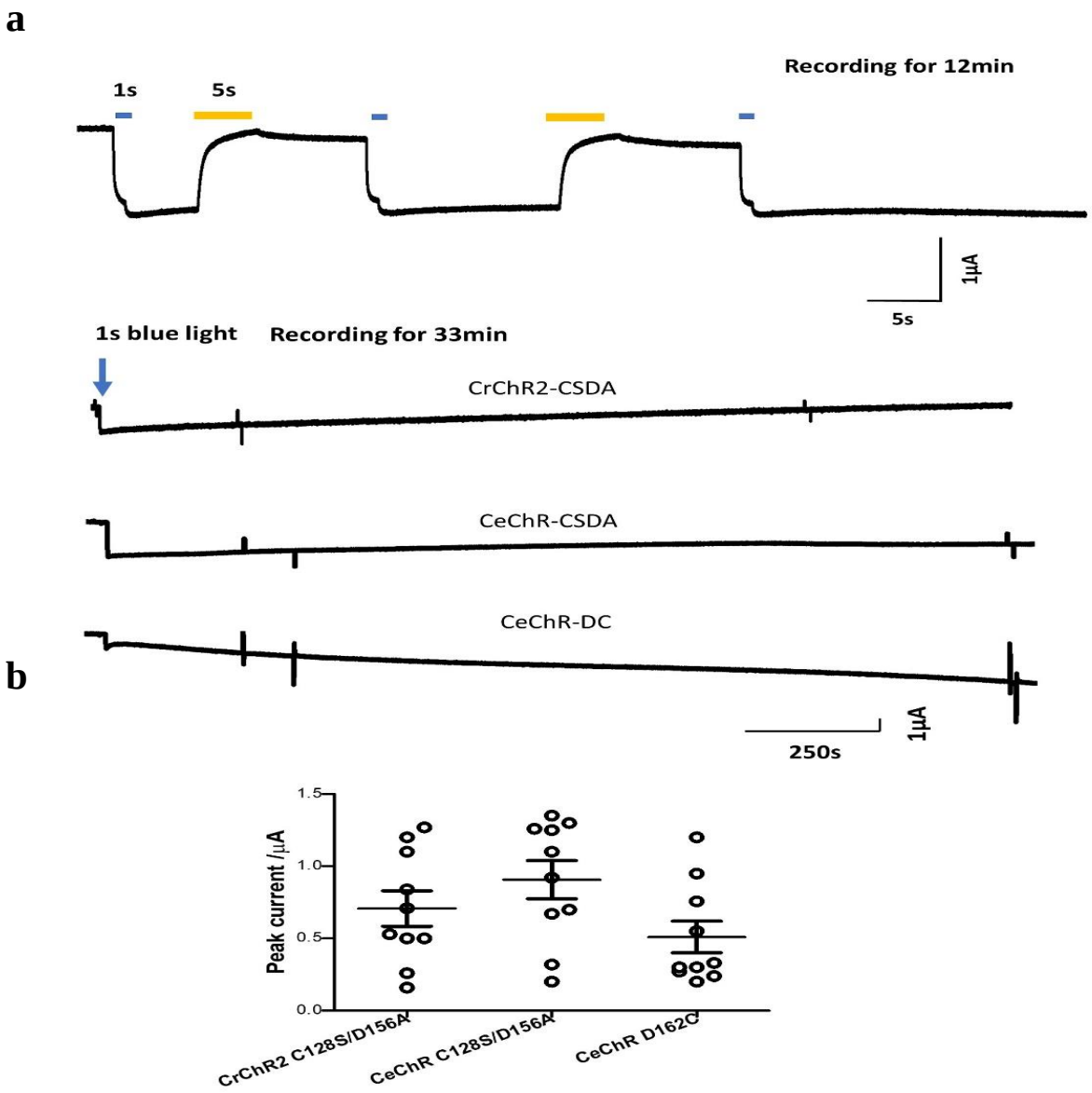

Figure 3.20 Engineering novel bi-stable channelrhodopsin with slow kinetic. **(a)** representative photocurrent of LR-*Ce*ChR(D162C) expressing Oocytes, 1s 470nm blue light-induced stable inward photocurrent, 5s 590nm yellow light switch off-channel to the closed state. Were cultured in $ND96^{++}$ solution. **(b)** Photocurrent traces and peak photocurrent of three bio-stable channelrhodopsin measurement under low sodium and high potassium solution contain 2mM $BaCl_2$ at -60 mV. 470 nm laser-generated blue light for illumination.

Discussion

Optogenetics is initialized by the characterization and application of ChR2 in neuroscience. Optogenetic tools have been expanding during the last decade [13, 92-94]. Most of them belong to microbial rhodopsins, such as light-gated cation channel ChRs, light-gated anion channel ACRs as well as light-driven proton pump BR, sodium pump KR2 and chloride pump HR[95]. Rhodopsin-based optogenetic tools combined with optical approaches are used to explore the mechanism underlying the causal link between cellular events, neural circuit and a specific behavior in diverse animal models, from the nematode *C. elegans* and *Drosophila* to mouse and non-human primates [14, 82, 96, 97].

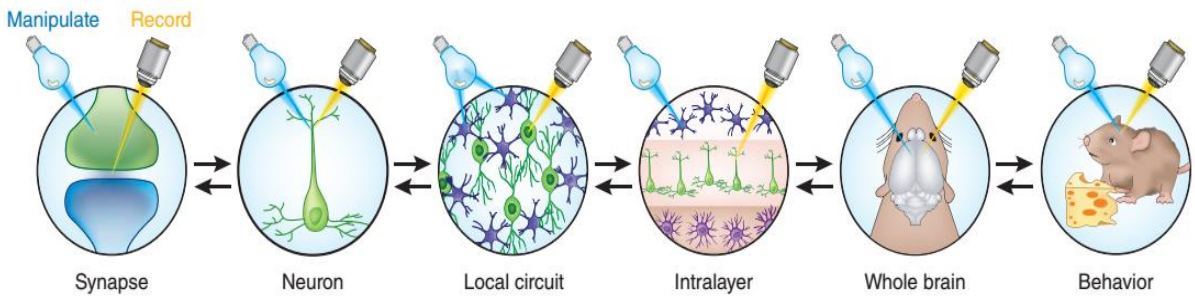

Figure 4.1 Combination of optogenetics with optical approaches can be used at all levels of brain function.

A variety of applications use optogenetic actuators and optical sensors to both readout and control neural activity in a specific type of neural populations. The picture was taken from[94].

4.1 New trafficking peptide to expand the optogenetic toolbox

The crucial step of developing optogenetics is to engineer high-functional optogenetic tools[1, 7, 94]. Several strategies have been used by many researchers aiming at designing improved optogenetic tools. Here, I summarise these strategies as the following five classes. First, the naturally rhodopsin-based optogenetic tools, such as wild type ChR1/2, wild type *Vc*ChR1/2, Chronos, Chrimson, *Ps*ChR are based on the genome-mining analysis; Second, structure-guided mutagenesis of rhodopsin which generates massive variations with diverse characters. The most commonly used tools like ChR2 (H134R)[47], ChrimsonR[73], ChR2 (ETA)[81], ChR2(ET/TC)[98], Jaw[23], CheRiff, ChR2-XXM and ChR2-XXL are coming from mutated opsin genes; The third class is the homology-based molecular engineering Chimeras like *Rea*ChR, C1V1, ChIEF and so on. Traditional single mutation of rhodopsin rarely altered the properties obviously and seems less effective. Recently, the fourth class is based on large-scale screening system including machine learning-guided and multidimensional screening methods which yield tools like ChromeT and ChromeQ, ChRger1, ChRger2, and ChRger3[99]. In addition to the above strategies, the last class was developed by topological inversion membrane targeting strategies generating a light-driven cation pump termed FLInChR, a new hyperpolarizing tool for neural inhibition[100]. Typically, all the above strategies contributed to 2 to 5-fold increase in photocurrent amplitude for 90% channelrhodopsin variants. And more than 90% of light-driven pump variations showed even worse performance[31, 33].

In our study, I tested a novel plasma membrane trafficking module for improving the optogenetic tools. This module contains three motifs: LR signal peptide, membrane trafficking and ER export signal peptide. Interestingly, the terminal modification of multiple rhodopsins with these motifs enhanced its functional photocurrent by a factor of three to ten. For example, red-shifted channelrhodopsin：Chrimson is highly welcome for neuroscientists as it enables deep tissue penetration. So far, no Chrimson variations which exhibit more than two times larger photocurrent than wild type were reported.[68]. In comparison to other engineering strategies, our novel trafficking module could increase stationary photocurrent of Chrimson by a factor of more than five. Furthermore, I tested it effect on other optogenetic tools, such as CheRiff, ACRs, HR, BR and KR2. Our results demonstrated that all LR modified rhodopsins show at least three to five times larger photocurrents than that of original versions. This easy-handling and high-efficiency fusion strategies could be a universal method for neuroscientists to improve the plasma membrane trafficking of rhodopsins, consequently, enhancing their functional photocurrent. Furthermore, it could also contribute to discovering uncharacterized but functional rhodopsins as some rhodopsins cannot be functionally characterized because of the mistargeting.

4.2 Engineering high-performance optogenetic tools

Channelrhodopsin with the ability to generate large photocurrent while maintaining fast kinetic and less desensitization is always welcome. In this study, I obtained several ChR2 and *Ps*ChR variations

with higher photocurrent and faster kinetic properties. For example, *Ps*CatCh 2.0f shows appropriate fifteen-fold larger photocurrent that CatCh and still has fast off kinetic and much less desensitization. Therefore, *Ps*CatCh 2.0f could be the most powerful depolarizing tools within ten millisecond closing time, further in *vivo* implementation of *Ps*CatCh 2.0f for neural activation is on the way.

In contrast, tools with slow kinetics are not suitable for ultra-fast multiple stimulations but preferred for experiments that require low light power density and long-time stimulation. The prolonged open times were accompanied by elevated light sensitivities. In our research work, a series of tools with ultra-high photocurrent and light sensitivity was designed. For instance, ChR2-XXM 2.0 and ChR2-XXL 2.0, *Ps*ChR D139C and *Ps*ChR D139H 2.0 became the order of magnitude increase in both photocurrent amplitude and light sensitivity, probably due to improved both plasma membrane expression level and single-channel conductance. These super high light-sensitive channelrhodopsin could be ideal optogenetic tools for efficient deep brain stimulation with infrared light in combination with up-conversion nanoparticles (UCNPs). These tools need to be further tested in mammalian systems[69].

Efforts on reducing proton permeability or designing a light-gated specific cation (Ca^{2+}, Na^{+} or K^{+}) permeable channelrhodopsin, is one of the most important and interesting work. The putative ChR ion-conducting pore was formed by helix1, 2, 3 and 7. Mutation analysis along the cation conducting pathway generated lots of ChR variants with moderately altered ion selectivity [101, 102]. Here, I demonstrated

that the conserved aspartate of transmembrane helix 4 (TM4) within multiple channelrhodopsins plays an important role in controlling both monovalent and divalent ion conductance. For example, mutated aspartate within TM4 to histidine contributes to improved sodium permeability by a factor of four for ChR2 and five for *Ps*ChR. This mutation also gives rise to higher calcium and potassium permeability, probably due to reduced proton selectivity. I also generated a series of high calcium permeability channelrhodopsin variations with fast off kinetics, such as *Ps*CatCh 2.0f, *Ps*CatCh 2.0e. *Ps*CatChs also displayed larger reversal potential shift than CatCh when reducing extracellular barium concentration. All these variants capable of generating five to ten-fold larger calcium photocurrent than CatCh. These tools could potentially become ‘calcium-actuators’ for researcher to study calcium signaling in a spatiotemporal way.

4.3 Integration of optogenetics and optical strategies

A central goal of neuroscience is to understand how the neural system communicates to integrate and process input-output information. Understanding complex mechanisms underlying neutrally-encoded information based on approaches to tracing important neural events, including neuron transmembrane voltage change, intracellular calcium transient and neurotransmitters or neuromodulators release, at the cellular level [103-105]. Currently, a population of FP-based genetically encoded sensors or indicators have been developed to monitor neural activities. Here, I would like to discuss combination of high-performance optical sensors with powerful optogenetic tools to

achieve observation and manipulation of neural activities in a single experiment setting.

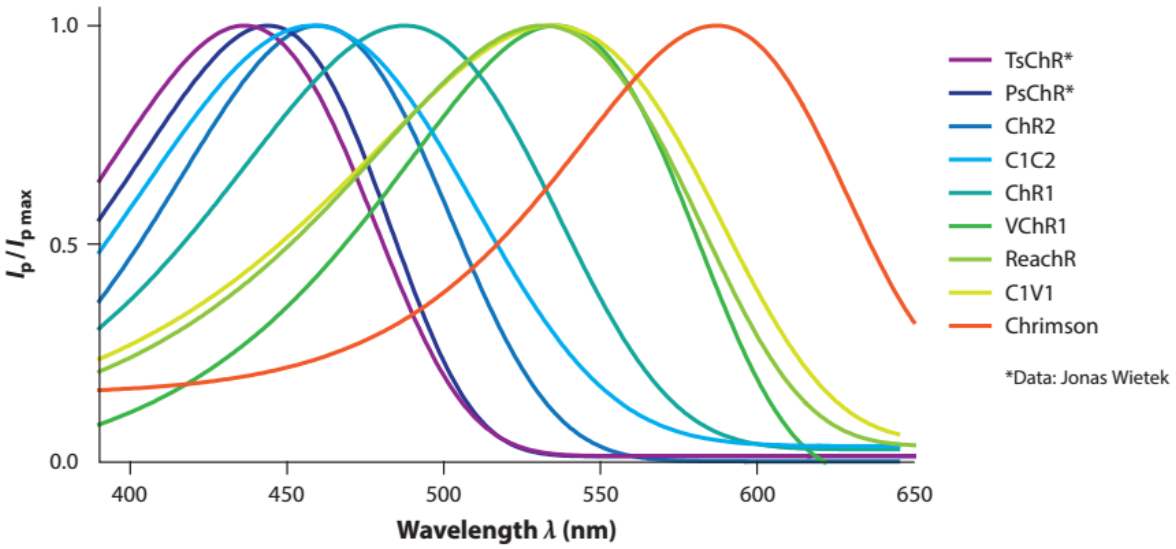

Figure 4.2 Colour-tuned channelrhodopsin.

The ChRs exhibit action spectrum maxima between 436nm (*Ts*ChR) and 590nm (Chrimson). Above figure was taken from (Franziska Schneider et.al;2015)

Genetically encoded calcium indicators (GECIs) are the most popular and widely used optical sensors for neural activities observation [106]. Nowadays, researchers use blue-shifted channelrhodopsin CheRiff as excitatory tools and jRCaMP1a as an optical sensor to achieve all-optical electrophysiological recording. But there is still light-induced cross-talk because 561 nm light for calcium imaging still causes steady inward-photocurrent by CheRiff which would disturb the transmembrane voltage [107]. However, under the same imaging illumination condition, *Ps*CatCh variations do not show any light response. Consequently, blue-shifted channelrhodopsin with large photocurrent like *Ps*CatCh variations could be the ideal optogenetic

actuator for the goal of all-optical recording without crosstalk. In addition, *Ps*CatCh variations exhibit much higher light sensitivity and even more blue-shifted action spectrum than that of CheRiff. Thus, all-optical recording achieved by *Ps*CatCh-jRCaMP1 pairs without crosstalk should be confirmed in neuron or brain tissue.

In addition to conjunction with these calcium sensors, *Ps*CatCh variations can also be combined with genetically encoded voltage indicators (GECIs). Among these *Ps*CatCh variations, pairing *Ps*CatCh 2.0f with VARNAM and Ace-mNeon could enable us to achieve all-optical manipulation and dual-color imaging of voltage dynamics in different neural ensemble with minimal cross talk and timed temporal resolution[108, 109]. To our knowledge, under normal experimental routine, voltage indicators that show good application both in vitro and in vivo are not available, as all published voltage probes either suffer from low brightness or need strong light irradiation.

The next important generation of neural sensors are genetically encoded indicators for optical imaging neurotransmitter or neuromodulator dynamic in the nervous system[110]. Recently, a series of genetically encoded neurotransmitter or neuromodulator indicators (GENIs) have been engineered and tested in all kinds of organisms and animal models[111]. Peak excitation wavelength around 520-560 nm GENIs like R-iGluSnFR1, GlyFS and iTango2 can be used together with our blue-shifted channelrhodopsin ChR2, *Ce*ChR and *Ps*ChR variations as well as enhanced ACRs. Enhanced Chrimson variations could be used together with GENIs which show peak excitation at blue light range including dLight, $GRAB_{DA}$, GRCh2.0 and $GRAB_{NE}$ to

tracing and control dopamine (DA), GABA, acetylcholine (ACh) and norepinephrine (NE) dynamic in freely moving animal under different contextual conditions[112-114].

In summary, our novel optogenetic toolbox with improved properties provides new options for neuroscientists to design rational optogenetic approaches for controlling neural activities, select suitable actuator-reporter pairs for optical observation and manipulation in tracing neural activity and monitoring specific animal behavior.

Reference

1. Schneider, F., C. Grimm, and P. Hegemann, *Biophysics of Channelrhodopsin.* Annu Rev Biophys, 2015. **44**: p. 167-86.
2. Volkov, O., et al., *Structural insights into ion conduction by channelrhodopsin 2.* Science, 2017. **358**(6366).
3. Deisseroth, K. and P. Hegemann, *The form and function of channelrhodopsin.* Science, 2017. **357**(6356).
4. Yoshida, K., et al., *A unique choanoflagellate enzyme rhodopsin exhibits light-dependent cyclic nucleotide phosphodiesterase activity.* J Biol Chem, 2017. **292**(18): p. 7531-7541.
5. Gao, S., et al., *Optogenetic manipulation of cGMP in cells and animals by the tightly light-regulated guanylyl-cyclase opsin CyclOp.* Nat Commun, 2015. **6**: p. 8046.
6. Tian, Y., et al., *A novel rhodopsin phosphodiesterase from Salpingoeca rosetta shows light-enhanced substrate affinity.* Biochem J, 2018. **475**(6): p. 1121-1128.
7. Zhang, F., et al., *The microbial opsin family of optogenetic tools.* Cell, 2011. **147**(7): p. 1446-57.
8. Nagel, G., et al., *Channelrhodopsin-2, a directly light-gated cation-selective membrane channel.* Proc Natl Acad Sci U S A, 2003. **100**(24): p. 13940-5.
9. Govorunova, E.G., et al., *NEUROSCIENCE. Natural light-gated anion channels: A family of microbial rhodopsins for advanced optogenetics.* Science, 2015. **349**(6248): p. 647-50.
10. Inoue, K., et al., *A natural light-driven inward proton pump.* Nat Commun, 2016. **7**: p. 13415.
11. Inoue, K., et al., *A light-driven sodium ion pump in marine bacteria.* Nat Commun, 2013. **4**: p. 1678.
12. Tian, Y., et al., *Two-component cyclase opsins of green algae are ATP-dependent and light-inhibited guanylyl cyclases.* BMC Biol, 2018. **16**(1): p. 144.
13. Yizhar, O., et al., *Optogenetics in neural systems.* Neuron, 2011. **71**(1): p. 9-34.
14. Liu, X. and S. Tonegawa, *Optogenetics 3.0.* Cell, 2010. **141**(1): p. 22-4.

15. Govorunova, E.G., et al., *Microbial Rhodopsins: Diversity, Mechanisms, and Optogenetic Applications.* Annu Rev Biochem, 2017. **86**(1): p. 845-872.
16. Chow, B.Y., et al., *High-performance genetically targetable optical neural silencing by light-driven proton pumps.* Nature, 2010. **463**(7277): p. 98-102.
17. Waschuk, S.A., et al., *Leptosphaeria rhodopsin: bacteriorhodopsin-like proton pump from a eukaryote.* Proc Natl Acad Sci U S A, 2005. **102**(19): p. 6879-83.
18. Ihara, K., et al., *Evolution of the archaeal rhodopsins: evolution rate changes by gene duplication and functional differentiation.* J Mol Biol, 1999. **285**(1): p. 163-74.
19. Shevchenko, V., et al., *Inward H(+) pump xenorhodopsin: Mechanism and alternative optogenetic approach.* Sci Adv, 2017. **3**(9): p. e1603187.
20. Matsuno-Yagi, A. and Y. Mukohata, *Two possible roles of bacteriorhodopsin; a comparative study of strains of Halobacterium halobium differing in pigmentation.* Biochem Biophys Res Commun, 1977. **78**(1): p. 237-43.
21. Lanyi, J.K., *Halorhodopsin: a light-driven chloride ion pump.* Annu Rev Biophys Biophys Chem, 1986. **15**: p. 11-28.
22. Zhang, F., et al., *Multimodal fast optical interrogation of neural circuitry.* Nature, 2007. **446**(7136): p. 633-9.
23. Chuong, A.S., et al., *Noninvasive optical inhibition with a red-shifted microbial rhodopsin.* Nat Neurosci, 2014. **17**(8): p. 1123-9.
24. Inoue, K., et al., *A light-driven sodium ion pump in marine bacteria.* Nat Commun, 2013. **4**: p. 1678.
25. Gushchin, I., et al., *Structure of the light-driven sodium pump KR2 and its implications for optogenetics.* FEBS J, 2016. **283**(7): p. 1232-8.
26. Gushchin, I., et al., *Crystal structure of a light-driven sodium pump.* Nat Struct Mol Biol, 2015. **22**(5): p. 390-5.
27. Kandori, H., K. Inoue, and S.P. Tsunoda, *Light-Driven Sodium-Pumping Rhodopsin: A New Concept of Active Transport.* Chem Rev, 2018. **118**(21): p. 10646-10658.

28. Kato, H.E., et al., *Structural basis for Na(+) transport mechanism by a light-driven Na(+) pump.* Nature, 2015. **521**(7550): p. 48-53.
29. Balashov, S.P., et al., *Light-driven Na(+) pump from Gillisia limnaea: a high-affinity Na(+) binding site is formed transiently in the photocycle.* Biochemistry, 2014. **53**(48): p. 7549-61.
30. Beja, O. and J.K. Lanyi, *Nature's toolkit for microbial rhodopsin ion pumps.* Proc Natl Acad Sci U S A, 2014. **111**(18): p. 6538-9.
31. Tsunoda, S.P., et al., *Functional characterization of sodium-pumping rhodopsins with different pumping properties.* PLoS One, 2017. **12**(7): p. e0179232.
32. Zhao, H., et al., *Coexistence of light-driven Na(+) and H(+) transport in a microbial rhodopsin from Nonlabens dokdonensis.* J Photochem Photobiol B, 2017. **172**: p. 70-76.
33. Grimm, C., et al., *Electrical properties, substrate specificity and optogenetic potential of the engineered light-driven sodium pump eKR2.* Sci Rep, 2018. **8**(1): p. 9316.
34. Avelar, G.M., et al., *A rhodopsin-guanylyl cyclase gene fusion functions in visual perception in a fungus.* Curr Biol, 2014. **24**(11): p. 1234-40.
35. Scheib, U., et al., *The rhodopsin-guanylyl cyclase of the aquatic fungus Blastocladiella emersonii enables fast optical control of cGMP signaling.* Sci Signal, 2015. **8**(389): p. rs8.
36. Scheib, U., et al., *Rhodopsin-cyclases for photocontrol of cGMP/cAMP and 2.3 A structure of the adenylyl cyclase domain.* Nat Commun, 2018. **9**(1): p. 2046.
37. Mahn, M., et al., *High-efficiency optogenetic silencing with soma-targeted anion-conducting channelrhodopsins.* Nat Commun, 2018. **9**(1): p. 4125.
38. Messier, J.E., et al., *Targeting light-gated chloride channels to neuronal somatodendritic domain reduces their excitatory effect in the axon.* Elife, 2018. **7**.
39. Raimondo, J.V., et al., *Optogenetic silencing strategies differ in their effects on inhibitory synaptic transmission.* Nat Neurosci, 2012. **15**(8): p. 1102-4.
40. Wietek, J., et al., *Identification of a Natural Green Light Absorbing Chloride Conducting Channelrhodopsin from Proteomonas sulcata.* J Biol Chem, 2016. **291**(8): p. 4121-7.

41. Govorunova, E.G., et al., *The Expanding Family of Natural Anion Channelrhodopsins Reveals Large Variations in Kinetics, Conductance, and Spectral Sensitivity.* Sci Rep, 2017. **7**: p. 43358.
42. Govorunova, E.G., et al., *Extending the Time Domain of Neuronal Silencing with Cryptophyte Anion Channelrhodopsins.* eNeuro, 2018. **5**(3).
43. Bi, A., et al., *Ectopic expression of a microbial-type rhodopsin restores visual responses in mice with photoreceptor degeneration.* Neuron, 2006. **50**(1): p. 23-33.
44. Boyden, E.S., et al., *Millisecond-timescale, genetically targeted optical control of neural activity.* Nat Neurosci, 2005. **8**(9): p. 1263-8.
45. Ishizuka, T., et al., *Kinetic evaluation of photosensitivity in genetically engineered neurons expressing green algae light-gated channels.* Neurosci Res, 2006. **54**(2): p. 85-94.
46. Li, X., et al., *Fast noninvasive activation and inhibition of neural and network activity by vertebrate rhodopsin and green algae channelrhodopsin.* Proc Natl Acad Sci U S A, 2005. **102**(49): p. 17816-21.
47. Nagel, G., et al., *Light activation of channelrhodopsin-2 in excitable cells of Caenorhabditis elegans triggers rapid behavioral responses.* Curr Biol, 2005. **15**(24): p. 2279-84.
48. Ardevol, A. and G. Hummer, *Retinal isomerization and water-pore formation in channelrhodopsin-2.* Proc Natl Acad Sci U S A, 2018. **115**(14): p. 3557-3562.
49. Berndt, A., et al., *Structural foundations of optogenetics: Determinants of channelrhodopsin ion selectivity.* Proc Natl Acad Sci U S A, 2016. **113**(4): p. 822-9.
50. Bamann, C., et al., *Structural guidance of the photocycle of channelrhodopsin-2 by an interhelical hydrogen bond.* Biochemistry, 2010. **49**(2): p. 267-78.
51. Gradinaru, V., et al., *Molecular and Cellular Approaches for Diversifying and Extending Optogenetics.* Cell, 2010. **141**(1): p. 154-165.
52. Kleinlogel, S., et al., *A gene-fusion strategy for stoichiometric and co-localized expression of light-gated membrane proteins.* Nat Methods, 2011. **8**(12): p. 1083-8.

53. Ma, D., et al., *Golgi export of the Kir2.1 channel is driven by a trafficking signal located within its tertiary structure.* Cell, 2011. **145**(7): p. 1102-15.
54. Rost, B.R., et al., *Optogenetic Tools for Subcellular Applications in Neuroscience.* Neuron, 2017. **96**(3): p. 572-603.
55. Tkatch, T., et al., *Optogenetic control of mitochondrial metabolism and Ca(2+) signaling by mitochondria-targeted opsins.* Proc Natl Acad Sci U S A, 2017. **114**(26): p. E5167-E5176.
56. Asano, T., et al., *Organelle Optogenetics: Direct Manipulation of Intracellular Ca(2+) Dynamics by Light.* Front Neurosci, 2018. **12**: p. 561.
57. Rost, B.R., et al., *Optogenetic acidification of synaptic vesicles and lysosomes.* Nat Neurosci, 2015. **18**(12): p. 1845-1852.
58. Kakegawa, W., et al., *Optogenetic Control of Synaptic AMPA Receptor Endocytosis Reveals Roles of LTD in Motor Learning.* Neuron, 2018. **99**(5): p. 985-998 e6.
59. Nagel, G., et al., *Channelrhodopsin-1: a light-gated proton channel in green algae.* Science, 2002. **296**(5577): p. 2395-8.
60. Mattis, J., et al., *Principles for applying optogenetic tools derived from direct comparative analysis of microbial opsins.* Nat Methods, 2011. **9**(2): p. 159-72.
61. Hochbaum, D.R., et al., *All-optical electrophysiology in mammalian neurons using engineered microbial rhodopsins.* Nat Methods, 2014. **11**(8): p. 825-33.
62. Bedbrook, C.N., et al., *Machine learning to design integral membrane channelrhodopsins for efficient eukaryotic expression and plasma membrane localization.* PLoS Comput Biol, 2017. **13**(10): p. e1005786.
63. Cho, Y.K., et al., *Multidimensional screening yields channelrhodopsin variants having improved photocurrent and order-of-magnitude reductions in calcium and proton currents.* J Biol Chem, 2019. **294**(11): p. 3806-3821.
64. Scholz, N., et al., *Mechano-dependent signaling by Latrophilin/CIRL quenches cAMP in proprioceptive neurons.* Elife, 2017. **6**.

65. Dawydow, A., et al., *Channelrhodopsin-2-XXL, a powerful optogenetic tool for low-light applications.* Proc Natl Acad Sci U S A, 2014. **111**(38): p. 13972-7.
66. Mardinly, A.R., et al., *Precise multimodal optical control of neural ensemble activity.* Nat Neurosci, 2018. **21**(6): p. 881-893.
67. Rajasethupathy, P., et al., *Projections from neocortex mediate top-down control of memory retrieval.* Nature, 2015. **526**(7575): p. 653-9.
68. Oda, K., et al., *Crystal structure of the red light-activated channelrhodopsin Chrimson.* Nat Commun, 2018. **9**(1): p. 3949.
69. Chen, S., et al., *Near-infrared deep brain stimulation via upconversion nanoparticle-mediated optogenetics.* Science, 2018. **359**(6376): p. 679-684.
70. Lin, J.Y., *A user's guide to channelrhodopsin variants: features, limitations and future developments.* Exp Physiol, 2011. **96**(1): p. 19-25.
71. Govorunova, E.G., et al., *Characterization of a highly efficient blue-shifted channelrhodopsin from the marine alga Platymonas subcordiformis.* J Biol Chem, 2013. **288**(41): p. 29911-22.
72. Pan, Z.H., et al., *ChR2 mutants at L132 and T159 with improved operational light sensitivity for vision restoration.* PLoS One, 2014. **9**(6): p. e98924.
73. Klapoetke, N.C., et al., *Independent optical excitation of distinct neural populations.* Nat Methods, 2014. **11**(3): p. 338-46.
74. Schild, L.C. and D.A. Glauser, *Dual Color Neural Activation and Behavior Control with Chrimson and CoChR in Caenorhabditis elegans.* Genetics, 2015. **200**(4): p. 1029-34.
75. Lin, J.Y., et al., *Characterization of engineered channelrhodopsin variants with improved properties and kinetics.* Biophys J, 2009. **96**(5): p. 1803-14.
76. Kim, Y.S., et al., *Crystal structure of the natural anion-conducting channelrhodopsin GtACR1.* Nature, 2018. **561**(7723): p. 343-348.
77. Sineshchekov, O.A., et al., *Gating mechanisms of a natural anion channelrhodopsin.* Proc Natl Acad Sci U S A, 2015. **112**(46): p. 14236-41.

78. Govorunova, E.G., O.A. Sineshchekov, and J.L. Spudich, *Structurally Distinct Cation Channelrhodopsins from Cryptophyte Algae.* Biophys J, 2016. **110**(11): p. 2302-2304.
79. Schneider, F., D. Gradmann, and P. Hegemann, *Ion Selectivity and Competition in Channelrhodopsins.* Biophysical Journal, 2013. **105**(1): p. 91-100.
80. Vierock, J., et al., *Molecular determinants of proton selectivity and gating in the red-light activated channelrhodopsin Chrimson.* Sci Rep, 2017. **7**(1): p. 9928.
81. Gunaydin, L.A., et al., *Ultrafast optogenetic control.* Nat Neurosci, 2010. **13**(3): p. 387-92.
82. Deubner, J., P. Coulon, and I. Diester, *Optogenetic approaches to study the mammalian brain.* Curr Opin Struct Biol, 2019. **57**: p. 157-163.
83. Kim, C.K., A. Adhikari, and K. Deisseroth, *Integration of optogenetics with complementary methodologies in systems neuroscience.* Nat Rev Neurosci, 2017. **18**(4): p. 222-235.
84. Mahn, M., et al., *Biophysical constraints of optogenetic inhibition at presynaptic terminals.* Nat Neurosci, 2016. **19**(4): p. 554-6.
85. Wiegert, J.S. and T.G. Oertner, *How (not) to silence long-range projections with light.* Nat Neurosci, 2016. **19**(4): p. 527-8.
86. Shepard, B.D., et al., *A cleavable N-terminal signal peptide promotes widespread olfactory receptor surface expression in HEK293T cells.* PLoS One, 2013. **8**(7): p. e68758.
87. Berndt, A., et al., *Bi-stable neural state switches.* Nat Neurosci, 2009. **12**(2): p. 229-34.
88. Perny, M., et al., *Chronic activation of the D156A point mutant of Channelrhodopsin-2 signals apoptotic cell death: the good and the bad.* Cell Death Dis, 2016. **7**(11): p. e2447.
89. Hirooka, S., et al., *Acidophilic green algal genome provides insights into adaptation to an acidic environment.* Proc Natl Acad Sci U S A, 2017. **114**(39): p. E8304-E8313.
90. Yizhar, O., et al., *Neocortical excitation/inhibition balance in information processing and social dysfunction.* Nature, 2011. **477**(7363): p. 171-8.

91. Stahlberg, M.A., et al., *Investigating the feasibility of channelrhodopsin variants for nanoscale optogenetics.* Neurophotonics, 2019. **6**(1): p. 015007.
92. Boyden, E.S., *Optogenetics and the future of neuroscience.* Nat Neurosci, 2015. **18**(9): p. 1200-1.
93. Deisseroth, K., *Optogenetics: 10 years of microbial opsins in neuroscience.* Nat Neurosci, 2015. **18**(9): p. 1213-25.
94. Hausser, M., *Optogenetics: the age of light.* Nat Methods, 2014. **11**(10): p. 1012-4.
95. Govorunova, E.G., et al., *Microbial Rhodopsins: Diversity, Mechanisms, and Optogenetic Applications.* Annu Rev Biochem, 2017. **86**: p. 845-872.
96. Hegemann, P. and A. Moglich, *Channelrhodopsin engineering and exploration of new optogenetic tools.* Nat Methods, 2011. **8**(1): p. 39-42.
97. Lerner, T.N., L. Ye, and K. Deisseroth, *Communication in Neural Circuits: Tools, Opportunities, and Challenges.* Cell, 2016. **164**(6): p. 1136-1150.
98. Berndt, A., et al., *High-efficiency channelrhodopsins for fast neuronal stimulation at low light levels.* Proc Natl Acad Sci U S A, 2011. **108**(18): p. 7595-600.
99. Moorhouse, A.J. and J.M. Power, *Making light work of fine-tuning channelrhodopsins.* J Biol Chem, 2019. **294**(11): p. 3822-3823.
100. Brown, J., et al., *Expanding the Optogenetics Toolkit by Topological Inversion of Rhodopsins.* Cell, 2018. **175**(4): p. 1131-1140 e11.
101. Lorenz-Fonfria, V.A., et al., *Temporal evolution of helix hydration in a light-gated ion channel correlates with ion conductance.* Proc Natl Acad Sci U S A, 2015. **112**(43): p. E5796-804.
102. Takemoto, M., et al., *Molecular Dynamics of Channelrhodopsin at the Early Stages of Channel Opening.* PLoS One, 2015. **10**(6): p. e0131094.
103. Gong, Y., et al., *Imaging neural spiking in brain tissue using FRET-opsin protein voltage sensors.* Nat Commun, 2014. **5**: p. 3674.

104. Inagaki, S. and T. Nagai, *Current progress in genetically encoded voltage indicators for neural activity recording.* Curr Opin Chem Biol, 2016. **33**: p. 95-100.
105. McIsaac, R.S., C.N. Bedbrook, and F.H. Arnold, *Recent advances in engineering microbial rhodopsins for optogenetics.* Curr Opin Struct Biol, 2015. **33**: p. 8-15.
106. Shen, Y., et al., *A genetically encoded Ca(2+) indicator based on circularly permutated sea anemone red fluorescent protein eqFP578.* BMC Biol, 2018. **16**(1): p. 9.
107. Farhi, S.L., et al., *Wide-area all-optical neurophysiology in acute brain slices.* J Neurosci, 2019.
108. Kannan, M., et al., *Fast, in vivo voltage imaging using a red fluorescent indicator.* Nat Methods, 2018. **15**(12): p. 1108-1116.
109. Piatkevich, K.D., et al., *A robotic multidimensional directed evolution approach applied to fluorescent voltage reporters.* Nat Chem Biol, 2018. **14**(4): p. 352-360.
110. Wang, H., M. Jing, and Y. Li, *Lighting up the brain: genetically encoded fluorescent sensors for imaging neurotransmitters and neuromodulators.* Curr Opin Neurobiol, 2018. **50**: p. 171-178.
111. Piatkevich, K.D., M.H. Murdock, and F.V. Subach, *Advances in Engineering and Application of Optogenetic Indicators for Neuroscience.* Applied Sciences, 2019. **9**(3).
112. Helassa, N., et al., *Ultrafast glutamate sensors resolve high-frequency release at Schaffer collateral synapses.* Proc Natl Acad Sci U S A, 2018. **115**(21): p. 5594-5599.
113. Jing, M., et al., *A genetically encoded fluorescent acetylcholine indicator for in vitro and in vivo studies.* Nat Biotechnol, 2018. **36**(8): p. 726-737.
114. Patriarchi, T., et al., *Ultrafast neuronal imaging of dopamine dynamics with designed genetically encoded sensors.* Science, 2018. **360**(6396).

Appendix

Supplement table

*Ce*ChR primer	Sequence
*Ce*ChR NewS BgATG5F	GA**agatct**ATGGTGTTCCTTGAAGCCGCAGAAG
*Ce*ChR BhATG5F	cG**ggatcc**accATGTCtCAGTACGGCTGCATCA
*Ce*ChR NewL BgATG5F	GA**agatct**atGGCACTCTCTTCATTCGGTTTTCAGTACCTTAGCCA GTTCCCAGCCAATCCTTATCTGTCCACAACAAGTGAAACATGC CAAGGGTCtCAGTACGGCTGCATCA
*Ce*ChR-LL BgATG5F	GA**agatct**accATGCTcAAgACTAAAGAgAAAGCCGAAATTCAGGC ACTCTCTTCATTCGGT
*Ce*ChR CS qcF	TTCACCaGCCCAGTAATCCTTATC
*Ce*ChR CS qcR	TACTGGGCtGGTGAAAAGCCACTC
*Ce*ChR CD qcF	TTCACCgaCCCAGTAATCCTTATCC
*Ce*ChR CD qcR	TACTGGGtgGGTGAAAAGCCACTC
*Ce*ChR DA qcF	CGTTTCAGCTATCGGATGCGTGGT
*Ce*ChR DA qcR	TCCGATAGCTGAAACGAGGAGTCG
*Ce*ChR DC qcF	CGTTTCATGTATCGGATGCGTGGTATG
*Ce*ChR DC qcR	TCCGATACATGAAACGAGGAGTCGCA
*Ce*ChR DH qcF	CGTTTCACATATCGGATGCGTGGTATG
*Ce*ChR DH qcR	TCCGATATGTGAAACGAGGAGTCGCA
*Ce*ChR DF qcF	CGTTTCATTCATCGGATGCGTGGTATG
*Ce*ChR DF qcR	TCCGATGAATGAAACGAGGAGTCGCA
*Ce*ChR DY qcF	CGTTTCATATATCGGATGCGTGGTATG
*Ce*ChR DY qcR	TCCGATATATGAAACGAGGAGTCGCA
*Ce*ChR H134Q qcF	CCTTATCCAGTTGTCCAATCTTACtGGTC
*Ce*ChR H134Q qcR	GATTGGACAAcTGGATAAGGATTACTGG

ChR2 primmer	sequence
ChR2-N17+Cv10	CG**ggatcc**GGtatggctgtgcaccagattggagaa ggcggaacgaacccagtagtcgtca
ChR2-N13+Cv10	CG**ggatcc**GGtatggctgtgcaccagattggagaa ggcggactgctatttgtaacgaacccag
ChR2-N17+Cv12	CG**ggatcc**GGtatggctgtgcaccagattggagaa ggcggacttgtcacgaacccagtagtcgtca
ChR2-N15	CG**ggatcc**GGttttgtaacgaacccagtagtc
ChR2-N17	CG**ggatcc**GGtacgaacccagtagtcgtca
ChR2-N19	CG**ggatcc**GGtccagtagtcgtcaatggct
ChR2-N13	CG**ggatcc**GGtctgctatttgtaacgaacccag
ChR2-N11	GA**agatct**GGTAGTcgcgagctgctatttgtaac
ChR2-N24	GA**agatct**GGTAGTggctctgtacttgtgcct

PsChR primer	Sequence
*Ps*ChR L115 C qcF	CAGTCATTTGCATACATTTGAGTAACATTACAGG
*Ps*ChR L115 C qcR	CAAATGTATGCAAATGACTGGGCAGGTCAA
*Ps*ChR H117Q qcF	CTCATACAgTTGAGTAACATTACAGGAC
*Ps*ChR H117Q qcR	GTTACTCAACTGTATGAGAATGACTGG
*Ps*ChR F202Y qcF	CAGCGGTATATTTTACAAGTTGGTTCATGTTTCCC
*Ps*ChR F202Y qcR	CAACTTGTAAAATATACCGCTGCCATCG
*Ps*ChR D139C qcF	ACATCCTGCCTGGGAGGCAT
*Ps*ChR D139C qcR	CCCAGGCAGGATGTGATCAGGGA
PsChR-35+Cv12	CG**ggatcc**GGtacgaacccagtagtcgtcaatggctctgtacttgtgcctgaggaccagtgttactgcgcgggctggattgagtcCCGAGGTACGCAATGGTT
PsChR-N33+Cv10	CG**ggatcc**GGtATGGCTGTGCACCAGATTGGAGAAGGCGGACTGGTTGCCCGAGGTACGCAAT
PsChR-N19	CG**ggatcc**GGtACGCCAATCTATCTGAACGT
PsChR-N12	CG**ggatcc**GGtACAATTTTGCTGGACGACTGT
PsChR-C29	CGAGAAGTCACGGTGTCGTGTTTTGTCGATAAAGAAGAGGAGGATGAAGACGAACGTATCAGCACTAAGACCTACGCGAACCGGGCA
PsChR-C20	GATAAAGAAGAGGAGGATGAAGACGAACGTATCAGCACTAAGACCTACGCGAACCGGGCA

Abbreviation

Ace-mNeon	Genetically encoded voltage sensor
ACR	Anion-conducting channelrhodopsin
ANOVA	Analysis of variance
AP	Action potential
AR-3	Archaerhodopsin-3
Arch	*Halorubrum sodomense* archaerhodopsins
ArchT	*Halorubrum* strain T009 archaerhodopsins
ATR	All-*trans* retinal
BAPTA	Fast Ca^{2+} chelator (1,2-bis (o-aminophenoxy) ethane-N, N, N', N'-tetraacetic acid, potassium-salt
BLINK1	Blue-light induced K+ channel 1
BLUF	Blue light utilizing FAD
BeCyClOp	Light-regulated guanylyl-cyclase opsin from *blastocladiella emersonii*
BR	Bacteriorhodopsin
CatCh	Calcium translocating ChR
$CatCh^{+}$	$ChR2^{T159C/S}$
C1C2	Chimeric ChR composed of *Cr*ChR1/2
*Ce*ChR	Acidophilic green alga *Chlamydomonas eustigma*
CG	Central gate
C1V1	Chimeric ChR composed of *Vc*ChR1 and *Cr*ChR1

CheRiff	*Scherffelia dubia* channelrhodopsin E154A
ChR	Channelrhodopsin
ChR1/2	*Chlamydomonas reinhartii* ChR1/2
Chrimson	*Cn*ChR1 *Chlamydomonas noctigama* ChR1
ChrimsonSA	ChrimsonS169A
Chronos	*Stigeoclonium helveticumCs*ChR
*Cs*Chrimson	*Cn*ChR1 with N-terminal sequence from
*Cs*R	*Coccomyxa subellipsoidea* rhodopsin
cRNA	cDNA-derived mRNA
DMEM	Dulbecco's modified eagle medium
DMSO	Dimethyl sulfoxide
dNTP	Deoxynucleotide triphosphate
*Ds*ChR1	*Dunaliella salina* ChR1
dLight1/2	Genetically encoded sensor of dopamine
eACR	Engineered ACR
*ED*50	Half-maximal effective light dose
EDTA	Ethylenediaminetetraacetic
EGFP	Enhanced green fluorescent protein
ER	Exports signal
FP	Fluorescence protein
FLInChR	Full-length inversion of ChR
GECIs	Genetically encoded calcium indicator
GENIs	Neurotransmitter or neuromodulator indicator
*Gt*CCR2/3	Light gated cation channel from cryptophyte
algae	
GPCRs	G protein-coupled receptors

$GRAB_{DA}$	Genetically encoded GPCR-activation-based-DA sensors dopamine sensors
GRCh2.0	Genetically encoded sensor for GACh2.0
$GRAB_{NE}$ GHK	Goldman-Hodgkin-Katz equation
*Hs*HR	*Halobacterium salinarum*
*Np*HR	*Natronomonas pharaonis* named
Jaw	*Natronomonas pharaonis* halorhodopsin K200R and W214F
jRCaMP1	Genetically encoded red calcium sensor
KR2	*Krokinobacter eikastus* termed
LR	Leucine rich
LOVSIK	Light control STIM1 fragment
NTM	Contain three motifs
*Mv*ChR1	*Mesostigma viride* ChR1
opto-CRAC	Light activated CRAC channel
opto-STIM1	Light-induced Ca2+ influx module
PACR	Light sensitive calcium actuator
PsChR	*Marine Alga Platymonas subcordiformis* ChR
PhotonSABER	Photon-sensitive ASR-based endocytosis regulator
SD/ SEM	Standard deviations/standard error mean
*Sr*RhoPDE	Rhodopsin phosphodiesterase from *Salpingoeca rosetta*
SSFO	Stable step function opsin

TYE Trafficking signal, yellow fluorescence protein and ER export signal

UCNPs Upconversion nanoparticles

VARNAM Voltage activated red neuronal activity monitor （Ace-WR-mRuby3 N81S）

*Zip*ACR *Psu*ACR_973

Acknowledgments

I am very grateful to have received the supervision and support from Prof. Dr. Georg Nagel who provided me the opportunity to work on this meaningful and interesting research project and gave me the freedom to pursue my goal. Many thanks to my second supervisor Prof. Dr. Robert J. Kittel who provided the technical platform for my research work.

Special thanks to Dr. Shiqiang Gao, a co-worker with my supervisor, who helped me a lot on designing my research works and teaching experimental skills from which I benefit a lot.Many thanks to my collaborators from Goethe University, Prof. Dr. Alexander Gottschalk and Hamburg University, Dr. Christine Gee, for cooperation in *Ps*ChRs work.

I would like to thank my colleagues from our research group. Thanks to Yu Jing teach me electrophysiological techniques. And other members, Dr. Yuehui Tian, Dr. Sebastian Beck, Shang Yang, Yang Zhou, Ruijing Tang, Meiqi Jing, Maximilian Pitsch, Eike Jöst. And thanks to all my friends in Würzburg for help in my life.

I would also like to sincerely thank my family who provided the best care and selfless support throughout my study time. Many thanks to my girlfriend Yu Shi (KiKi) accompany me during my last year of PhD-journey.

I was supported by the Chinese Scholarship Council and DAAD fellowship for Ph.D. study at Würzburg University.

Table of figures and tables